LBL-6325 1/3

Energy and Environment Division

Telluric And D.C. Resistivity Techniques Applied To The Geophysical Investigation Of Basin And Range Geothermal Systems, Part I: The E-Field Ratio Telluric Method

J.H. Beyer
(Ph.D. thesis)

June 1977

Lawrence Berkeley Laboratory University of California/Berkeley

Prepared for the U.S. Energy Research and Development Administration under Contract No. W-7405-ENG-48

TELLURIC AND D.C. RESISTIVITY TECHNIQUES APPLIED TO THE GEOPHYSICAL INVESTIGATION OF BASIN AND RANGE GEOTHERMAL SYSTEMS

PART I

THE E-FIELD RATIO TELLURIC METHOD

J. H. Beyer

ABSTRACT

This paper describes a natural field electrical exploration technique, the E-field ratio telluric method. The method employs a collinear three-electrode array to measure successive electric field ratios as the array is leap-frogged along a survey line. The 0.05 and 8 Hz responses observed over numerous simple resistivity structures, based upon numerical modeling, are presented. From the model study it can be concluded that: the method is well suited for the rapid electrical reconnaissance exploration of survey areas of several hundred square kilometers, in search of deep conductive targets such as might be associated with hydrothermal systems; the frequencies used for the model study (0.05 and 8 Hz) are appropriate to exploration in Basin and Range valleys, and afford a rudimentary means of depth discrimination.

PREFACE

Starting in the Summer of 1973, the Lawrence Berkeley Laboratory of the University of California has been involved in a geothermal assessment program with three main goals:

1) To evaluate, on the basis of detailed geological, geochemical and geophysical data, some geothermal systems in the mid Basin and Range geologic province.

2) To compare and evaluate geophysical techniques used in the exploration and delineation of geothermal reservoirs.

3) To develop new exploration techniques, and the instrumentation required, specifically for the deep penetration desired in geothermal investigations.

This report addresses various aspects of each of these points.

It is well documented that hot water geothermal reservoirs tend to have lower electrical resistivity than surrounding cold and/or dry rock by virtue of: (1) increased ion mobility, (2) more dissolved solids, and (3) increased permeability and porosity of the reservoir rocks as a result of convection of the geothermal fluids. Vapor dominated geothermal systems are resistive in the steam zone, but display anomalously conductive halos in intermediate temperature regions where there is condensation. Thus, one distinctive feature of geothermal reservoirs is that they may be electrically conductive targets which, to be of economic importance, may be a few cubic kilometers in size, but with a depth of burial of one or more kilometers.

When confronted with the problem of initial exploration of a several hundred square kilometer region in the vicinity of a hot spring, a rapid reconnaissance electrical method is important to locate areas of low resistivity for more intensive investigation. The E-field ratio telluric method described in Part I of this report appears to satisfy this need quite adequately.

Subsequent to the location of conductive anomalies by reconnaissance techniques an electrical method providing higher resolution and affording more quantitative interpretation capability is needed. For this purpose, and for correlation with and evaluation of other electrical exploration techniques, d.c. resistivity measurements using the polar dipole-dipole array were performed as a part of the LBL geothermal exploration program. A second resistivity electrode configuration, the Schlumberger method, has been widely used by other investigators. Part II of this report is a numerical model study and comparison of these two resistivity techniques.

An extensive program of geophysical exploration was undertaken by LBL in the vicinity of Leach Hot Springs in Grass Valley, Nevada. The detailed interpretation of E-field ratio telluric, dipole-dipole resistivity, and bipole-dipole resistivity mapping data is treated in Part III of this report, along with a description of the implementation of high-power d.c. resistivity exploration techniques. Several areas in Grass Valley emerge as being worthy of further investigation for their geothermal potential, and the interpretation process has provided a means of evaluating and comparing the exploration techniques.

ACKNOWLEDGEMENTS

The major portion of this work was supported by the U.S. Energy Research and Development Administration through the University of California - Lawrence Berkeley Laboratory. Some computer time was provided by the U.C. Berkeley Computer Center.

Special thanks are due: Professor H.F. Morrison for numerous profitable ideas and discussions throughout the course of this work; Ki Ha Lee for his helpfullness in the use of his computer codes for the model studies presented in this paper; and Art Paradis for his aid in assembling the computer graphics code necessary to display the models.

TABLE OF CONTENTS

Part I: The E-Field Ratio Telluric Method

INTRODUCTION

Electrical current flow in the ionosphere and lightening discharges in the troposphere are sources of natural electromagnetic fields which can be used for electrical probing of the earth. Depth discrimination is afforded by the increased penetration of longer periods.

This paper deals with the theoretical analysis and model studies of a particular natural electric (telluric) field reconnaissance technique hereby called the Electric (E) Field Ratio Telluric Method. The advantageous aspects of this method are the ease of data acquisition over large (several hundred square kilometer) survey areas, and the simplicity and low cost of data recording and reduction.

For a bit of historical perspective, Boissonnas and Leonardon (1948) have noted that the first definite proof that currents flow in the ground and create potential differences between two points was acquired by Barlow in 1847 as a result of his measurements on English telegraph lines. The initial application of this discovery to geophysical exploration appears to have been made by Leonardon. In 1928 he described an experiment which is the basis of the electric field ratio telluric method. He quite accurately deduced that the ratio of potential differences measured with dipoles perpendicular to strike on opposite sides of a fault would be proportional to the resistivities on either side, and that this ratio would be independent of the telluric current direction because the component of the current normal to the fault is continuous. To prospect for faults he moved an array of two collinear dipoles laid end-to-end along a line perpendicular to strike, and located the fault where the potential difference ratio deviated most from unity. With the complete array on either side of the fault he found the ratio to be unity.

(There is no mention of the frequency band measured). Leonardon also mentions that this technique can locate ore deposits because they "attract the currents flowing in the ground . . . As a result, in the vicinity of the extremities of the conducting masses an abnormal density of current is observed in the surrounding rocks themselves."

What has now become the conventional means of telluric prospecting was first described by Schlumberger in 1939. The method employs two electrode arrays, each consisting of an orthogonal pair of dipoles 500 to 1000 meters long to measure simultaneously the total telluric field at two locations. One array remains fixed at a base station as a reference while the second array is mobile. As has been described by various researchers (Boissonnas and Leonardon, 1948; Tuman, 1951; Berdichevskiy, 1960; Yungul, 1966) the ratio of the areas of ellipses or closed figures simultaneously drawn by the tips of the electric field vectors at the base and mobile stations is roughly proportional to the ratio of the apparent resistivities at the two locations for the frequency band of the measurement.

Shortly after the electromagnetic character of magnetotelluric fields became known Cagniard (1953) developed the theory which revealed the full potential of the magnetotelluric method. If the magnetic as well as the electric telluric fields are measured over layered structure the apparent resistivity can be calculated as a function of frequency, which can be interpreted in terms of the approximate resistivity as a function of depth.

The magnetotelluric method of Cagniard, upgraded by tensor impedance calculations of the apparent resistivity, is a very powerful exploration tool, but is hardly a rapid reconnaissance technique. And the telluric

method of Schlumberger (1939) as presently practiced is rather cumbersome in either instrumentation or data reduction.

A rapid telluric prospecting method, similar to that of Leonardon (1928), was devised by Neuenschwander and Metcalf (1942). They used a collinear three electrode array to measure electric field ratios, and leap-frogged the array along a profile line, successively multiplying the ratios to obtain a relative amplitude profile. (This is the field procedure and data presentation used in the E-field ratio telluric method.) For measurements over ground having a resistivity of 3 to 45 ohm-meters their data, narrow banded at 10 kHz, showed good correlation with shallow d.c. resistivity measurements.

A lower frequency range of 0.5 to 10 Hz was used by Dahlberg (1945) in his experiments with this method. With the profile direction oriented parallel to the maximum electric field direction he found good correlation with resistivity measurements, but determined that if the telluric current flow was predominantly in one direction, data obtained for electrode spreads at right angles to this direction would be greatly influenced by even small amounts of current path curvature. He also notes that occasionally in the vicinity of pipelines the signals from the two dipoles were 180 degrees out of phase as if the current flow were toward or away from the center electrode.

This three electrode ratioing technique has been applied more recently by Yungul (1965, 1973) to mapping deeply buried reefs in Texas.

The aforementioned practitioners determined the electric field intensity from galvanometer measurements or recorded two traces of the electric field intensity as a function of time, seeking portions of the record which were in phase for amplitude comparison. The method

described below is a much easier and faster means of determining the electric field ratio using a portable x-y plotter. Previous reference to work with this reconnaissance telluric method has been made by Beyer, et al. (1975, 1976a, and 1976b).

Before describing this telluric method in detail, however, a theoretical discussion of the behavior of the magnetotelluric field would be appropriate.

ELECTROMAGNETIC THEORY FOR TELLURIC AND MAGNETOTELLURIC EXPLORATION

The natural electromagnetic field of the earth has two sources (Bleil, 1964). Long period variations, below 1-5 H, have for some time been associated with sunspot activity. Solar wind bombardment of the magnetosphere induces currents to flow in the ionosphere, which in turn induces telluric currents in the earth. Higher frequency electromagnetic fields are generated by lightening discharges in the lower atmosphere. Constructive interference occurs for waves whose wavelengths are multiples of the earth's circumference. These propagate around the earth in the earth-ionosphere cavity giving rise to high amplitude resonances, the Schumann resonances, at 8 Hz and multiples thereof. The electromagnetic field travels through the atmosphere and is reflected and refracted at the earth's surface. The equations describing the behavior of the field are given by many authors (e.g., Cagniard, 1953; Price, 1962; Vozoff, et al., 1964; Ward, 1967; Slankis, 1970).

The experimental evidence of Faraday and Ampere led to the first two of Maxwell's four equations relating the vectors of electric field intensity E, magnetic induction B, dielectric displacement D, magnetic field intensity H, and current density J:

$$\nabla \times E + \frac{\partial B}{\partial t} = 0 \qquad (I\text{-}1)$$

$$\nabla \times H - \frac{\partial D}{\partial t} = J \qquad (I\text{-}2)$$

If all media are homogeneous, isotropic, and contain no sources then $B = \mu H$, $D = \epsilon E$, and $J = \sigma E$ where μ, ϵ and σ are the material properties permeability, permittivity, and conductivity.

If a harmonic time variation of $e^{-i\omega t}$ is assumed we have

$$\nabla \times E - i\omega\mu H = 0 \tag{I-3}$$

$$\nabla \times H + (i\omega\epsilon - \sigma)E = 0. \tag{I-4}$$

In rectangular coordinates the field vectors satisfy the Helmholtz equations

$$\nabla^2 E + k^2 E = 0 \tag{I-5}$$

$$\nabla^2 H + k^2 H = 0 \tag{I-6}$$

where $k^2 = \mu\epsilon\omega^2 + i\mu\sigma\omega$.

For the material properties of most geophysical problems and at the frequencies used in telluric exploration the propagation constant k is dominated by the conduction term so that in the earth $k = \delta + i\delta$ where

$$\delta = \sqrt{\frac{\omega\mu\sigma}{2}}. \tag{I-7}$$

As an electromagnetic field propagates into a conductive material it induces currents to flow. These currents in turn produce an electro-

magnetic field which tends to cancel the primary field. The skin depth δ is the depth in the material at which the amplitude of the total field is reduced to $1/e$ of the incident field at the surface. In practical units, with $\mu = \mu_o$

$$\delta \simeq 503 \sqrt{\rho/f} \qquad (1\text{-}8)$$

where $\rho = 1/\sigma$ is the resistivity in ohm-meters and f is the frequency in Hertz.

In the air the displacement term of the propagation constant must dominate because the conductivity of the air is negligible, so $k = \omega \sqrt{\mu \epsilon}$. The propagation constant is much greater in the earth than in the air, so regardless of the angle of incidence of the source field the refracted electromagnetic wave will travel straight downward.

To make geophysical use of natural electromagnetic fields, for which distance and location of the source are unknown, it is necessary that the fields propagating into the earth can be considered to be plane waves over the lateral dimensions of the survey area. Wait (1954) and Price (1962) have shown that this is not the case unless the incident field is uniform over horizontal distances much larger than its skin depth in the ground. However, Srivastava (1965) has concluded that the effect of the wavelength of the source can be assumed to be negligible for periods less than 1000 seconds over moderate resistivity distributions for depths of 10 to 20 kilometers.

A practical test of the plane wave assumption for natural fields is the repeatibility of data. As is discussed in a later section of this

paper, for a 19-kilometer line of electric field ratio telluric data obtained in Grass Valley, Nevada, and repeated several months later, the correspondence between the two sets of data was excellent.

For the one-dimensional problem of harmonic plane electromagnetic waves propagating downward (+ z direction) into a homogeneous or layered earth the E and H fields are laterally uniform ($\partial/\partial x = \partial/\partial y = 0$) so that we can consider any horizontal orthogonal components of the electric (E_x) and magnetic (H_y) fields. Equations (I-3) and (I-4) become

$$\frac{\partial E_x}{\partial z} - i\mu\omega H_y = 0 \qquad (I\text{-}9)$$

$$\frac{\partial H_y}{\partial z} + \sigma E_x = 0 \qquad (I\text{-}10)$$

and the Helmholtz equations, (I-5) and (I-6), become

$$\frac{\partial^2 E_x}{\partial z^2} + k^2 E_x = 0 \qquad (I\text{-}11)$$

$$\frac{\partial^2 H_y}{\partial z^2} + k^2 H_y = 0 \qquad (I\text{-}12)$$

where $k^2 = -i\omega\mu_0\sigma$. Solutions of equations (I-9) and (I-10) which satisfy the Helmholtz equations, (I-11) and (I-12), for downward travelling waves are, respectively,

$$E_x = E_x^{\,o} e^{-ikz} \qquad (I\text{-}13)$$

$$H_y = H_y^{\,o} e^{-ikz} \qquad (I\text{-}14)$$

where E_x^o and H_y^o are constant amplitudes at the surface ($z = 0$). Substitution of equation (I-13) into equation (I-9), or equation (I-14) into equation (I-10), will yield

$$\frac{E_x^o}{H_y^o} = \sqrt{\frac{i\omega\mu_o}{\sigma}} \qquad (I\text{-}15)$$

which defines the electromagnetic plane wave impedance, E_x^o/H_y^o, of a homogeneous medium. The phase of the electric field is seen to lead that of the magnetic field by 45 degrees.

If equation (I-15) is converted from rationalized MKS units to convenient geophysical units, the electric field in millivolts per kilometer and the magnetic field in gammas, it can be written as

$$\rho \simeq 0.2\, T \left| \frac{E_x^o}{H_y^o} \right|^2 \qquad (I\text{-}16)$$

where $T = 2\pi/\omega$, the period in seconds. Thus, if for a particular frequency the orthogonal components of the electric and magnetic fields are simultaneously measured at the surface of a homgeneous half-space, equation (I-16) will give the resistivity of that half-space in ohm-meters.

For a vertically stratified medium an apparent resistivity ($\rho = \rho_a$) will be calculated as a function of frequency due to the combined effects of the various layer resistivities and thicknesses, with higher frequency incident fields penetrating less deeply due to skin effect attenuation (see equation I-8). This is the basis of the magnetotelluric exploration technique.

Let us now consider the case of a plane electromagnetic wave incident upon a half-space containing two-dimensional conductivity inhomogeneities

which are of infinite extent in the $\pm$ y (strike) direction, as is depicted in Figure I-1. It will always be true that the incident field can be separated into two components: one with the magnetic field parallel to strike and with the associated electric field in the plane of incidence ($E_\perp$ and $H_\parallel$), and the other with the electric field parallel to strike and the magnetic field in the plane of incidence ($E_\parallel$ and $H_\perp$). The former has been called by various authors the transverse magnetic (TM), H-polarization, or E-perpendicular case, while the latter is known as the transverse electric (TE), E-polarization, or E-parallel case.

The two-dimensionality described here dictates that the field is invariant in the strike direction ($\partial/\partial y = 0$); for the TM case $H_x = H_z = E_y = 0$, so that from Ampere's Law (equation I-4) we obtain for this situation

$$\frac{\partial H_y}{\partial x} - \sigma E_z = 0 \qquad (I\text{-}17)$$

and

$$\frac{\partial H_y}{\partial z} - \sigma E_x = 0 . \qquad (I\text{-}18)$$

As a result of the zero conductivity of the air, the normal component of the current density at the surface (z = 0) is zero, which in turn necessitates that the vertical component of the electric field be zero ($E_z\big|_{z=0} = 0$). From equation (I-17) it follows that

$$\left.\frac{\partial H_y}{\partial x}\right|_{z=0} = 0 . \qquad (I\text{-}19)$$

The strike-component of the magnetic field at the surface of the earth is invariant in the presence of two-dimensional conductivity inhomogeneities. This significant result indicates that $E_{\perp}(f)$ measured at any location with respect to two-dimensional structures will be proportional to the TM apparent resistivity at that location, which has the practical application that in performing magnetotelluric surveys over linear features, $H_{\parallel}(f)$ need be measured at only one location.

For the two-dimensional ($\partial/\partial y = 0$) TE case $E_x = E_z = H_y = 0$, however the remaining components, H_x, H_z, and E_y, are continuous across the air-earth interface ($z = 0$). Problems in this class, as well as three-dimensional problems, require numerical solutions which include consideration of the free space above the earth.

THE ELECTRIC (E) FIELD RATIO TELLURIC METHOD

The E-field ratio telluric method is intended to be used as a qualitative technique for electrical reconnaissance of the upper couple kilometers of the earth's crust. It is applicable to survey areas of several hundred square kilometers across which electrode locations can be established along straight lines at several hundred meter intervals. The method was successfully used in Basin and Range valleys of north central Nevada by the University of California - Lawrence Berkeley Laboratory for the exploration of hydrothermal systems.

An array of three electrodes emplaced along the traverse line is used to form two consecutive grounded electric dipoles, with the central electrode as common. As shown in Figure I-2 the signals from the two dipoles are amplified, narrow bandpass filtered, and used, respectively, as the x and y inputs to an x-y plotter. If the phase difference between the two signals is small the plotter will draw a straight line whose slope is equal to the ratio of the potential differences observed across the two dipoles. The ratio of the electric fields across the two dipoles will be

$$\frac{E_2}{E_1} = \frac{\Delta V_2 / L_2}{\Delta V_1 / L_1} = \frac{L_1}{L_2} \tan \phi$$

where for dipoles 1 and 2

E = the instantaneous average electric field along the dipole

ΔV = the instantaneous potential across the dipole

L = the dipole length

ϕ = the acute angle between the line drawn by the plotter and its x (horizontal) axis.

For many exploration areas the dipole length can remain constant ($L_1 = L_2$) for any particular survey line so that the ratio of the electric fields will equal the slope of the line drawn on the plotter. Henceforth it will be assumed that this is the case.

Over a uniform or layered earth the average electric fields seen by the two dipoles will be equal, so ϕ will equal 45°. If more resistive structure underlies the second dipole E_2 will be greater than E_1 so that ϕ will be greater than 45°, and conversely.

The array is leapfrogged along the survey line to obtain a continuous set of relative electric field intensity ratios. When successively multiplied together these ratios yield a relative amplitude profile of the component of the electric field in the traverse line direction. Dipole lengths of 500 meters, or 250 meters if higher resolution is desired, have been found to be practical for geothermal exploration in Nevada. These lengths are short enough to detect anomalies of interest to a reconnaissance geothermal survey, yet sufficiently large to reduce the effects of minor surficial anomalies and to allow rapid data acquisition. Figure I-3 depicts three successive E-field ratio telluric stations and the means by which the relative E-field amplitude is calculated and displayed. The angle ϕ can be obtained in the field with a protractor and the slope, tan ϕ, can be found with a pocket calculator.

Exploration depth is an inverse function of the frequency of the incident electromagnetic field. In using the E-field ratio telluric method for reconnaissance, two frequencies which have consistently high amplitude in the natural electromagnetic spectrum, and which are appropriate to the investigation of Basin and Range valleys with I-20

ohm-meter sediments overlying more resistive bedrock, have been employed: 0.05 Hz (bandpass filters set at 0.03-0.06 Hz) for deep probing, and the 8 Hz Schumann resonance band (filters set at 6-10 Hz) for determining the effects of shallow features.

The electric fields observed by the two collinear dipoles of the E-field ratio array are not necessarily in phase. Let us assume that the field has a harmonic time variation of $e^{-i\omega t}$. Then the average electric fields across the dipoles, 1 and 2, will be

$$E_1 = E_1^{\circ} e^{-i(\omega t - \theta_1)}$$

and (I-20)

$$E_2 = E_2^{\circ} e^{-i(\omega t - \theta_2)}$$

where E_1° and E_2° are constant maximum amplitudes, and

$$\theta = \theta_2 - \theta_1$$

is the phase difference between E_1 and E_2. If these signals are used as inputs to the y and x channels, respectively, of an x-y plotter, as shown in Figure I-2, the tip of the resulting E-field ratio "vector" will trace an ellipse with the properties shown in Figure I-4. Note that the major axis of the ellipse lies in the second and fourth quadrants due to the inverted polarity of one of the input signals.

The ellipse will have x and y extremes of $\pm E_1^{\circ}$, and $\pm E_2^{\circ}$, respectively, tilt angle ϕ, semi-minor axis b, and semi-major axis a. The ellipticity ϵ can be defined as $+ b/a$ for left-hand (counter-clockwise) rotation, and $- b/a$ for right-hand (clockwise) rotation of the E-field ratio "vector". Positive ϵ corresponds to

the phase of E_2 leading E_1 ($\theta > 0$), and negative ϵ refers to the phase of E_2 lagging E_1 ($\theta < 0$).

To determine the electric field ratio from the plotter drawn ellipse the amplitudes $2E_1^o$, and $2E_2^o$ (see Figure I-3) can be measured. In practice, however, this is sometimes difficult. The source field varies in amplitude with a frequency less than ω (see equations I-20) so that for practical purposes E_1^o and E_2^o are slowly varying functions of time. It was observed however, that for the 0.05 Hz data the tilt angle ϕ of the ellipse remains reasonably constant, and can quite easily be measured in the field by visually aligning a straight edge with the major axis of the ellipse, and using a protractor. The tangent of ϕ is approximately equal to E_2^o/E_1^o.

The proportions of the ellipse are uniquely defined by the amplitude ratio E_2^o/E_1^o and the phase difference θ , or alternatively by the tilt angle ϕ and the ellipticity $\pm \epsilon$. The relationship between the two pairs of parameters can be shown to be

$$\frac{E_2^o}{E_1^o} = \left[\frac{g-h}{g+h}\right]^{1/2}$$

and

$$\theta = \sin^{-1}\left[\frac{2\epsilon}{(g^2-h^2)^{1/2}}\right]$$

where

$$g = 1 + \epsilon^2$$

and

$$h = \left[g^2 - \frac{g^2 \tan^2 2\phi + 4\epsilon^2}{1 + \tan^2 2\phi} \right]^{1/2}$$

with h equal to the positive root of the right-hand term for $-45^\circ < \phi < 45^\circ$, and h equal to the negative root for $45^\circ < \phi < 135^\circ$.

From these relationships we can determine the error in using tan ϕ as the E-field ratio rather than E_2°/E_1°. For $E_2^\circ = E_1^\circ$ (homogeneous or layered geology) tan ϕ correctly equals 1 regardless of the phase difference or ellipticity. In the extreme cases of the ellipse having a tilt angle of 0° or 90°, either $E_2^\circ = 0$ or $E_1^\circ = 0$, respectively, or the phase difference equals $\pm 90^\circ$, which means that E_2°/E_1° is independent of the tilt angle. Such a case was never encountered in the field (except as an indication of incorrect instrument settings or equipment malfunction). The tan ϕ approximation for E_2°/E_1° grows progressively worse as the tilt angle deviates from 45° and the ellipticity increases, however, for $30^\circ \leq \phi \leq 60^\circ$ and $|\epsilon| < 0.25$ the error is less than 7%. The E_2/E_1 phase difference θ in this case is $\pm 32^\circ$. For all but a few of the 500 or so E-field ratio telluric stations occupied in Nevada during the UCB-LBL geothermal program, the ellipticity of the E-field ratio trace drawn by the x-y plotter was less than 0.1, yielding less than 7% error for the tan ϕ approximation of E_2°/E_1° over a range of $15^\circ \leq \phi \leq 75^\circ$. For $\phi = 15^\circ$ or 75° and $\epsilon = \pm 0.1$, the E_2/E_1 phase difference is $\pm 22^\circ$.

Should stations be encountered at which the x-y plotter ellipse has a high ellipticity <u>and</u> a tilt angle significantly greater or less than 45°, the x and y amplitudes of an ellipse can be measured to obtain the E-field ratio.

Sample Data

Figures I-5 and I-6 show representative field records of 0.05 Hz E-field ratio telluric data. Several traces are obtained at each station so that an average tilt angle can be calculated. The measured tilt angle ϕ is noted by each trace. The traces labeled "Cal" are calibration lines obtained by connecting both x and y inputs of the plotter to a single dipole so that both channels will receive identical signals. If both channels of the amplifier, filter, and plotter produce the same gain the slope of the calibration lines will be 45°.

The 8 Hz signals are not handled in quite the same manner as the long period (f = 0.05 Hz) tellurics due to two considerations: variable phase shift has been observed between the signals seen by the two in-line dipoles, and the x-y plotter which has been used to date has a maximum frequency response of 2 Hz. For these reasons, each of the two incoming telluric signals is rectified and integrated--stored capacitively, but with a slow discharge rate (time constant about 1 second). The capacitor voltages are used as inputs to the x and y channels of the plotter. A burst of 8 Hz telluric signal will cause the plotter to rapidly trace a line in the + x, + y quadrant (owing to the rectification of the signal), and between bursts the capacitor voltages decay so that the plotter pen moves back toward the origin. The tangent of the angle ϕ that this oscillating trace makes with the x-axis of the plotter is the time average of the E-field ratio as seen by the two receiver dipoles.

Figures I-7 and I-8 show representative field records of 8 Hz E-field ratio telluric data. As with the 0.05 Hz data, several traces are obtained so that an average tilt angle can be calculated.

Instrumentation

The x-y plotter which was used for geothermal exploration in Nevada is commercially available: The Simpson Model No. 2745 x-y, y-t Recorder. It measures 26 x 21 x 11 centimeters, weighs 3.8 kg, and is powered by eight "D" cells.

The telluric receivers were designed and built at Lawrence Berkeley Laboratory. The LBL Mark III A Telluric Receiver is a two channel device containing amplifiers (10-2000 gain), tunable high and low pass filters (0.01 to 1000 Hz with 24 db/octave roll-off), d.c. buckout capability, integration circuitry for 8 Hz signals, and a transient suppressor ("auto zero") for accelerated damping of the filters when tuned for long period signals. The instrument measures 28 x 18 x 20 cm, weighs 4 kg, and will operate for over 100 hours powered by twelve penlight batteries.

Non-polarizing copper-copper sulfate porous pot electrodes were used.

The equipment is shown in Figure I-9, and a schematic diagram of the telluric receiver is given in Figure I-10. Questions regarding this instrument should be directed to the Manager, Special Projects Group, Lawrence Berkeley Laboratory, Berkeley, California, 94720.

MODEL STUDY OF THE E-FIELD RATIO TELLURIC METHOD

In order to help assess the usefullness of the E-field ratio telluric method for reconnaissance of potential geothermal sites a two-part numerical model study has been conducted. The first part displays the E-field ratio telluric anomaly observed along a traverse line perpendicular to the strike of a number of simple two-dimensional resistivity structures. The second part is a parametric study for two resistivity models which demonstrates the effects of varying (1) the traverse line direction with respect to strike, and (2) the incident electromagnetic field ellipticity and (3) polarization direction.

The computer code used for this study was developed by Ryu (1971) with some modification by Lee (1976). It employs the finite element approach for numerical solution of the electromagnetic response of two-dimensional resistivity models for harmonically varying plane wave incident fields of either transverse magnetic or transverse electric mode. For combining the TM and TE responses to obtain the observed electric field in any traverse direction for arbitrary incident field polarization and ellipticity, a program written by Lee (1976, personal communication), with modification by the author.

In addition to the anomaly profiles presented below, Slankis, et al. (1972) have calculated what amount to the 8 Hz E-field ratio telluric responses for an assortment of conductive bodies.

E-Field Ratio Telluric Response Perpendicular to the Strike of Two-Dimensional Structures

Appendix I-A (Figures I-A1 through I-A34) constitutes a numerical model study of E-field ratio telluric anomalies along profile lines perpendicular to the strike of two-dimensional resistivity features for frequencies of 0.05 and 8 Hz. This geometry involves only the TM electromagnetic field. As was demonstrated in the previous section, the transverse magnetic field ($H_{\parallel}$) is invariant at all points on the surface, which results in the electric field ($E_{\perp}$) being proportional to the apparent resistivity.

The electric field amplitude and phase have been calculated at 250 meter intervals (to represent receiver dipoles of this length) across the surface of the model; the E-field ratio has been measured with respect to the electric field amplitude at the left edge (x = -8.) of the model shown at the bottom of each figure. The phase of the TM electric field does not vary appreciably over the surface of the earth. For all the data displayed in these figures, the highest phase difference observed between two successive dipoles was 6 degrees, found at the central location for the infinite vertical contact shown in Figure I-A1. The ellipse which would be drawn by the x-y plotter method of determining the E-field ratio has a negligible ellipticity ϵ of 0.035. Thus, for all the models presented, an E-field ratio plot using the tan ϕ approximation for E_2^o/E_1^o would be identical to one using E_2^o/E_1^o itself.

An interval of 250 meters was used for the model dipole length rather than 500 meters, which was more commonly used in the field, to display more detail in the anomaly patterns. Should the anomaly for 500 meter dipoles be desired, the curve shown can quite accurately be

visually averaged over a 500 meter unit length.

The resistivity models shown at the bottom of Figures I-A1 through I-A35 have equal horizontal (x) and vertical (z) scales indicated in kilometers. For the purpose of computation of the electromagnetic field the models are not truncated at the right, left, or bottom as is suggested by the diagrams; they extend in these respective directions for a distance equal to several skin depths in the most resistive massive material in the model such that at the boundaries of the computational mesh the secondary fields due to lateral inhomogeneities located at the center of the model have become negligible. Horizontal layers which extend to the boundaries of the mesh are treated analytically to establish the proper boundary conditions. Although it is not relevant to the calculations involving TM fields, it should be mentioned that the effect of the air layer above the model is properly considered in the TE case, such that the secondary fields due to lateral inhomogeneities at the center of the model have become negligible at the top of the mesh.

For the ensuing discussion of the E-field ratio telluric models it should be remembered that the value which is plotted is a relative amplitude. For practical purposes this means that a curve of E-field ratio data can be slid up or down to any location on the "relative amplitude" axis. It also means that the E-field ratio anomaly for any model will not be greatly affected by the addition of any layered resistivity structure beneath the deepest lateral resistivity contrast.

As a convenience for analyzing the E-field ratio telluric models, Table 1 lists the skin depths in the materials used in the models at the frequencies employed.

Table 1

Resistivity in ohm-meters	Skin depth in km at 0.05 Hz	Skin depth in km at 8 Hz
1	2.25	0.18
10	7.11	0.56
30	12.3	0.95
100	22.5	1.78
1000	71.1	5.62

The semi-infinite vertical contact.

Figure I-A1 shows the 0.05 and 8 Hz E-field ratio telluric anomalies over a semi-infinite vertical contact at x = 0 which separates regions with resistivities ρ_1 = 10 and ρ_2 = 100 ohm-meters. At two locations distant from the fault in the -x and +x directions, equation (I-16) will give, respectively,

$$\rho_1 \simeq 0.2\,T \left| \frac{E_{1x}^{o}}{H_{1y}^{o}} \right|^2$$

and

$$\rho_2 \simeq 0.2\,T \left| \frac{E_{2x}^{o}}{H_{2y}^{o}} \right|^2$$

For the TM mode magnetic fields $H_{1y}^{o} = H_{2y}^{o}$, so that

$$\frac{E_{2x}^{o}}{E_{1x}^{o}} = \sqrt{\frac{\rho_2}{\rho_1}} \quad . \tag{I-20}$$

Thus, the ratio of the telluric intensity simultaneously measured perpendicular to strike on either side of the contact, and distant from

it, equals the square root of the resistivity ratio (or apparent resistivity ratio for the case of layered structure separated by a vertical contact). We see in Figure I-A1 that for the 8 Hz data at the extreme edges of the diagram $E_{2x}/E_{1x} = 3.2$, which satisfies equation (I-20). The 0.05 Hz data has nearly reached its asymptotic value at x = -8 km due to the skin depth in the 10 ohm-meter material being 7 km, whereas on the 100 ohm-meter side of the contact the skin depth is 22 km, requiring a greater separation than x = 8 km before the effect of the contact becomes negligible.

At the contact (x = 0) the normal component of the current density (J_x) must be continuous. Ohm's Law ($J_x = 1/\rho\, E_x$) demands that the electric field be discontinuous across the contact, with

$$\left.\frac{E_{2x}}{E_{1x}}\right|_{x=0} = \left.\frac{\rho_1}{\rho_2}\right|_{x=0} \qquad (I\text{-}21)$$

Thus, at the contact the telluric field ratio equals the resistivity ratio for any frequency. Figure I-A1 does not reflect the discontinuity or the ratio given by equation (I-20) due to the use of finite length dipoles--the electric field is averaged over the length of a 250 meter dipole. The decrease in the E-field ratio as the contact is approached from the conductive side is the result of a downward component of current flow for current moving to the right. This is necessitated by the fact that the distribution of the horizontal component of the current density as a function of depth must be different on the two sides of the contact. On the resistive side a greater proportion of the lateral current flow is deeper than on the conductive side.

If the depth extent of the vertical contact is reduced to 1 km, as is the case in Figure I-A2, the 8 Hz anomaly remains unchanged as a result of the inability of the 8 Hz signal to penetrate the 10 ohm-meter layer. At 0.05 Hz the offset across the contact is virtually identical to that in Figure I-A1 due to the discontinuity of the electric field. The increase in the E-field ratio as the contact is approached from the resistive side results from the upward flow of current moving to the left; current is concentrated near the surface to enter the conductive layer. Notice that for the two frequencies the anomaly profile positions along the "relative amplitude" axis bear no relationship to the apparent resistivities which would be calculated at a particular location for the respective frequencies. In practice it is impossible to determine the absolute relationship between E-field ratio telluric profiles at different frequencies without additional information, such as might be provided by a magnetotelluric station at some location along the survey line.

In comparing Figures I-A1 and I-A2 it can be seen that long period telluric or magnetotelluric measurements made near a thin conductive layer will be more greatly affected than if the conductive material were very thick.

Buried faults or contacts.

Figures I-A3, I-A4, and I-A5 depict the 0.05 Hz E-field ratio response over faults or contacts buried under a 10 ohm-meter overburden layer. For each of these models the inflection point is seen to be located on the side of the fault with the more conductive section. The "undershoot" and "overshoot" which were observed in Figures I-A1 and I-A2 are not present due to the lack of a lateral resistivity contrast

at the surface to produce a discontinuity in the horizontal electric field. In comparing Figures I-A4 and I-A5, the latter, for a fault with half the vertical offset and a greater average depth, produces very nearly half the anomaly. This indicates that the 0.05 Hz electromagnetic field, with a skin depth of 7 kilometers in 10 ohm-meter material, undergoes very little attenuation, and the overriding factor is simply the laterally discontinuous structure. As will be seen from subsequent models, the 8 Hz field does not sufficiently penetrate a 1 km thick 10 ohm-meter layer to produce an anomaly.

Figures I-A6 and I-A7 show the models of the previous two figures with the addition of a resistive extension of the fault into the conductive overburden layer. This represents a portion of the fault which has become resistive owing to precipitation from hydrothermal fluid flow. The 8 Hz telluric anomaly for the model in Figure I-14 would be a small bump at x = 0.

Figure I-A8 for a dipping contact might represent the margin of a sedimentary basin. It is important to notice that the 0.05 Hz data reach a minimum and level off at about x = 4 km where the model becomes horizontal. If the contact were to continue to greater depth, it is apparent from skin depth considerations that the 0.05 Hz E-field ratio would continue to decrease. The 8 Hz data on the other hand, level off at about x = 0 to 1 km, where the depth to the contact is less than 1 km. With the curves for the two frequencies normalized with respect to the electric field value at x = -8 km, where the apparent resistivity would be approximately 100 ohm-meters for both frequencies, the 8 Hz data at x = +8 km show a larger anomaly over the thickest conductive material than do the 0.05 Hz data.

If for each frequency the electric field ratio at x = 8 km is used to calculate the apparent resistivity using equation (I-20), results of 10 ohm-meters at 8 Hz and 18 ohm-meters at 0.05 Hz are obtained. This establishes that the 8 Hz electromagnetic field has not penetrated the thicker conductive region, while the 0.05 Hz field has, and demonstrates the usefullness of two such frequencies for reconnaissance exploration of conductive (about 10 ohm-meter) sedimentary areas.

If an E-field ratio survey were conducted across a sedimentary basin represented by the model in Figure I-A8, and the survey line were to end in the vicinity of the contact outcrop at x = -2.5, these data would not enable one to determine an absolute relationship between the data for the two frequencies.

Near surface resistivity contrasts.

Figures I-A9 through I-A12 show the effects that surface layer thickness can have upon E-field ratio telluric data. In the first two cases the surface layer is more conductive than the underlying medium, and in the second two cases it is more resistive. Variations in the thickness of a conductive surface layer can produce very large anomalies. Much of the horizontally flowing telluric current remains confined to this layer with the result that changes in the layer thickness tend to produce inversely proportional changes in the current density. For the resistive surface layer the 0.05 Hz anomalies are fairly small as a result of low skin effect attenuation in the 100 ohm-meter layer, whereas quite the reverse is found for 8 Hz signals.

Figure I-A13 displays the anomalies of a small conductive body and a small resistive body at the surface. The respective anomalies are virtually identical for the two frequencies, and show considerable

overshoot and undershoot, as a result of the dominant effect being the discontinuity of the normal component of the electric field across each lateral contrast. The bodies are small enough so that even at 8 Hz the skin effect attenuation is negligible.

Conductive bodies in a homogeneous half-space.

Figures I-A14 through I-A27 display the E-field ratio telluric anomalies for various conductive bodies in an otherwise homogeneous more resistive half-space. Various conclusions can be drawn by comparing these figures.

For a 1 km wide, 1 ohm-meter body buried 1 km in a 100 ohm-meter half-space (Figure I-A14) the anomaly is virtually unaffected by increasing the depth extent of the body (Figure I-A15), and is diminished only slightly by reducing the resistivity contrast of the body from 100:1 to 10:1 (Figure I-A16). However, if the lateral extent of the body is increased (Figures I-A17 and I-A18) the 0.05 Hz anomaly amplitude increases dramatically, partly as a result of more conductive material being closer to the surface, but more significantly as a result of increased coupling of the conductive body with the telluric current. In a homogeneous or layered earth telluric currents will flow horizontally in response to the vertical propagation of the electromagnetic field. If the resistivity contrast of a wide body is reduced (Figure I-A19) the anomaly suffers significantly because the current flow in the body is greatly reduced.

The 8 Hz anomaly reaches its asymptotic limit in a shorter lateral distance than does the 0.05 Hz response. Thus, the 8 Hz anomaly for the 1 km deep body increases as the width expands from 1 km (Figure I-A14) to 2 km (Figure I-A17), but then remains constant in amplitude with

further lateral extension (Figure I-A18).

The dipping body in Figure I-A20 yields a small 8 Hz response over only the shallowest portion of the body, whereas at the longer period excitation a significant anomaly is observed as a result of the body width and low 0.05 Hz attenuation in the 100 ohm-meter background. Massive conductive bodies at depths of 2 km and 3 km (Figures I-A21 and I-A22) yield significant 0.05 Hz anomalies, but no response at 8 Hz, for which the skin depth is less than 2 km in the background material.

From Figure I-A23 it can be seen that telluric fields clearly resolve two 1 km deep conductive bodies separated 1 km. (This is not the case for some d.c. resistivity methods [Beyer, 1977a].)

For conductive bodies buried at 250 or 500 meters in the 100 ohm-meter background (Figure I-A24) the anomalies at 0.05 and 8 Hz do not differ greatly because the depths of burial are small with respect to the skin depths.

If the background resistivity is reduced to 10 ohm-meters the 8 Hz signal does not penetrate to a depth of 1 km. At 0.05 Hz, however, the anomaly for a 1 km wide, 1 ohm-meter body buried 1 km (Figure I-A25) is only slightly reduced from that for the 100 ohm-meter earth containing a body with the same contrast (Figure I-A16). A wider body (Figure I-A26) once again produces a significantly larger anomaly.

At a depth of burial of 250 meters a 1 ohm-meter body (Figure I-A27) yields significant but distinctly different anomalies at the two frequencies.

Resistive bodies.

Figure I-A28 shows the telluric anomaly for a 1 km wide resistive body buried 1 km in a 100 ohm-meter half-space. The anomaly amplitudes

at both 0.05 and 8 Hz are larger than for the identical conductive body with 100:1 contrast (Figure I-A14). This result is observed because the horizontally flowing telluric current is not greatly deviated by a thin vertical conductive body, whereas a vertical resistive feature forces the current to flow around it. A thin horizontal resistive body, however, would deflect the telluric current very little resulting in only a small amplitude anomaly.

If the background resistivity is reduced to 10 ohm-meters (Figure I-A29) the 8 Hz anomaly is eliminated, while the 0.05 Hz response is only slightly attenuated.

Conductive bodies beneath an overburden layer.

If a 0.5 km thick, 30 ohm-meter overburden layer lies above a 1 km wide conductive body buried at 1 km (Figures I-A30 and I-A31) the telluric anomaly is naturally reduced from that seen without the overburden layer (Figures I-A14 and I-A16). If the overburden resistivity is reduced to 10 ohm-meters (Figure I-A32) even the 0.05 Hz anomaly becomes insignificant. It is interesting to note, however, that in each of these cases the anomaly is smaller than that seen for a background resistivity of 10 ohm-meters with no overburden (Figure I-A25). For the 0.05 Hz signal, attenuation in the overburden layer is clearly not the primary cause of the anomaly reduction, rather, the telluric current stays highly confined to the conductive layer so that the body produces little perturbation of the current flow at the surface.

Similarly, for the 2 km wide body with a 30 ohm-meter layer (Figure I-A33) the anomaly is somewhat reduced in comparison with Figure I-A17 without the layer, but it is still slightly larger than in the 10 ohm-meter background case (Figure I-A26). However, with a 10 ohm-meter

overburden (Figure I-A34) the anomaly is drastically reduced.

In Figure I-A35 a 10 ohm-meter layer overlies the same two conductive bodies shown in Figure I-A23. The bodies are still clearly resolved, but the anomaly amplitude is insignificant for this overburden resistivity.

Summary of observations.

To summarize the most significant results of this study:

1) Overshoot and undershoot are observed at lateral resistivity contrasts which reach the surface. This is reduced or eliminated by a thin surface layer of uniform resistivity.

2) Features which are at shallow depths (with respect to the skin depth in the overlying material) will yield essentially identical anomalies for both frequencies.

3) Conductive bodies with large lateral extent yield larger anomalies than those which are thin but of great vertical extent. The reverse is true for bodies which are more resistive than the background.

4) Depending upon the skin depth of the frequency in the overlying material, depth discrimination is afforded by the use of two or more frequencies.

5) Variations in the thickness of thin conductive overburden layers can produce high amplitude anomalies at high and low frequencies.

6) A conductive overburden layer can mask a buried anomalous body more severely than if the body lies within material of the overburden resistivity. This means that conductive targets which lie within basement rock beneath sedimentary basins are harder to locate than if they were to lie within the sedimentary section.

The effect of strike length.

The E-field ratio telluric models discussed above are intended to illustrate the types and amplitudes of anomalies which would be observed over some simple resistivity structures using 0.05 and 8 Hz telluric fields. However, the models are all two-dimensional and the profile lines are perpendicular to strike, so it is reasonable to ask what effect there would be on these anomalies if the bodies were finite in length and/or the profile lines were run at an arbitrary angle with respect to strike. While a complete analytical answer will not be presented here, some reasonable estimates can be made.

For the TM mode electromagnetic fields used for the models, the electric field normal to all lateral resistivity contrasts must be discontinuous with an offset equal to the conductivity contrast. This is the cause of the observed anomalies. If an anomalous body in the models were truncated in the strike (y) direction, the boundary condition for this face would only require that the electric field be continuous. This constraint is easily satisfied, so the dominant effect would still be the discontinuity of the electric field across faces which are normal to a component of the current flow, with the result that the modeled anomalies would undergo little change as a function of the strike length of a body.

A very useful paper by Weidelt (1975) confirms this conclusion with numerical modeling of electromagnetic plane wave excitation of three dimensional bodies. He presents diagrammatic representations of the secondary magnetotelluric field components over a conductive body which has a width of about 5 skin depth units, a strike length of 10 skin depths, and a thickness of 2 skin depths. (The body is 25 x 50 x 10

kilometers, has a resistivity of 1 ohm-meter, and is at the surface of a 10 ohm-meter half-space. The incident electromagnetic field has a period of 120 seconds [f = 0.0083 Hz]). The telluric anomaly along the long (strike) axis of the body (approximate TE case) is of comparable shape and amplitude to the anomaly along the short axis (approximate TM case). This demonstrates that the length of a conductive body in the direction perpendicular to the incident electric field is of only secondary importance to the E-field ratio telluric anomaly observed in the electric field direction.

The Effects of Incident Field Polarization Direction and Ellipticity on E-Field Ratio Telluric Anomalies

If the electric field is measured along a traverse line which is perpendicular to the strike of two-dimensional structures only the TM mode of the electromagnetic field need be considered. However, if the traverse line is at an arbirtary angle with respect to strike both the TM and TE components of the incident field must be taken into account. The relative amplitude and the phase relationship of these components, if they are harmonic, can be defined in terms of the polarization direction, or major axis direction of the polarization ellipse, and the ellipticity. To depict the effects that the source field can have upon the E-field ratio telluric anomaly, there is presented below an analysis of the 0.05 and 8 Hz anomaly patterns over a buried conductive body and an infinite vertical contact for a traverse line at 45 degrees with respect to strike.

Conventionally, the incident field is characterized by the ellipse described by the tip of the magnetic field vector. However, as we are dealing with telluric measurements, it will be more convenient to

consider the incident electric field polarization direction α and ellipticity. The direction of the rotation, as designated by the sign of the ellipticity, $\pm \epsilon$, will follow conventional notation such that positive is clockwise as seen by a viewer looking back toward the source. (This is not natural, but it is conventional). To conform to geological usage the electric field polarization and the traverse line directions will be measured with respect to strike, the y-axis direction. The situation is illustrated in Figure I-11. For each model and frequency there is a series of eight figures exhibiting, at several incident field polarization directions, the E-field ratio telluric anomaly which would result for incident field ellipticities of 0.0, $\pm$ 0.25, and $\pm$ 0.5. Additionally, the anomalies for circularly polarized incident fields with both rotation directions ($\epsilon = \pm 1.0$) are shown as limiting cases; these anomalies remain unchanged, of course, throughout the set of figures for a particular model and frequency as the incident field polarization direction is varied.

Appendix I-B (Figures I-B1 through I-B16) constitutes the E-field ratio parametric study for the conductive body shown in Figure I-A27; the 1 ohm-meter body is two-dimensional with a width of 1 km, thickness of 0.5 km, and depth of burial of 0.25 km in a 10 ohm-meter half-space. The first eight figures represent 0.05 Hz anomalies, and the latter eight, 8 Hz anomalies. The receiver dipole length is approximately 350 meters, and the horizontal axes indicate distance along the profile line direction at 45 degrees to strike.

Appendix I-C (Figures I-C1 through I-C16) is a similar treatment for the infinite vertical contact shown in Figure I-A1, with resistivities of 10 ohm-meters to the left and 100 ohm-meters to the right of the contact.

The buried conductive body.

At 0.05 Hz the transverse electric field is virtually unaffected by the presence of the buried conductive body. For this reason Figure I-B1 shows no anomaly for the incident electric field polarized parallel to strike with $\epsilon = 0$ (the purely TE case). As the angle of polarization increases toward the normal to strike (Figures I-B2 - I-B5) the anomaly for more highly polarized ($\epsilon = 0, \pm 0.25$) incident fields grows larger so that at a polarization angle of 90° and $\epsilon = 0$ (the purely TM case), we have an anomaly which is analogous to that in Figure I-A1.

For $\alpha = 135^{\circ}$ (Figure I-B7) the incident field is polarized perpendicular to the traverse line so that for small ellipticities the component of the electric field in the direction of the measuring dipoles is almost negligible. The anomalies are primarily the result of deviations in the polarization direction rather than in the amplitude of the total electric field vector at the surface of the earth. These situations are seen to produce "reversed" anomalies, that is to say, an apparent increase in the telluric field over a conductive body. For $\alpha = 157.5^{\circ}$ (Figure I-B8) reversed anomalies are also observed. An explanation for this is diagrammatically portrayed in Figure I-12, using the $\epsilon = 0$ data for a polarization direction of 157.5°. While a linearly polarized ($\epsilon = 0$) incident field is seldom observed in the field, it will serve to illustrate the principle while avoiding the complexity of a phase shift between the TM and TE components.

Figure 12 shows the undisturbed electric field at a large distance from the inhomogeneity, and, at several station locations, the total electric field at the surface of the earth, the components parallel and perpendicular to strike, and the observed component in the profile line

direction. At 0.05 Hz the TE field is virtually unaltered so $E_{\parallel}$ is constant in amplitude, while $E_{\perp}$ decreases over the conductive body. This rotates the E total vector clockwise over the body such that for this particular set of profile line and incident field polarization directions the component of the electric field in the profile line direction increases, producing a positive E-field ratio anomaly.

At 8.0 Hz the same conductive body yields a somewhat different set of E-field ratio anomalies as is seen in Figures I-B9 through I-B16. As a consequence of an 8 Hz skin depth of less than 200 meters in the 1 ohm-meter body, the TE component of the incident field yields as large an anomaly over the body as does the TM component.

The incident field polarization direction has relatively little effect upon the E-field ratio anomaly except, as in a previous case, when the profile line is perpendicular to a highly polarized incident field (see Figure I-B15 for ϵ = 0, 0.25). Even at a polarization direction of 157.5° (Figure I-B16) no reversed anomaly is encountered as a result of the attenuation of $E_{\parallel}$ as well as $E_{\perp}$ over the conductive body.

The semi-infinity vertical contact.

Many similar characteristics are seen in Appendix I-C, the telluric parametric study for the infinite vertical contact. The TE field displays a very gradual response to the contact at 0.05 Hz (see Figure I-C1, ϵ = 0). For larger ellipticities or polarization angles (Figures I-C2 - I-C5) the TM field dominates the E-field ratio response resulting in larger anomalies which approach the purely TM response (polarization direction perpendicular to strike, ϵ = 0).

As the polarization angle is increased beyond the normal to strike (Figure I-C6) exaggerated anomalies are observed for highly polarized incident fields. These conditions can produce large phase changes

between the electric fields observed at two consecutive dipoles. This phenomenon is depicted in Figure I-13 for an incident electric field polarized at 112.5 degrees to strike, with an ellipticity of -0.25. The profile line is at 45 degrees to strike with one dipole located on the 10 ohm-meter side of the contact and the other spanning the contact. At the center of each dipole are diagrammatically portrayed the average values of the $E_{\perp}$,$E_{//}$, E total, and E observed fields along that dipole. The fields are shown at four different instants in time as the incident electric field vector traces out an ellipse at a frequency of 0.05 Hz. The E-field ratio pattern drawn on the x-y plotter will be an ellipse with a tilt angle $\phi = 89^{\circ}$ and an ellipticity $\epsilon = -0.35$. Thus, the electric fields observed along the two consecutive dipoles are virtually out of phase with one another. An acceptable value for the E-field ratio can be found by measuring the x and y amplitudes $(E_2^{\circ}/E_1^{\circ})$ of the ellipse drawn by the plotter. Other electrode arrays along the survey line yield negligible phase shift between consecutive observed electric fields.

Another interesting case is observed for the 112.5° polarization direction if the incident field is linearly polarized. As is illustrated in Figure I-14, the E-field ratio for the array with one dipole over the 10 ohm-meter material and the second spanning the contact exhibits a 180 degree phase shift between the observed electric fields. The x-y plotter pattern is linear with a tilt angle $\phi = 100^{\circ}$. In this case the absolute value of the slope, $|\tan \phi|$, is an acceptable value to use for the E-field ratio. The complete E-field ratio profiles for this and the previous example are shown in Figure I-C6.

For the incident field perpencidular to the traverse line (Figure

I-C7) the anomaly for the linearly polarized field ($\epsilon = 0$) increases as the contact is approached from the left, the more conductive side. This is a result of the $E_{\parallel}$ component remaining relatively unchanged while $E_{\perp}$ decreases; the effect is to rotate the total E-field vector more nearly parallel to the contact (clockwise, as viewed in Figure I-14) as the contact is approached, producing an ever increasing component in the profile line direction.

The same effect is seen at a polarization direction of 157.5° (Figure I-C8). A reversed anomaly occurs for fields with nearly linear polarization ($\epsilon = 0, \pm 0.25$) as a result of the $E_{\parallel}$ component dominating $E_{\perp}$. The situation is analogous to that depicted in the right half of Figure I-12 for the buried conductive body. The ratio of the $E_{\parallel}$ field amplitudes at very large distances on either side of the contact, however, must reach the same ratio as does the $E_{\perp}$ field ratio.

The "notch" seen in some E-field ratio profiles near x = 0 km in Figures I-C7 and I-C8 is an artifact of locating an electrode precisely on the contact; the potential at that point must be an average of those observed at infinitessimal distances to the right or left. The same effect will be seen, however, for a dipole spanning a contact if the observed field along the dipole comprises out-of-phase elements which tend to cancel.

Figures I-C9 through I-C16 display the characteristics discussed above for an 8 Hz field incident upon the vertical contact. With a skin depth of 568 meters in the 10 ohm-meter material and 1.8 km in the 100 ohm-meter material, the TE field approaches its asymptotic limit relatively quickly so that the reversed anomalies in Figure I-C16

are seen only in the proximity of the contact.

Summary of observations and conclusions.

To summarize the observations of this parametric study:

1) For the incident electric field polarization direction α in the same quadrant as the profile line direction: at frequencies such that the skin depth is large with respect to the body the E-field ratio anomaly will increase as α approaches the normal to strike and/or as ϵ decreases; at high frequencies with respect to the skin depth in the body the anomaly undergoes relatively little change as a function of α and ϵ .

2) As the incident field polarization angle increases beyond the normal to strike outside the quadrant containing the profile line direction, and approaches the normal to the profile line, the anomaly becomes exaggerated for small ϵ , particularly in the case of long period incident fields. In areas where the electric field is changing rapidly, such as in the vicinity of a surface resistivity contrast, large phase differences can occur between the two electric fields observed at a particular station.

3) For the incident field polarized approximately perpendicular to the traverse line direction erratic anomalies can be observed as small deviations in the direction of the total electric field vector can reverse the polarity or greatly alter the amplitude ratio of the observed electric fields. The signal strength is at a minimum for this configuration.

4) For the incident field polarized in the range between the normal to the profile line and strike (-y axis reversed anomalies are found for small ϵ .

5) The observed signal amplitude will increase as the angle between the incident field polarization direction and the profile line direction is reduced.

6) As the traverse line becomes more nearly perpendicular to strike the anomaly becomes less variable as a function of the incident field polarization and ellipticity and approaches the purely TM anomaly.

The validity of using TE mode electric fields for two-dimensional (infinite) structures to calculate E-field ratio telluric anomalies along profile lines not perpendicular to strike could legitimately be questioned in terms of the finite strike length of real geologic structures. The factor to be considered is the size of the body in terms of the skin depth at the frequency of the field being measured. Thus, at 8 Hz the 1 ohm-meter buried conductive body need be only about 1 km long for the E-field ratio response along a traverse line across its center to be equivalent to that shown in the parametric study for the two-dimensional body. At 0.05 Hz the body would have to be about 8 km long. For the infinite vertical contact the 8 Hz response shown in the parametric study would be valid for a strike length of about 10 km, quite a reasonable length for structures such as the range-front faults in Basin and Range topography. However, at 0.05 Hz a skin depth of 23 km in the 100 ohm-meter material clearly precludes the observation of anomalies of precisely the form presented.

What is more to the point, however, is that the two-dimensional parametric study is a worst case analysis. The E-field ratio anomalies presented become distorted as a function of profile line direction and incident field polarization direction and ellipticity owing to the fact that the transverse electric field does not respond abruptly to

resistivity contrasts. The telluric anomalies will only be enhanced by the finite strike length of a body as a result of the electric field component parallel to strike behaving in a fashion similar to the TM mode electric field at the strike-length ends of the structure. This statement is borne out in a paper by Weidelt (1975) in which he shows successive curves for the $E_{//}$ component across a conductive body as the strike length of the body is increased from three skin depths to infinity. As for the reversed anomaly case presented in Figure I-12, and the large phase changes depicted in Figures I-13 and I-14, it is evident from a careful study of these figures that if the $E_{//}$ component were to behave in more nearly the same way as the $E_{\perp}$ component, as is the case for three-dimensional features, these exceptional traits would be reduced or eliminated.

On the basis of the parametric study it can be concluded that:

1) If survey lines are run perpendicular to the strike of linear geologic features repeatable anomalies will be obtained.

2) If the geologic strike of an area is undetermined, a traverse line direction which will avoid the possibility of reversed anomalies is parallel to the principal axis of the incident electric field ellipse. This direction will not necessarily produce the highest amplitude anomalies, however.

3) Traverse lines should not be run in a direction between strike and the normal to the incident field polarization direction lest reversed or erratic anomalies might be observed as the incident field ellipticity changes.

4) Traverse lines run at an angle between the normal to strike and the normal to the incident field polarization direction may, over near

surface resistivity contrasts, yield a high phase difference between the observed electric fields. However, this is not detrimental to gathering correctly interpretable data.

5) At higher frequencies the effects of points 3 and 4 are reduced.

6) If the strike length of geologic features is small (with respect to the skin depth) the effects of points 3 and 4 will be reduced or eliminated.

7) If an anomaly of interest is obtained over a feature of unknown strike direction, as would naturally be the case, a second line parallel to the first should be run to obtain a corresponding anomaly. In this way the strike direction can be found and, if necessary, a third line run perpencidular to it if the anomaly has been reversed due to an unfortunate initial choice of profile direction.

FIELD PROCEDURES AND REPEATABILITY OF DATA

It is impossible to determine precisely the polarization direction and ellipticity of the incident electric field based upon observations made at the surface of the earth. However, to determine an average principal axis direction of the electric field ellipse for the purpose of assessing optimum profile line directions for E-field ratio telluric surveys, the horizontal components of the total field can be recorded at several locations in the survey area which are free from lateral resistivity contrasts. To observe easily the field at these locations, an orthogonal array of two dipoles can be laid out and the signals used as inputs to the x and y channels of the x-y plotter.

Such recordings were periodically made at various locations by the Lawrence Berkeley Laboratory geothermal field crew operating in north-central Nevada. In Grass Valley the 0.05 Hz electric field away from surficial features was always observed to be polarized in a NW-SE direction with an ellipticity of 0.2 to 0.5. The direction of rotation would vary. For a particular location, constancy of the principal axis direction with varying ellipticity has also been noted by Schlumberger (1939), and Wescott and Hessler (1962), among others.

When the x and y components of the 8 Hz field were observed, the polarization direction and ellipticity were found to vary almost randomly. As has been discussed above, for the proper interpretation of E-field ratio telluric data it is less important that higher frequency signals be consistently polarized than it is for longer periods. This was empirically demonstrated by the field data obtained. While the 8 Hz E-field ratio data at a particular station often showed greater

variation in the ratio as a function of time than did the 0.05 Hz data, this variation was only rarely greater than 10 percent.

As the E-field ratio telluric method relies on successive measurements to obtain a running ratio of the electric field intensity, it is naturally susceptible to systematic or cummulative errors which might cause a false "regional gradient" along the length of a survey line. It is for this reason that calibration checks were run at every station to insure that both channels of the filter-amplifier system were equally balanced; small corrections were applied to the data if this was not the case. Figure I-15 displays a 0.05 Hz E-field ratio telluric profile which was run in several segments across Grass Valley, Nevada, starting in July 1974, and then was repeated in June 1975. The line spans 19 km at a station interval of 500 meters in most instances. The data gathered in July 1974, however, employed a 250-meter receiver dipole length and yield an interesting comparison with the 500-meter dipole data collected nearly one year later. The agreement between the two data profiles is excellent, and quite frankly, exceeded the expectations of the author. A long line of 8 Hz data was, unfortunately, never repeated in the field.

As was demonstrated by the parametric study, E-field ratio telluric anomalies can vary as a function of the incident field polarization direction and ellipticity. The fact that the repeated survey data presented in Figure 15 is in such good correspondence demonstrates a reasonably consistent incident 0.05 Hz field, at least in this survey area. E-field ratio data obtained in three geothermal survey areas in north central Nevada has shown very good correlation with other geophysical data and with known geologic features.

The Lawrence Berkeley Laboratory Geothermal field crews obtained

over 260 line-kilometers of E-field ratio telluric data in north central Nevada, generally at a station spacing of 500 meters, and occasionally at 250 meters. The profile lines were surveyed in advance to be used for various geophysical investigations.

The wire that was used for telluric surveys was approximately 20 gauge, containing a few steel strands in addition to several copper strands, making the wire exceptionally strong. It was found that a 500 meter length of wire could successfully be tied to the bumper of a jeep and dragged without stretching, along a straight line so that reeling and unreeling of wire was generally unnecessary. Abrasion of the insulation was not severe because the dragged wire would often be suspended by sage brush or would slide easily over soft playa deposits. This enabled the field crew to limit each data gathering team to two men and two four-wheel drive vehicles.

One man would operate the telluric equipment to obtain the data while the second man would move wire and electrodes to the next location. There were three lengths of wire on the ground, two which were in use gathering data, and the third which had been used for the previous station and was being dragged along the line into position for the next station. On the average, about eight stations per day were obtained along previously surveyed lines.

Without steel stranded wire or in terrain where insulation abrasion would be severe from dragging, the unused length of wire from a previous station must be reeled up and then laid out for the next station. Two men with a vehicle will generally have a hard time keeping up with the man recording the data.

Upon several occasions E-field ratio telluric data was obtained in

rugged terrain by men on foot. The telluric receiver, x-y plotter, and electrodes total about 8 kg in weight, and can easily be carried in a backpack. Additional equipment includes a small supply of copper sulfate and a jug of water for the electrodes, and a reel of wire. In some cases a length of 250 meters of wire could be dragged by a crewman from one location to the next along the survey line.

CONCLUSIONS AND RECOMMENDATIONS

1) The E-field ratio telluric method is a rapid electrical reconnaissance technique suited to the exploration of areas of several hundred square kilometers in terrain where in-line station locations can be established.

2) The method is well suited to exploration for massive conductive features such as might be associated with geothermal activity.

3) The use of two frequencies, which might have to be tailored for the formation or target resistivities in the survey area, yields a rudimentary depth discrimination. More frequencies could, of course, be used, but at some point the method would cease to be a rapid reconnaissance technique.

4) Only qualitative interpretation of the data is suggested, or even possible, as a result of the lack of complete measurement of the total field at the surface of the earth, with only one component of the electric field being recorded, and the magnetic field not being monitored at all.

5) The addition of two or three magnetotelluric stations along an E-field ratio telluric line affords a means of correlating the telluric data at different frequencies, allows some degree of interpretation in terms of apparent resistivity rather than electric field intensity, and offers a means of correcting for cumulative error along the telluric line.

REFERENCES

Berdichevskiy, M.N., 1960, Electrical surveying by means of telluric currents: Gostoptekhizdat, Moskow. English translation by: Bradley, J.E.S., 1963, National Lending Library, Boston Spa, England; also by: Keller, G.V., 1965, Quarterly of the Colorado School of Mines, v. 60, no. 1.

Beyer, H., 1977a, Telluric and d.c. resistivity techniques applied to the geophysical investigation of Basin and Range geothermal systems, Part II: A numerical model study of the dipole-dipole and Schlumberger resistivity methods, LBL-6325-2/3: Lawrence Berkeley Laboratory, University of California, Berkeley.

Beyer, H., 1977b, Telluric and d.c. resistivity techniques applied to the geophysical investigation of Basin and Range geothermal systems, Part III: The analysis of data from Grass Valley, Nevada, LBL-6325-3/3: Lawrence Berkeley Laboratory, University of California, Berkeley.

Beyer, H., Dey, A., Liaw, A., McEvilly, T.V., Morrison, H.F., and Wollenberg, H., 1976, Preliminary open file report: Geological and geophysical studies in Grass Valley, Nevada, LBL-5262: Lawrence Berkeley Laboratory, University of California, Berkeley.

Beyer, H., Morrison, H.F., and Dey, A., 1976, Electrical exploration of geothermal systems in Basin and Range valleys of Nevada: Proceedings: Second United Nations Symposium on the Development and Use of Geothermal Resources, May 1975, p. 889-894.

Beyer, H., Morrison, H.F., and Dey, A., 1975, Electrical exploration of geothermal systems in north central Nevada (Abstract): Geophysics, v. 40, no. 1, p. 174.

Bleil, D.F., ed., 1964, Natural electromagnetic phenomena below 30 Kc/s: Plenum Press, New York.

Boissonas, E., and Leonardon, E.G., 1948, Geophysical exploration by telluric currents with special reference to a survey of the Haynesville salt dome, Wood County, Texas: Geophysics, v. 13, no. 3, p. 387-403.

Cagniard, L., 1953, Basic theory of the magnetotelluric method of geophysical prospecting: Geophysics, v. 18, no. 3, p. 605-635.

Dahlberg, R.S., Jr., 1945, An investigation of natural earth currents: Geophysics, v. 10, no. 4, p. 494-506.

Leonardon, E.G., 1928, Some observations upon telluric currents and their applications to electrical prospecting: Terr. Mag., v. 33, p. 91-94.

Neuenschwander, E.F., and Metcalf, D.F., 1942, A study of electrical earth noise: Geophysics, v. 7, no. 1, p. 69-77.

Price, A.T., 1962, The theory of magnetotelluric methods when the source field is considered: J. Geophys. Res., v. 67, no. 5, p. 1907-1918.

Ryu, J., 1971, Low frequency electromagnetic sounding, unpublished Ph. D. thesis: University of California, Berkeley.

Schlumberger, M., 1939, The application of telluric currents to surface prospecting: A.G.U. Trans., Part III, p. 271-277.

Slankis, J.A., 1970, Telluric and magnetotelluric surveys at 8 Hz: unpublished Ph.D.thesis, Dept. of Mining Engineering and Applied Geophysics, McGill University, Montreal.

Slankis, J.A., Telford, W.M., and Becker, A., 1972, 8 Hz telluric and magnetotelluric prospecting: Geophysics, v. 37, no. 5, p. 862-878.

Srivastava, S.P., 1965, Method of interpretation of magnetotelluric data when source field is considered: J. Geophys. Res., v. 70, p. 945-954.

Tuman, V.S., 1951, Telluric method of prospecting and its limitations under certain geologic conditions: Geophysics, v. 16, p. 102-114.

Vozoff, K., Ellis, R.M., and Burke, M.D., 1964, Telluric currents and their use in petroleum exploration: Bull. AAPG, v. 48, p. 1890-1901.

Wait, J.R., 1954, On the relation between telluric currents and the earth's magnetic field: Geophysics, v. 19, no. 2, p. 281-289.

Ward, S.H., 1967, Electromagnetic theory for geophysical applications in Mining Geophysics, v. II: Society of Exploration Geophysicists, Tulsa, Oklahoma, p. 10-196.

Weidelt, P., 1974, Electromagnetic induction in three-dimensional structures: J. Geophys., v. 41, p. 85-109.

Wescott, E.M., and Hessler, V.P., 1962, The effect of topography and geology on telluric currents: J. Geophys. Res., v. 67, p. 4813-4823.

Yungul, S.H., 1966, Telluric sounding--a magnetotelluric method without magnetic measurements: Geophysics, v. 31, no. 1, p. 185-191.

Yungul, H., 1965, Telluric current method of determining ellipse area by simultaneously measuring two voltages with a collinear three electrode array: U.S. Patent Office, no. 3,188,559.

Yungul, S.H., Hembree, M.R., and Greenhouse, J.P., 1973, Telluric anomalies associated with isolated reefs in the Midland Basin, Texas: Geophysics, v. 38, no. 3, p. 545-556.

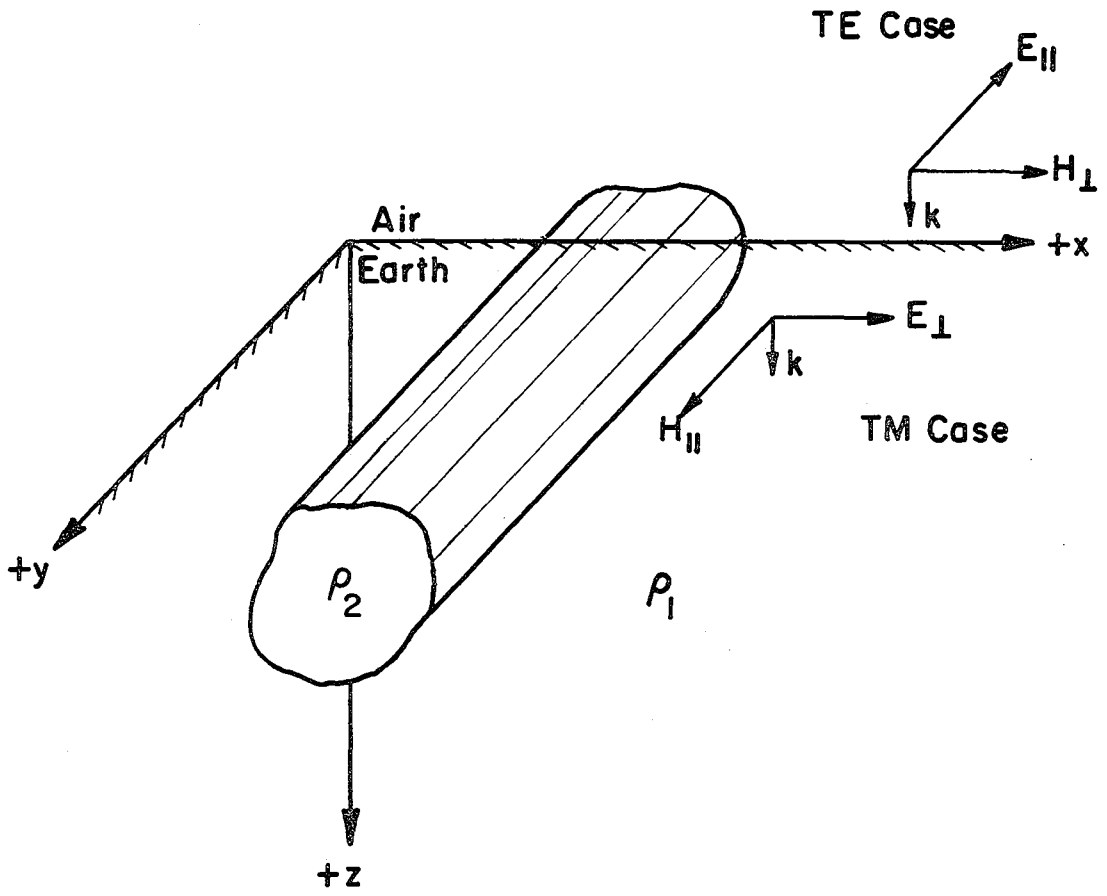

XBL 776-9366

Figure I-1. Coordinate system containing a two-dimensional resistivity inhomogeneity, and showing transverse electric and transverse magnetic field directions.

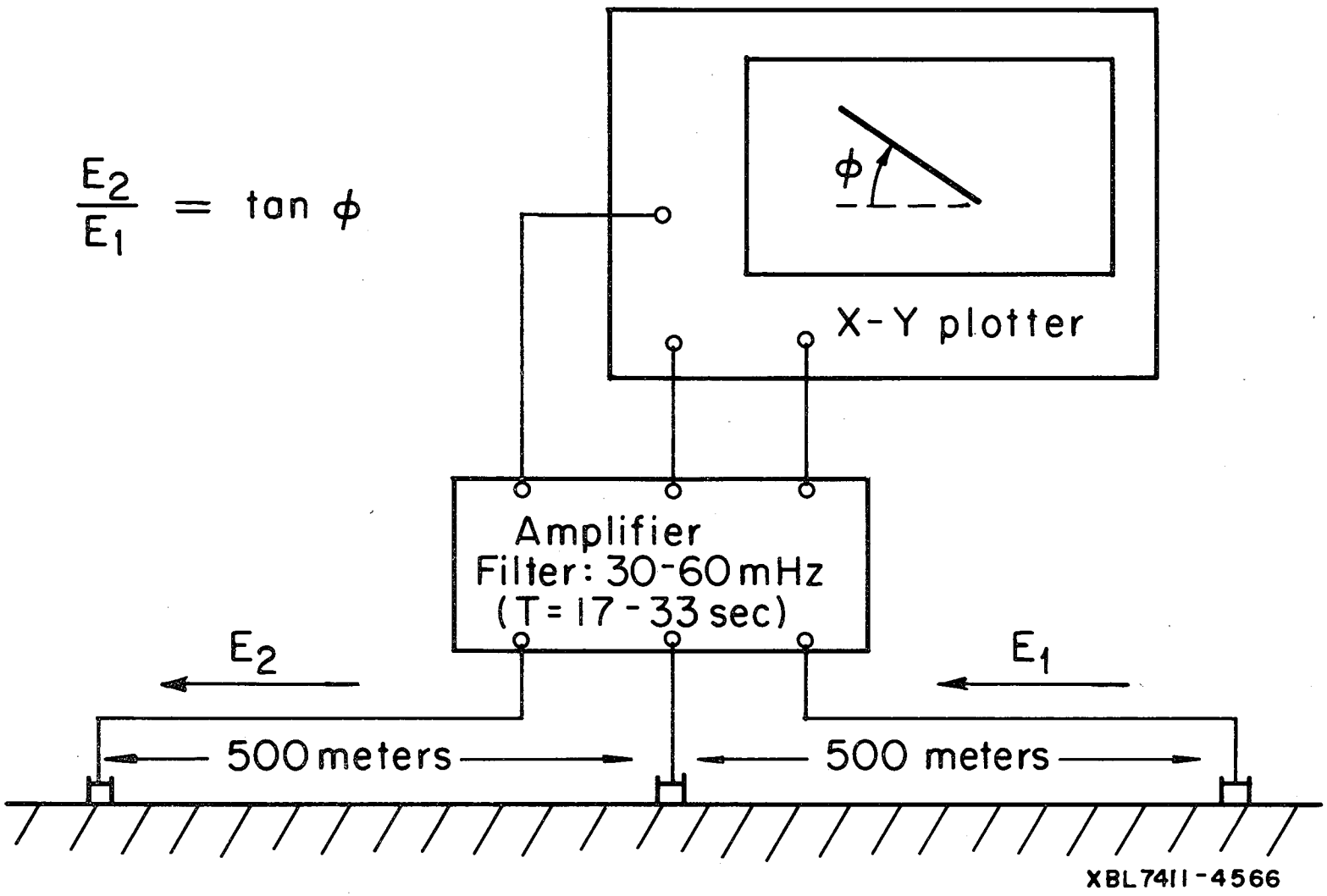

Figure I-2. Diagrammatic representation of the E-field ratio telluric system.

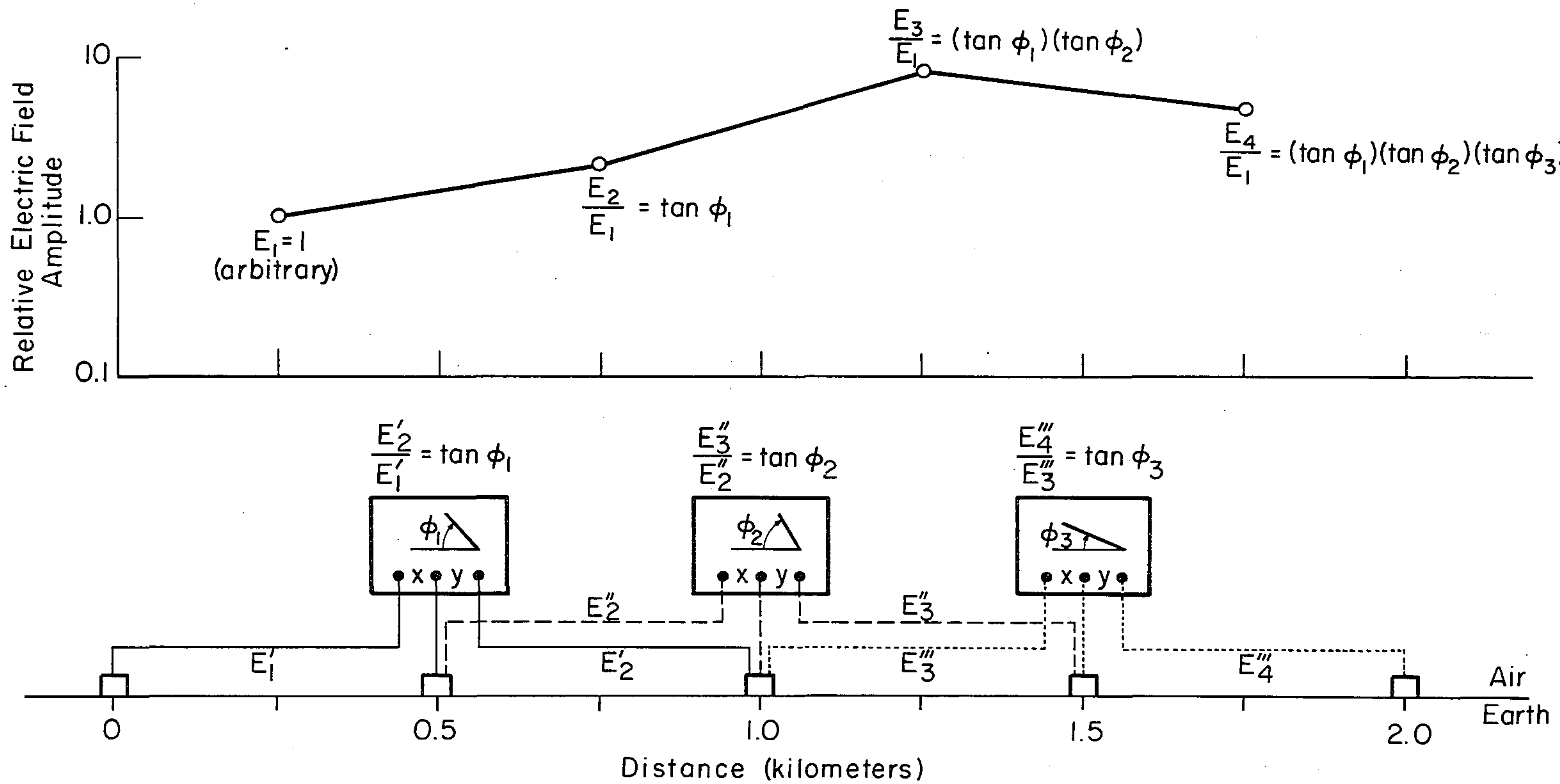

XBL 773-5229

Figure 1-3. Three successive E-field ratio telluric receiver stations and data plotting method.

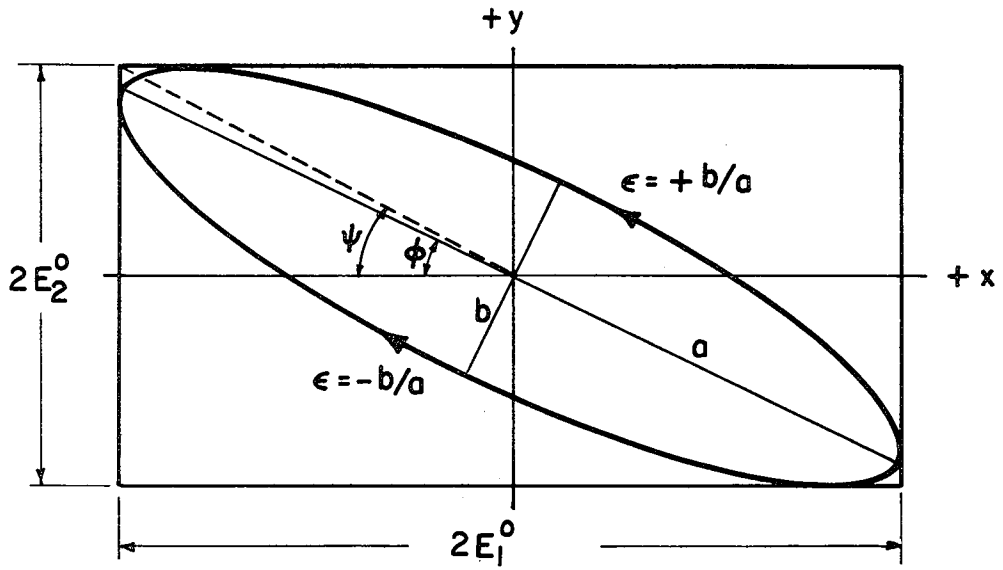

XBL 776-9365

Figure I-4. Electric field ratio ellipse as displayed on x-y plotter. E_1^o and E_2^o are the maximum amplitudes observed along the two respective in-line receiver dipoles. ϕ is the tilt angle of the ellipse, and ψ is the arc tangent of E_2^o/E_1^o.

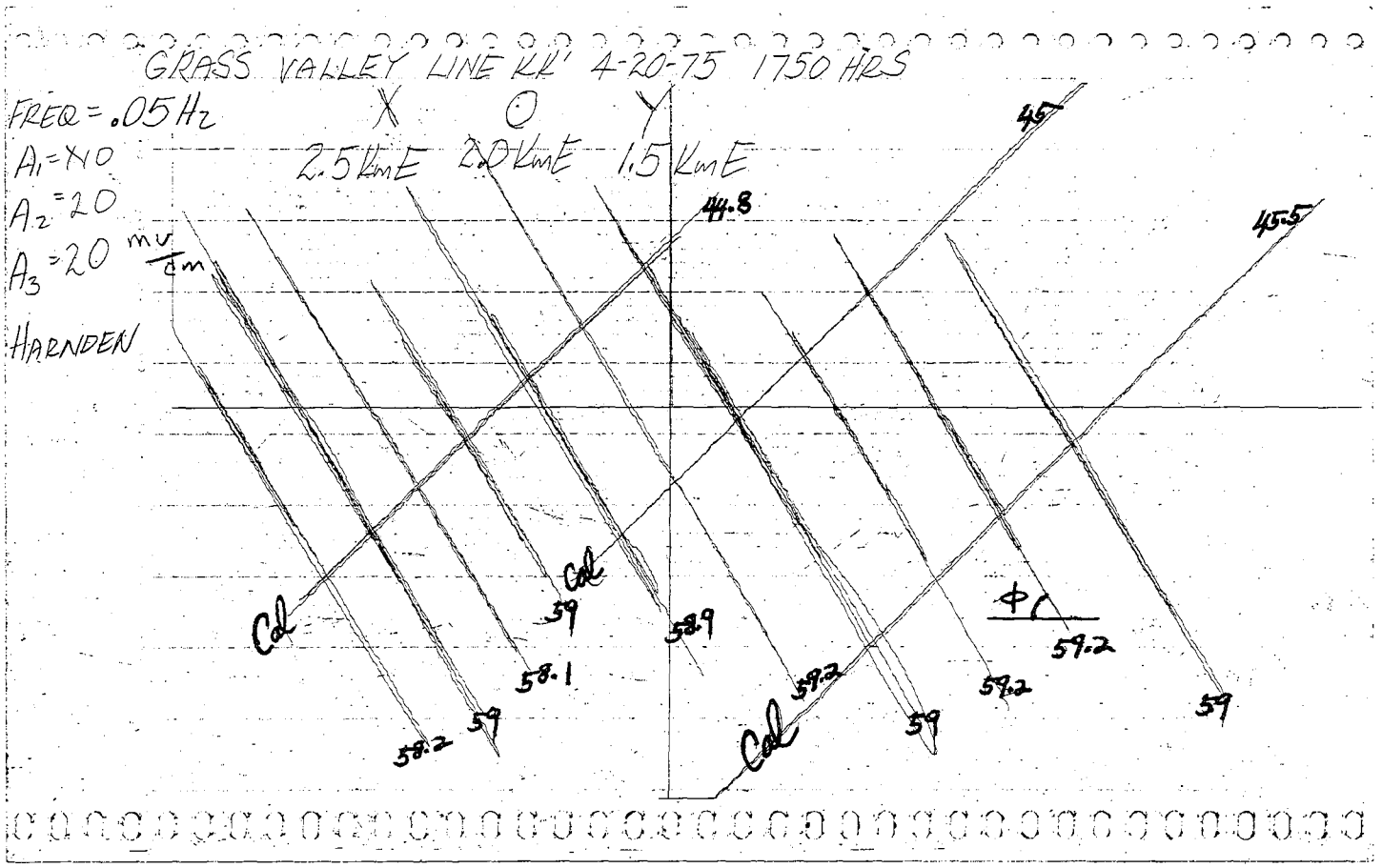

Figure 1-5. Typical 0.05 Hz E-field ratio telluric record drawn by x-y plotter (actual size) for one station location, showing several traces with tilt angles of $\phi \approx 59^{\circ}$. Traces marked "Cal", obtained for the identical signal being used as both x and y channel inputs, demonstrate that the two filter-amplifier channels are nearly perfectly balanced. The amplifier gain is 200, and the plotter gain is 20 mv/cm; both receiving dipoles are 500 meters long.

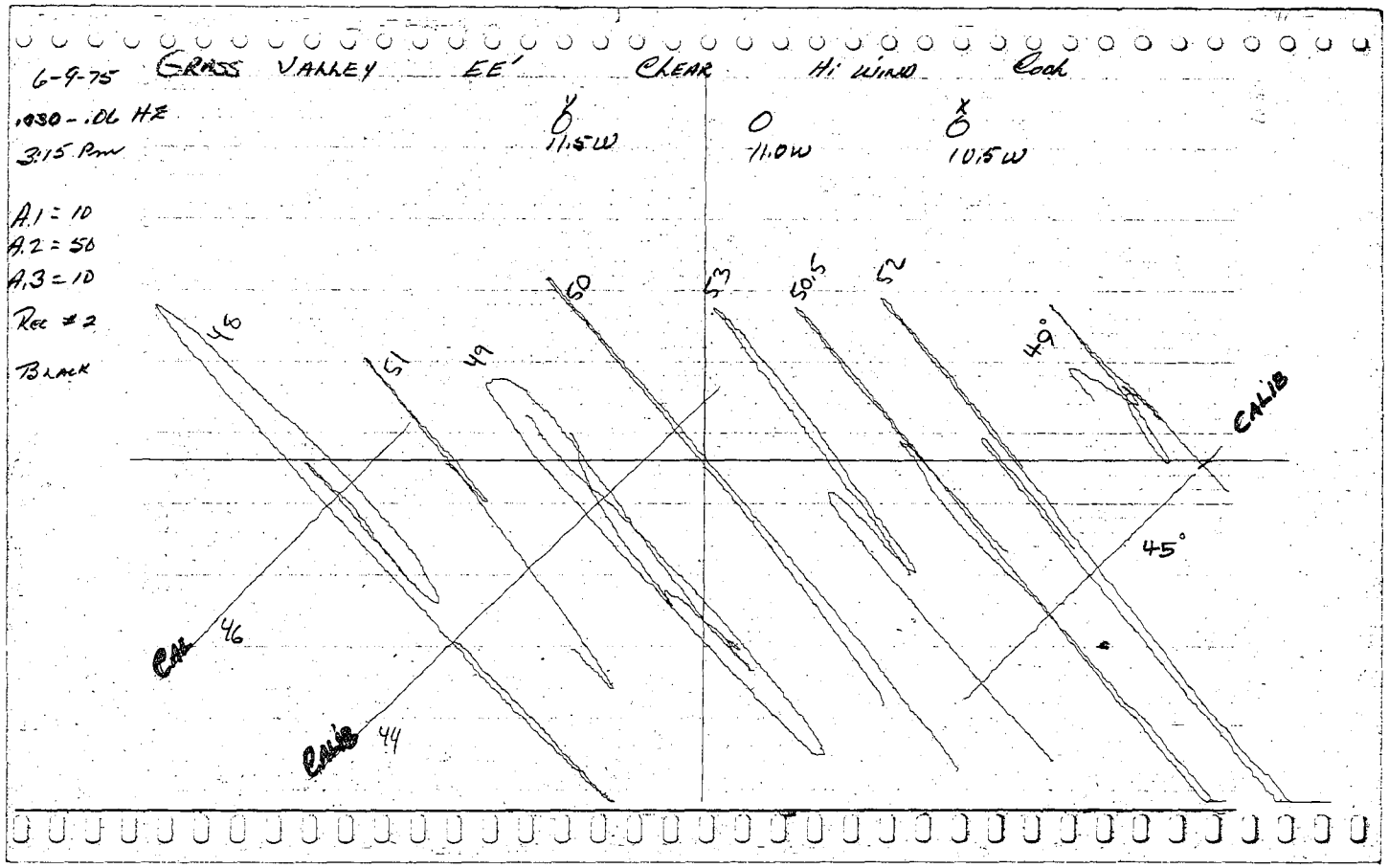

Figure 1-6. A worse than average 0.05 Hz E-field ratio telluric record showing traces with tilt angles ranging from 48° to 53°. Calibration lines demonstrate that both channels are perfectly balanced. Amplifier gain is 500, plotter gain is 10 mv/cm, and receiver dipoles are 500 meters long.

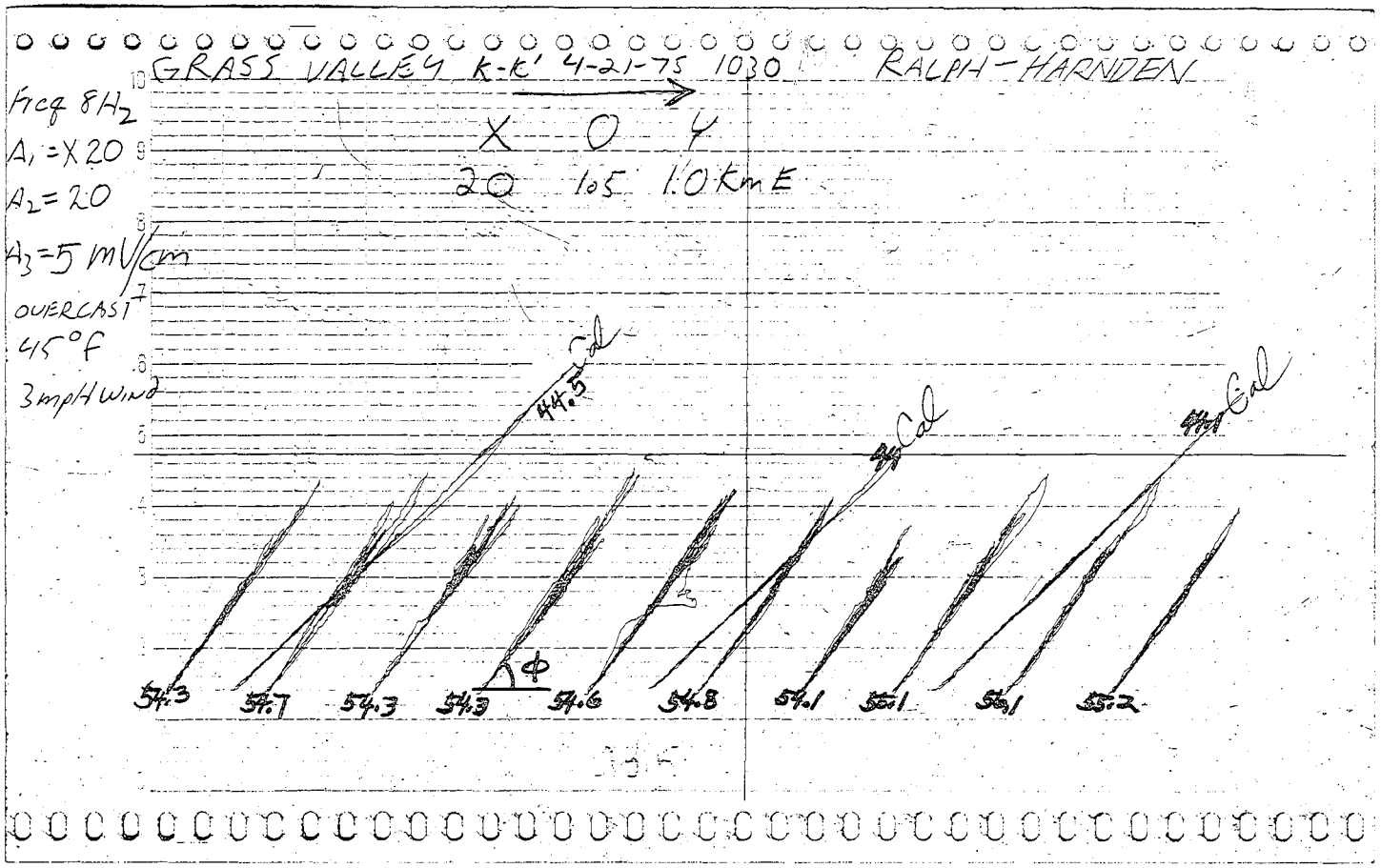

Figure I-7. A better than average 8 Hz E-field ratio telluric record for one station location showing several traces with an average tilt angle Φ of about 55°. Amplifier gain is 500, plotter gain is 5 mv/cm, and receiver dipole length is 500 meters.

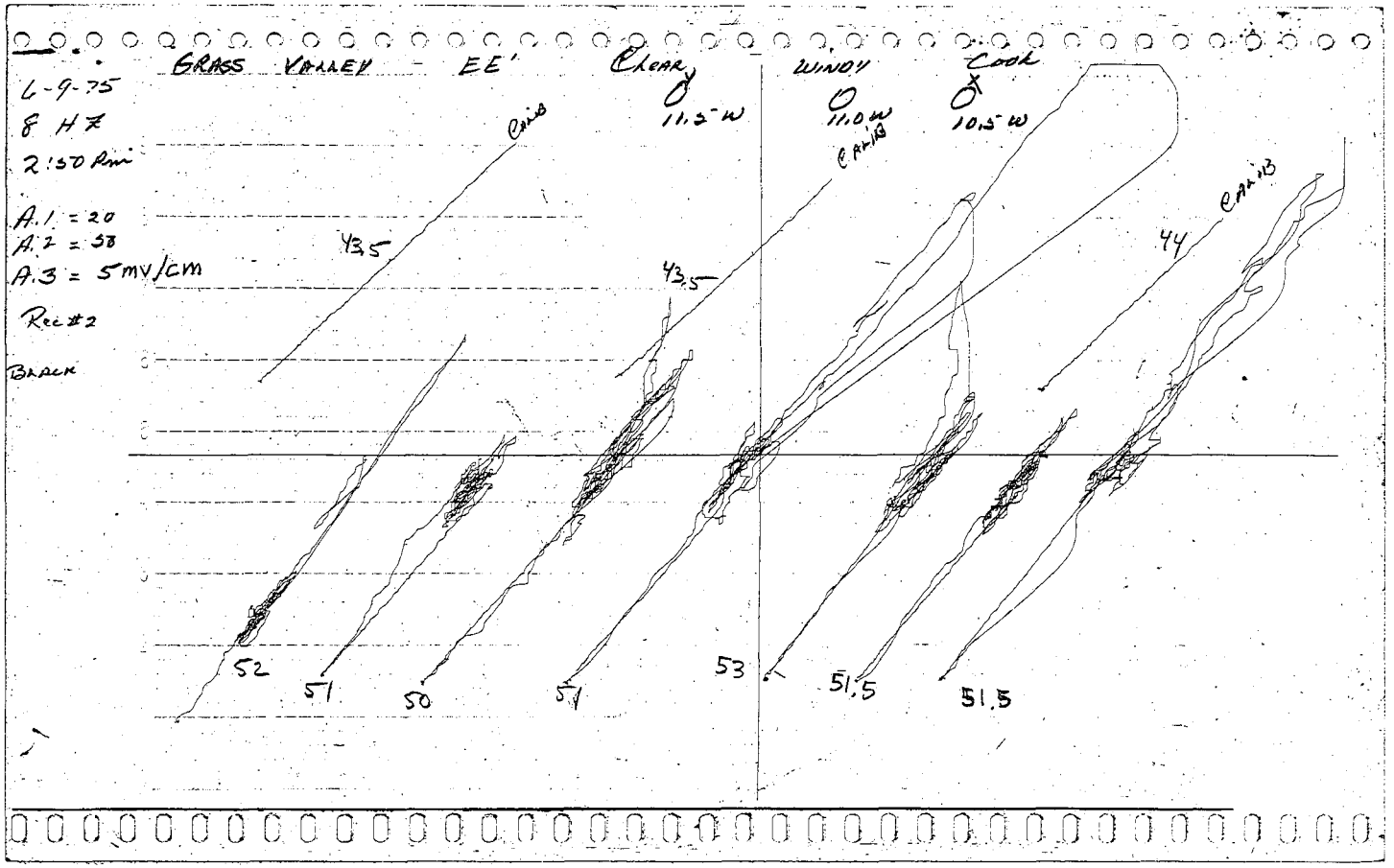

Figure I-8. A typical 8 Hz E-field ratio telluric record for one location showing several traces with tilt angles ranging from 50° to 53°. Calibration lines show a slight amplifier imbalance between the two channels. Amplifier gain is 1000, plotter gain is 5 mv/cm, and receiver dipole length is 500 meters.

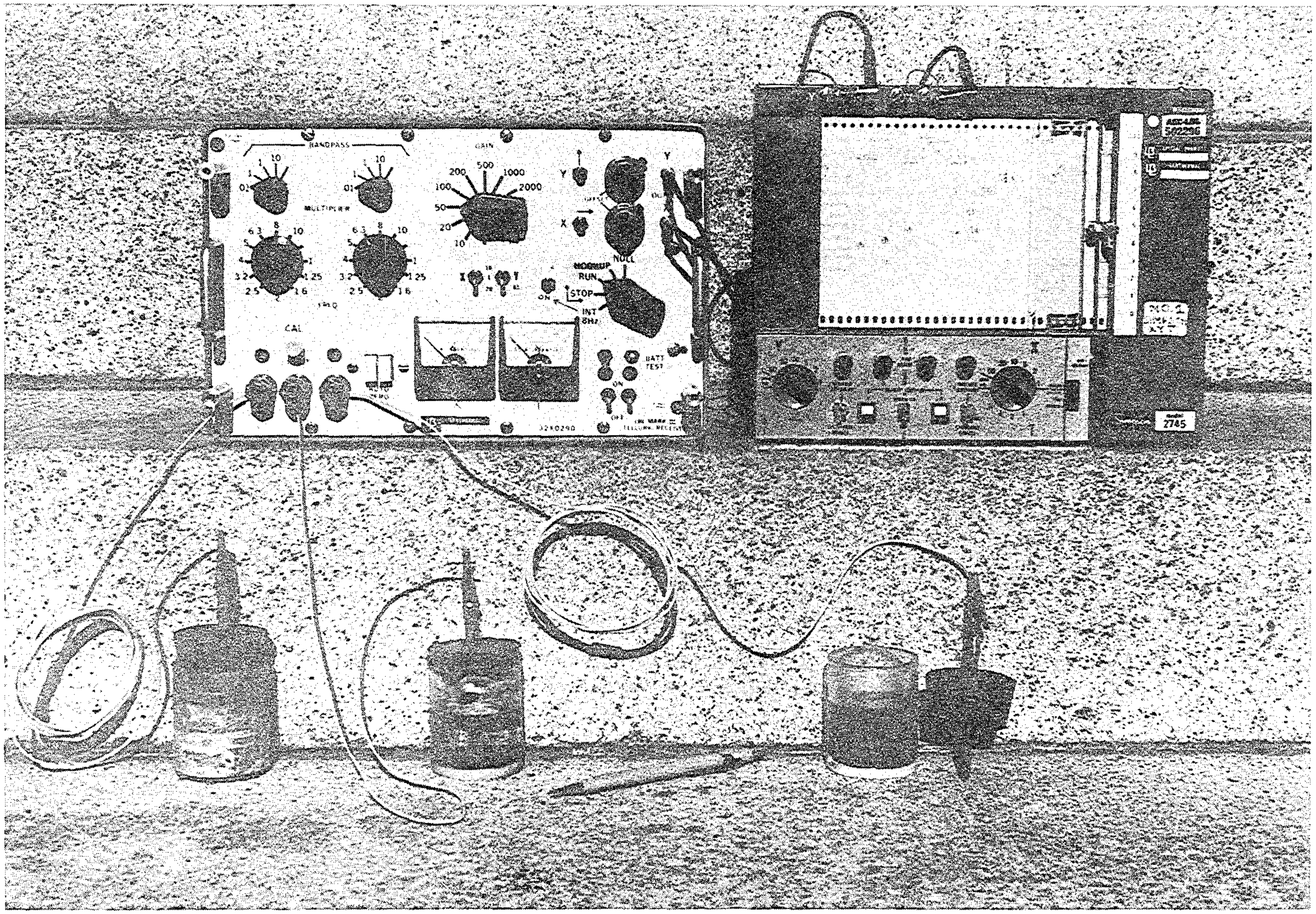

XBB 774-3840

Figure I-9. E-field ratio telluric field equipment: LBL Mark III A Telluric Receiver Simpson Model 2745 x-y, y-t Recorder, and three copper-copper sulfate porous pot electrodes.

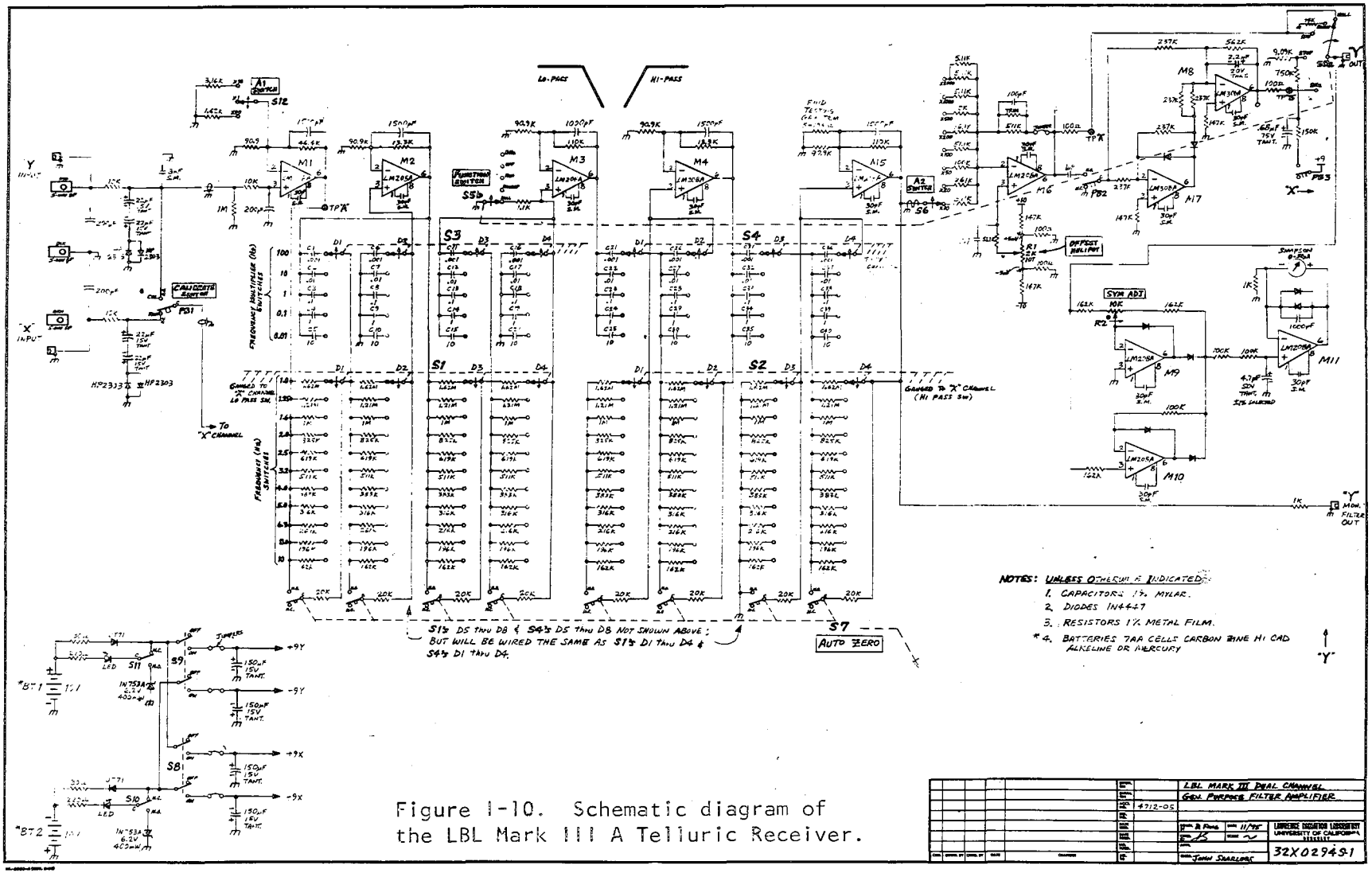

Figure 1-10. Schematic diagram of the LBL Mark III A Telluric Receiver.

XBL 773-8146

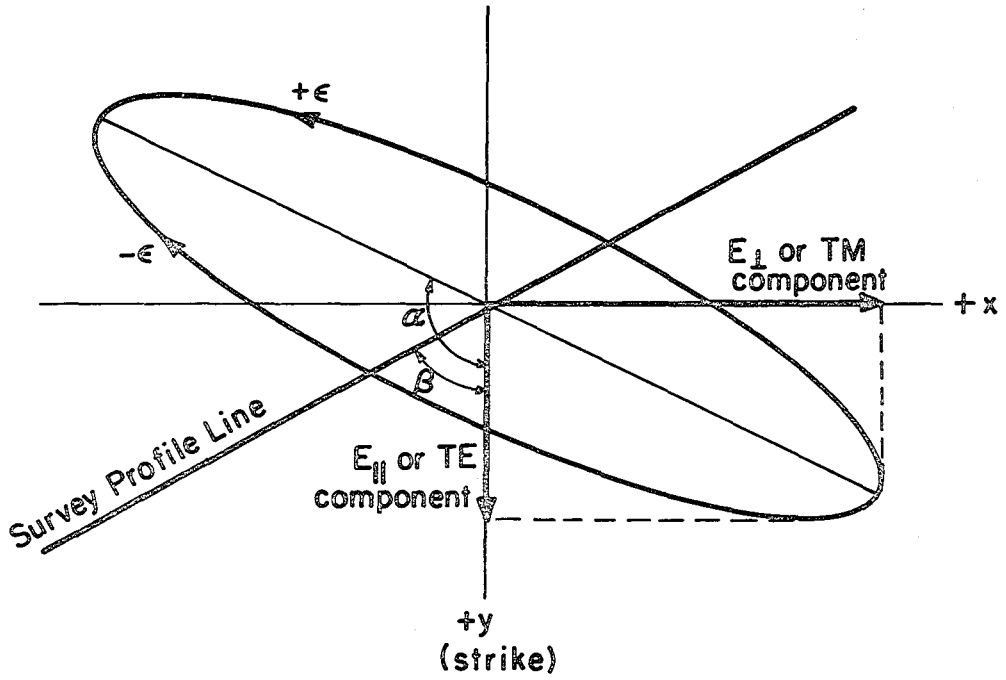

XBL 776-9364

Figure I-11. Incident electric field ellipse as viewed looking down on the surface of the earth (x-y plane). The polarization direction is α, measured with respect to strike.

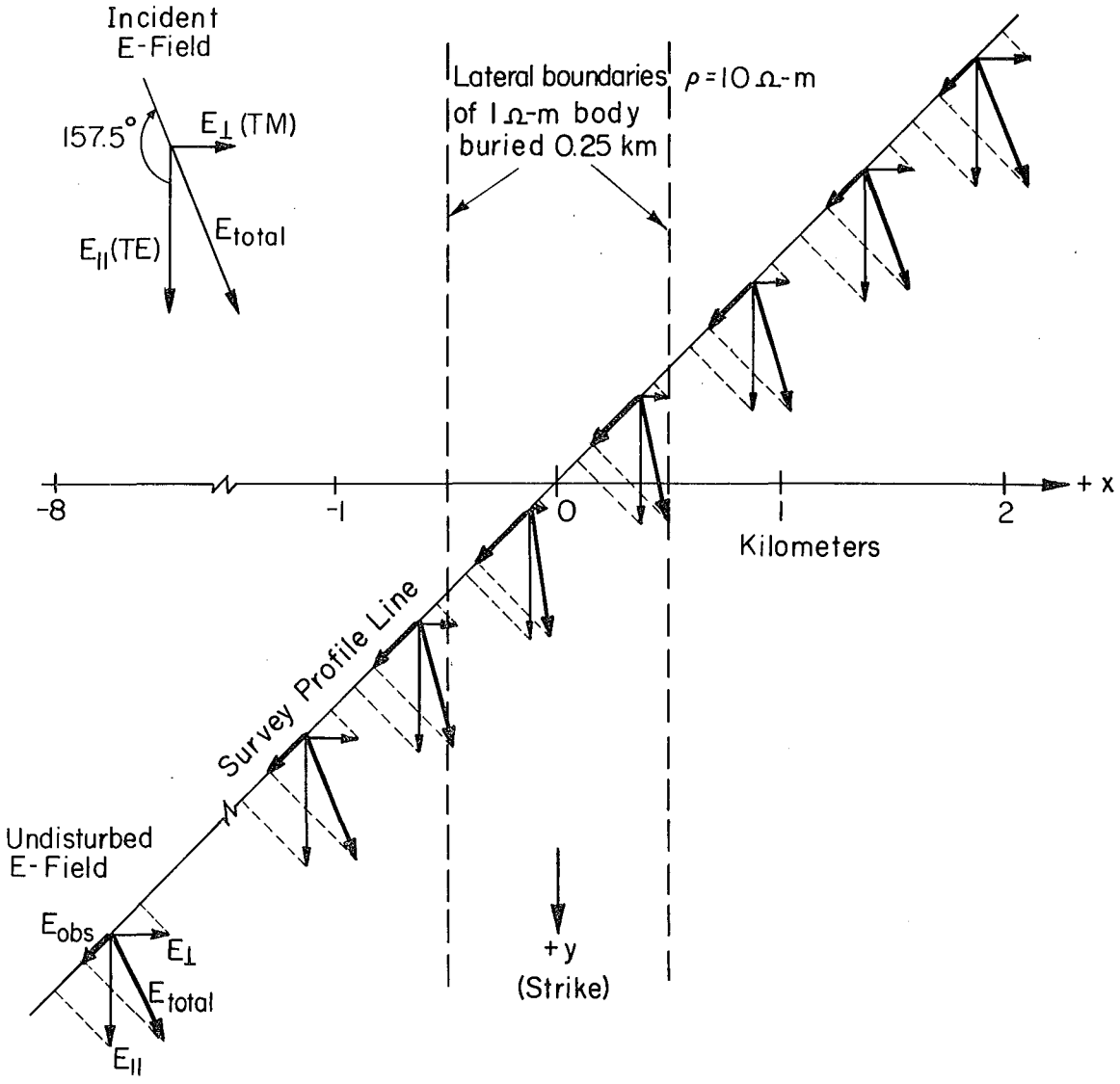

Figure I-12. Diagrammatic explanation of a reversed E-field ratio telluric anomaly over a buried two-dimensional conductive body for profile line at 45° to strike and a linearly polarized incident electric field at 157.5°.

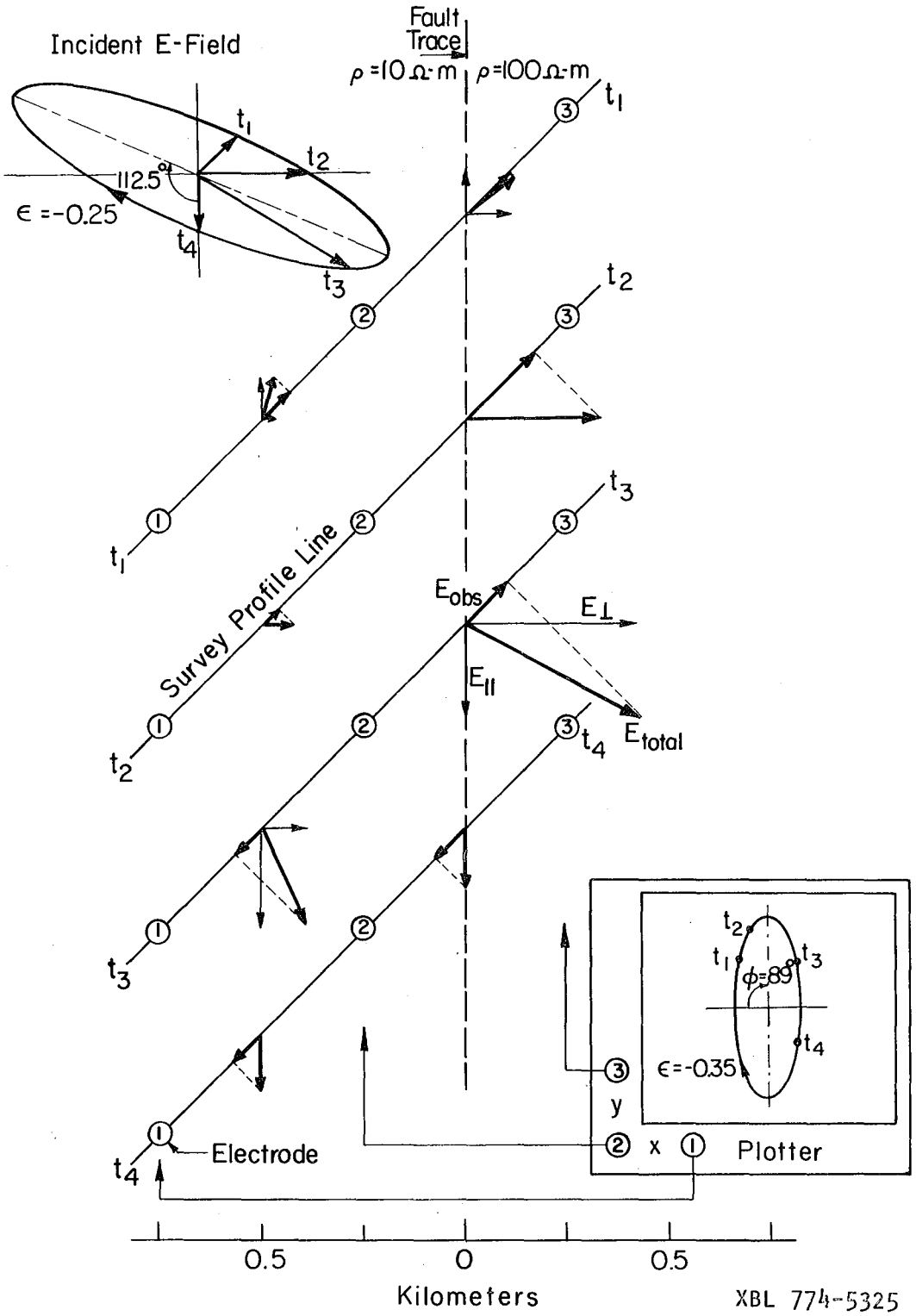

Figure I-13. Diagrammatic explanation, for an E-field ratio profile at 45° to a vertical contact, of the observed electric fields being out of phase. Shown at four successive times, t_1 through t_4, are the incident electric field vector, and the $E_{\perp}$, $E_{\parallel}$, E_{total}, and $E_{observed}$ vectors at the center of two receiver dipoles, and corresponding locations on the x-y plotter ellipse. In this particular case the plotter ellipse has a nearly vertical tilt angle and a large ellipticity.

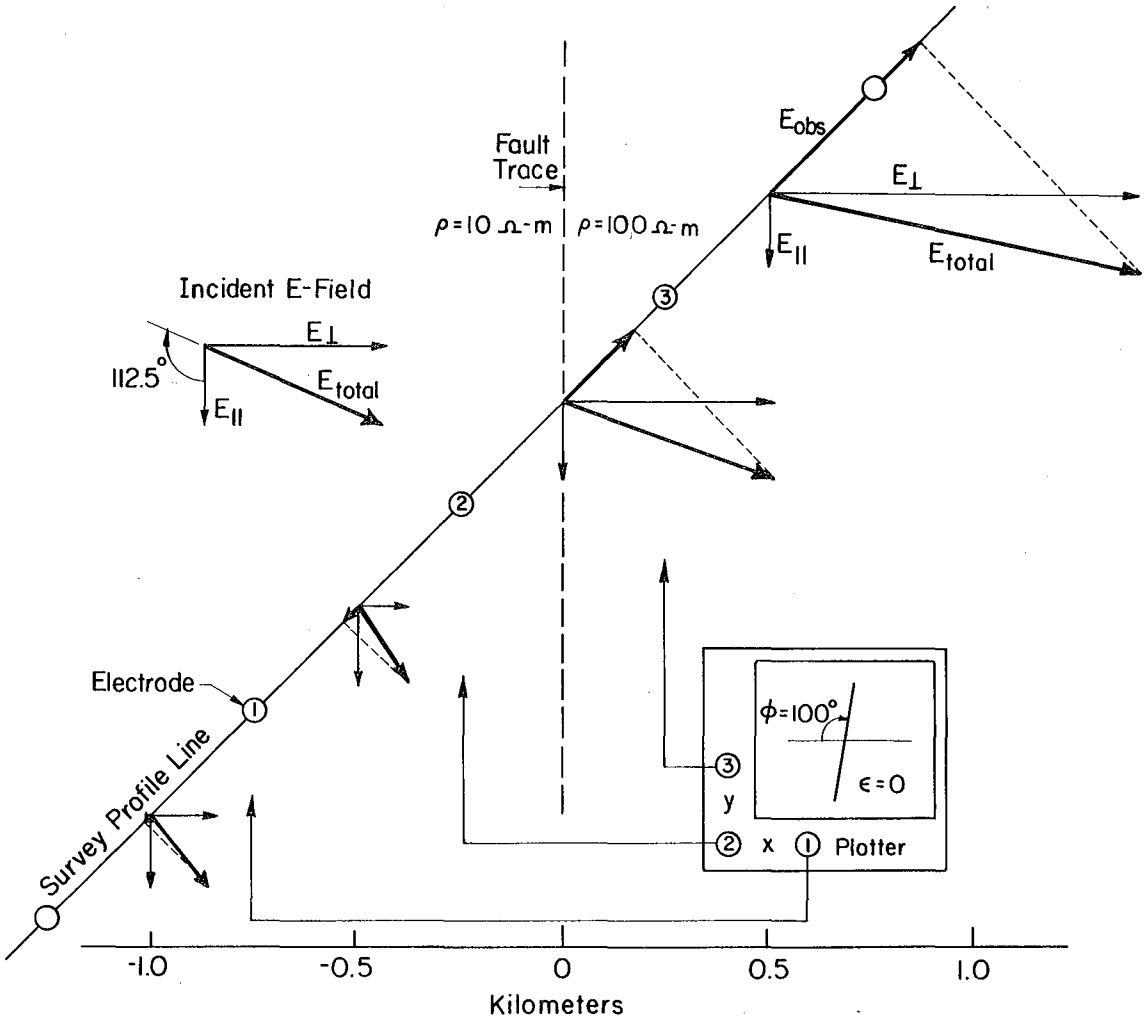

XBL 774-5324

Figure I-14. Diagrammatic explanation of a 180° phase shift in the observed electric fields across a vertical contact resulting in a linear x-y plotter ellipse with a tilt angle greater than 90°. Only for the station location with one dipole on the more conductive side of the contact and the second dipole straddling the contact is this phase reversal observed.

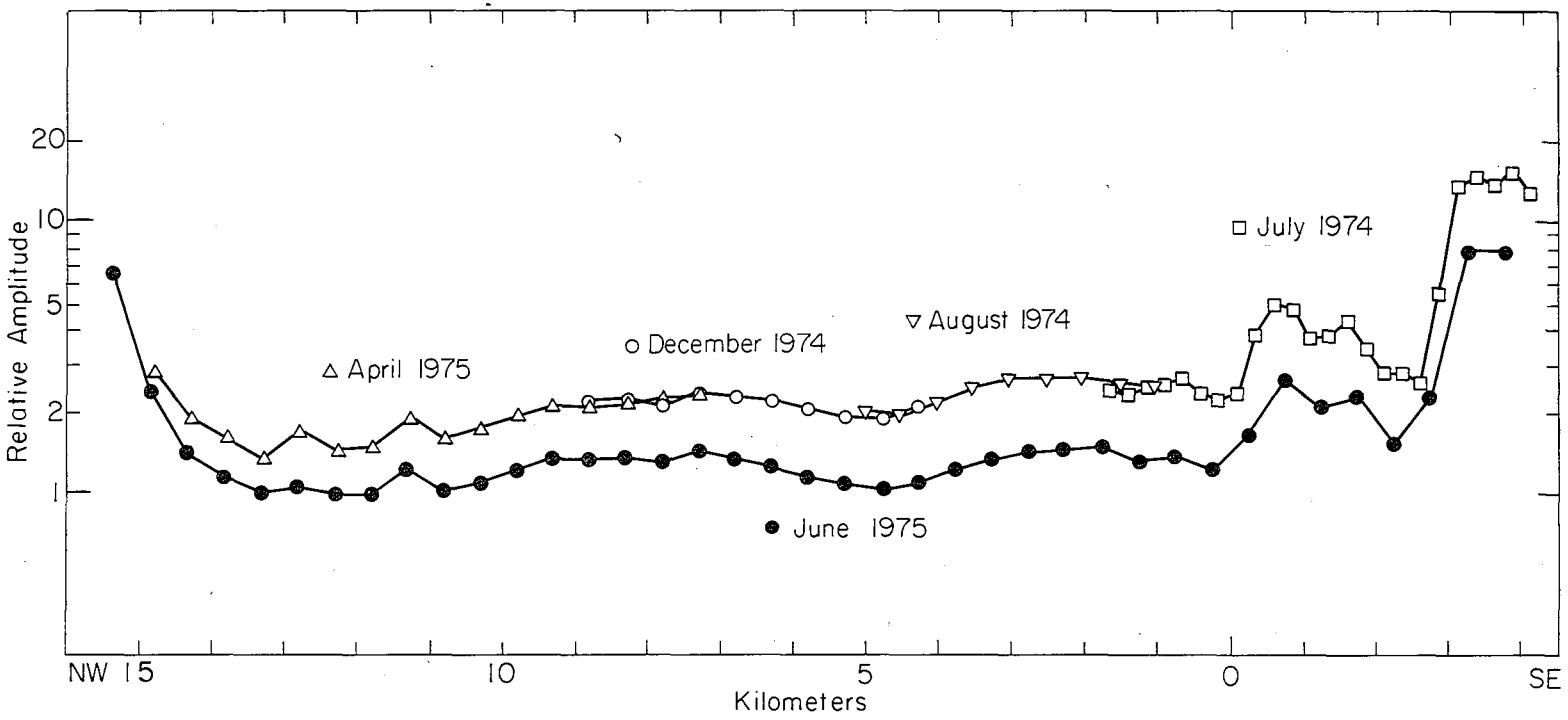

XBL774-5327

Figure I-15. A 19 km long 0.05 Hz E-field ratio telluric profile across Grass Valley, Nevada, conducted in several segments, and then repeated several months later. The July 1974 data were obtained at 250-meter station spacing, while all other data was obtained using 500-meter long dipoles. The survey line extends in a NW-SE direction parallel to the principal axis of the total electric field, and at about 45° to the geologic strike.

(for numbering sequence only)

APPENDIX I-A

E-Field Ratio Telluric Anomalies Perpendicular to the Strike of Two-Dimensional Structures

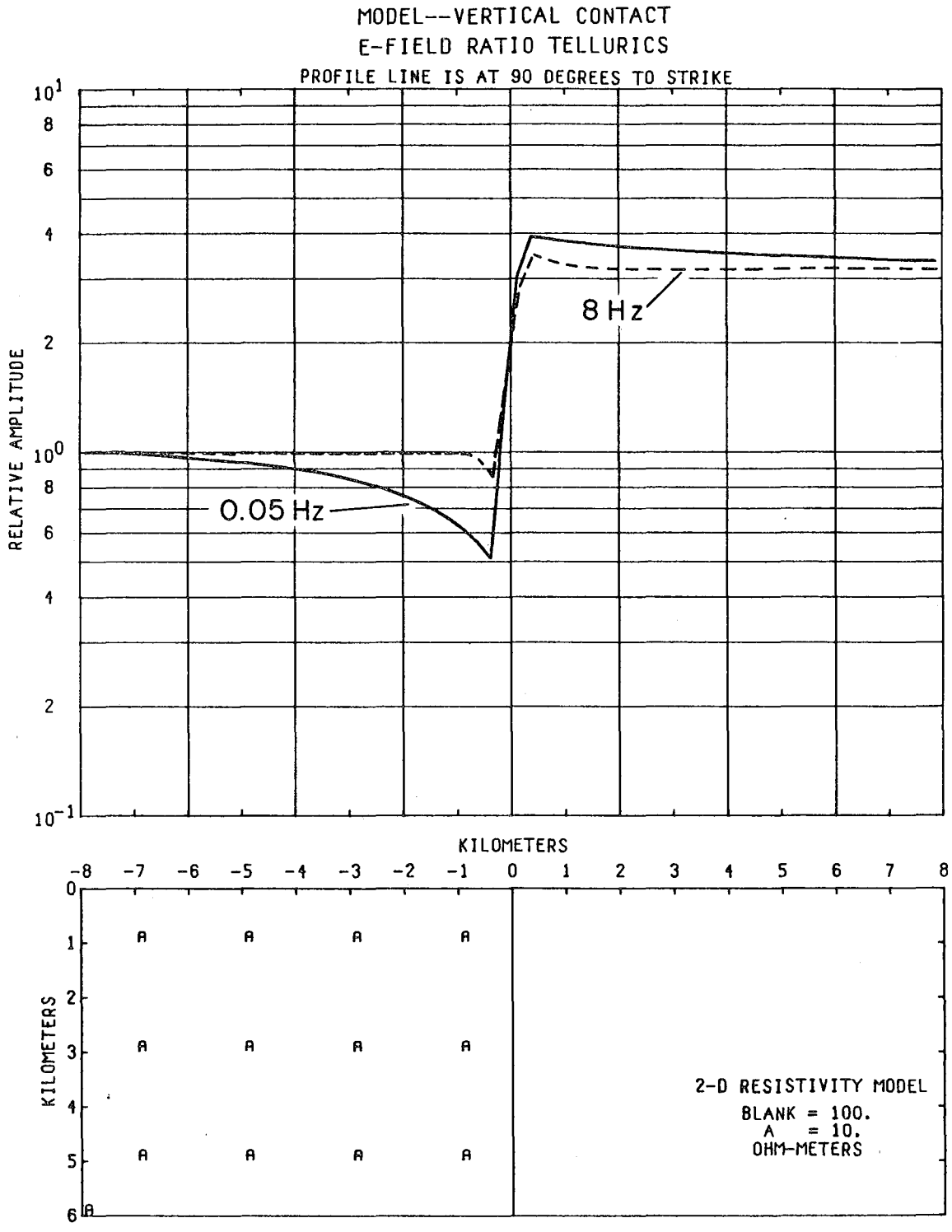
MODEL--VERTICAL CONTACT
E-FIELD RATIO TELLURICS
PROFILE LINE IS AT 90 DEGREES TO STRIKE
RELATIVE AMPLITUDE
8 Hz
0.05 Hz
KILOMETERS
KILOMETERS
2-D RESISTIVITY MODEL
BLANK = 100.
A = 10.
OHM-METERS

Figure I-A1

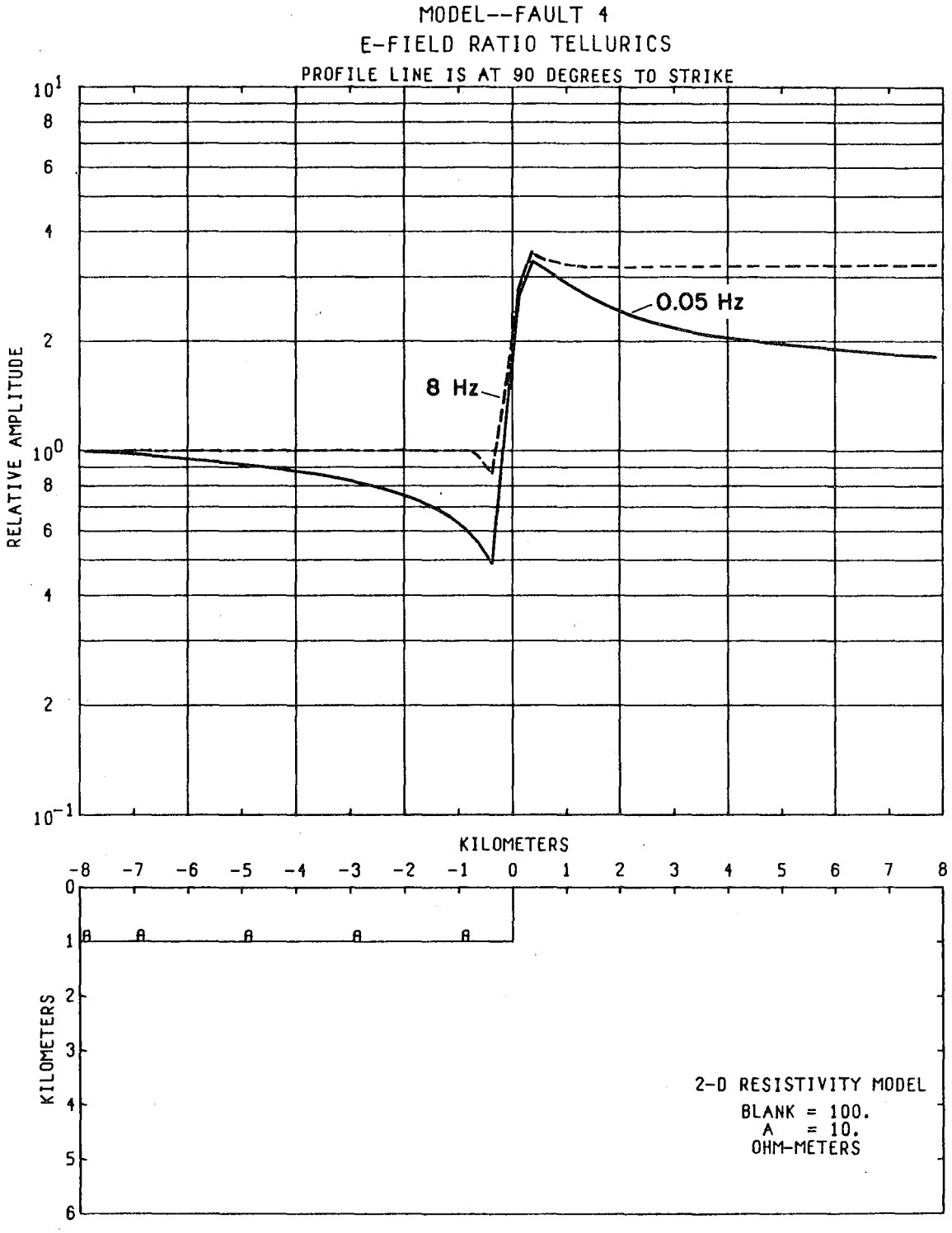

Figure I-A2

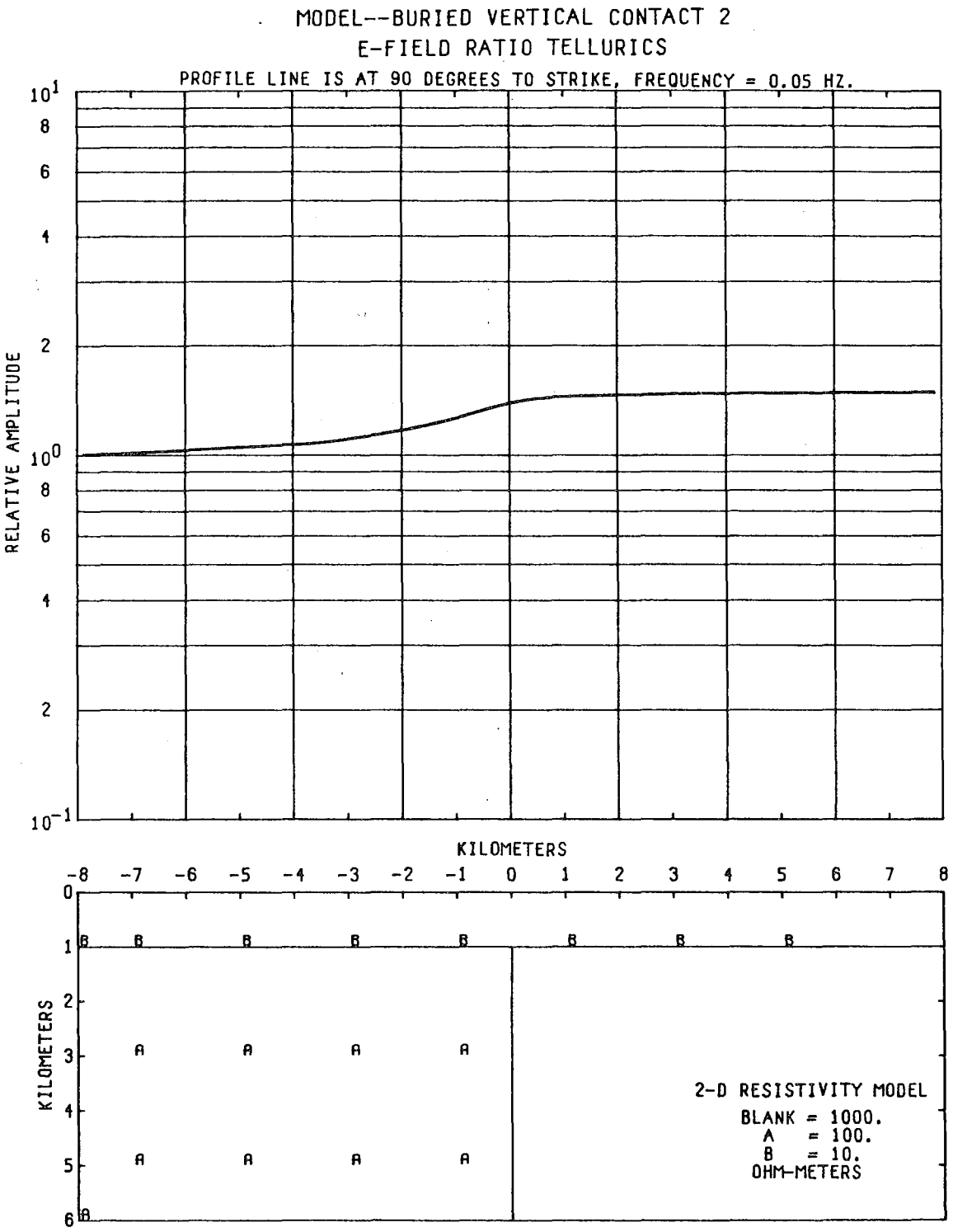
MODEL--BURIED VERTICAL CONTACT 2
E-FIELD RATIO TELLURICS
PROFILE LINE IS AT 90 DEGREES TO STRIKE, FREQUENCY = 0.05 HZ.
RELATIVE AMPLITUDE
KILOMETERS
KILOMETERS
2-D RESISTIVITY MODEL
BLANK = 1000.
A = 100.
B = 10.
OHM-METERS

Figure I-A3

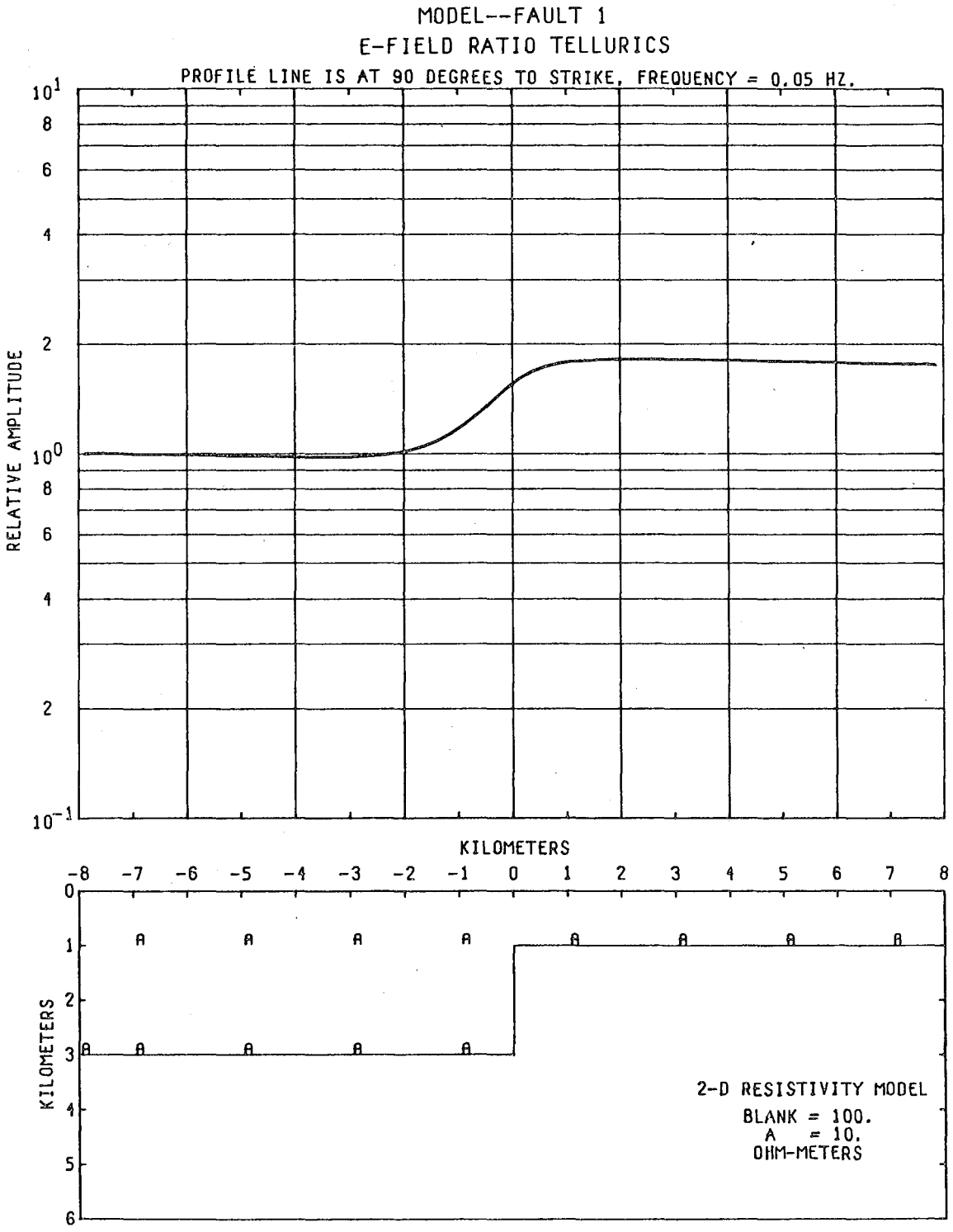

Figure I-A4

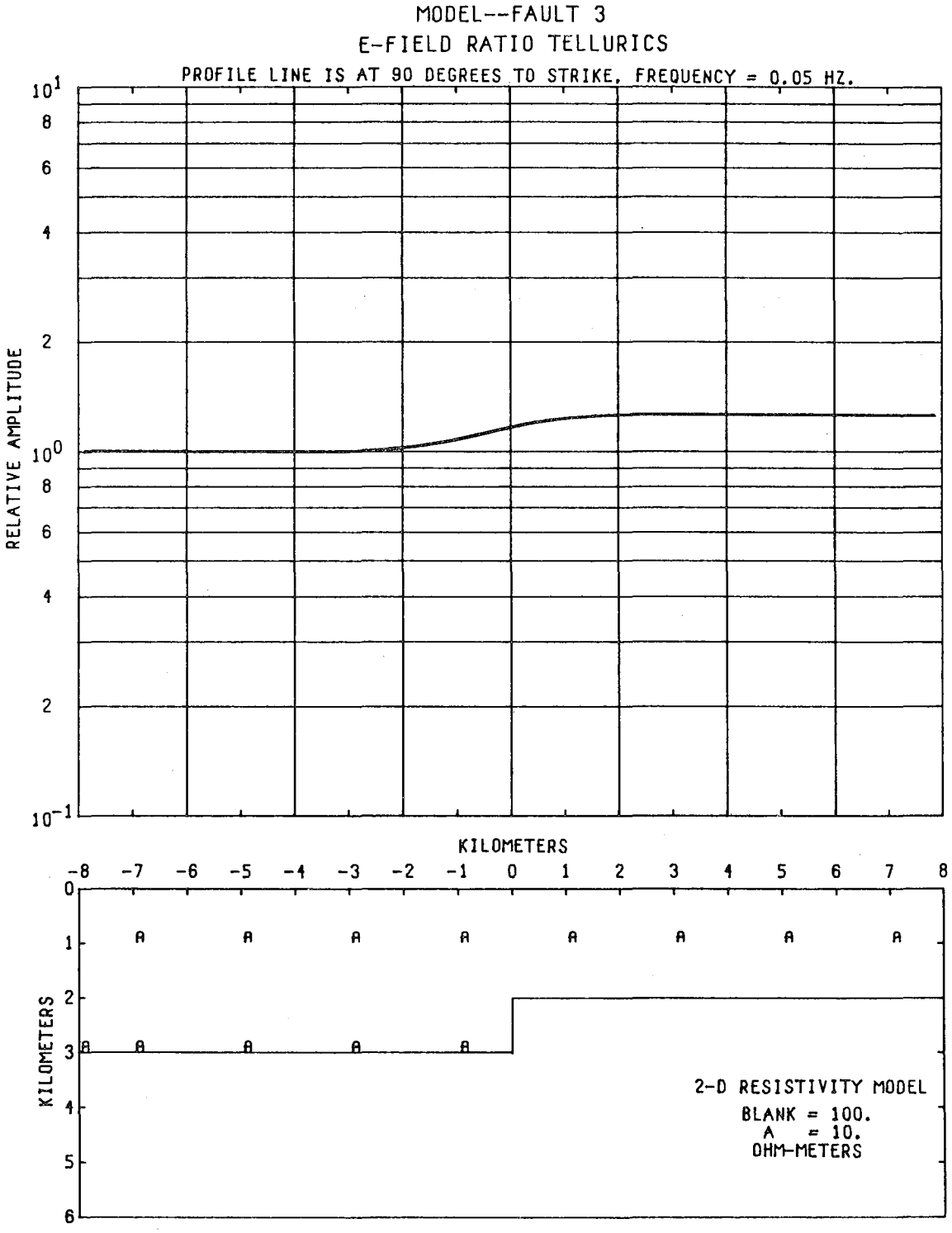
MODEL--FAULT 3
E-FIELD RATIO TELLURICS
PROFILE LINE IS AT 90 DEGREES TO STRIKE, FREQUENCY = 0.05 HZ.
RELATIVE AMPLITUDE
10^1
8
6
4
2
10^0
8
6
4
2
10^{-1}
KILOMETERS
-8 -7 -6 -5 -4 -3 -2 -1 0 1 2 3 4 5 6 7 8
KILOMETERS
0
1
2
3
4
5
6
2-D RESISTIVITY MODEL
BLANK = 100.
A = 10.
OHM-METERS

Figure I-A5

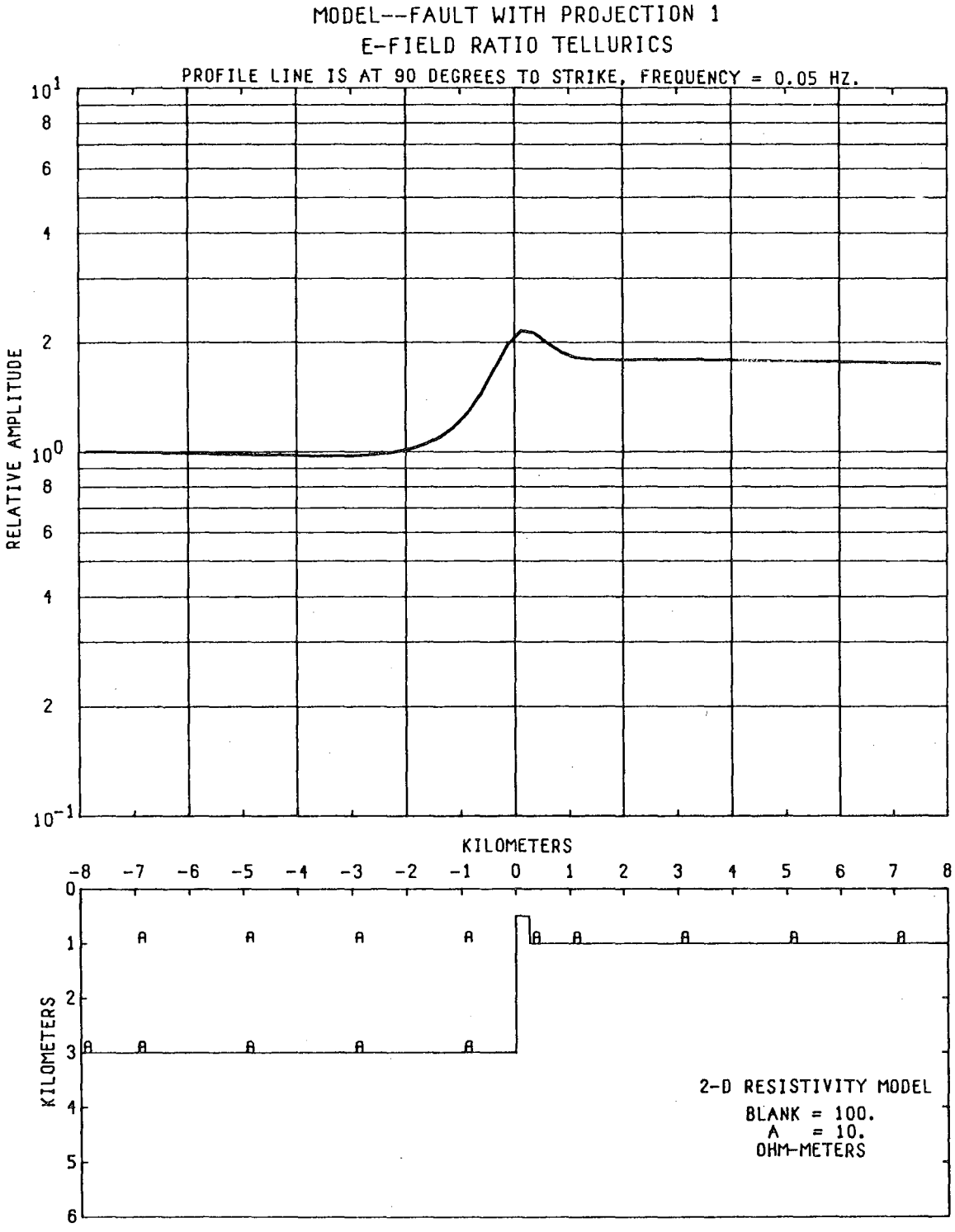

Figure I-A6

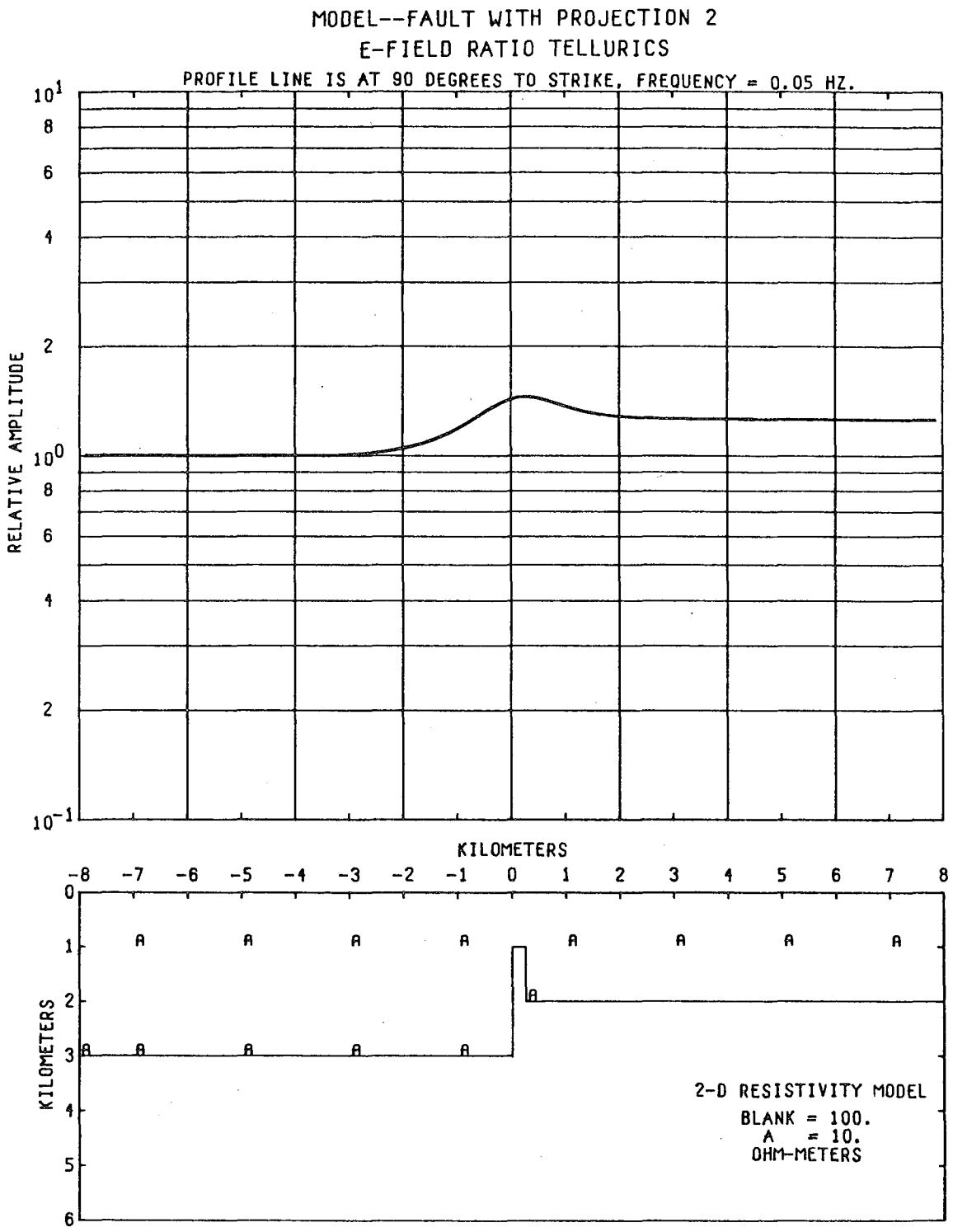
MODEL--FAULT WITH PROJECTION 2
E-FIELD RATIO TELLURICS
PROFILE LINE IS AT 90 DEGREES TO STRIKE, FREQUENCY = 0.05 HZ.
RELATIVE AMPLITUDE
KILOMETERS
KILOMETERS
2-D RESISTIVITY MODEL
BLANK = 100.
A = 10.
OHM-METERS

Figure I-A7

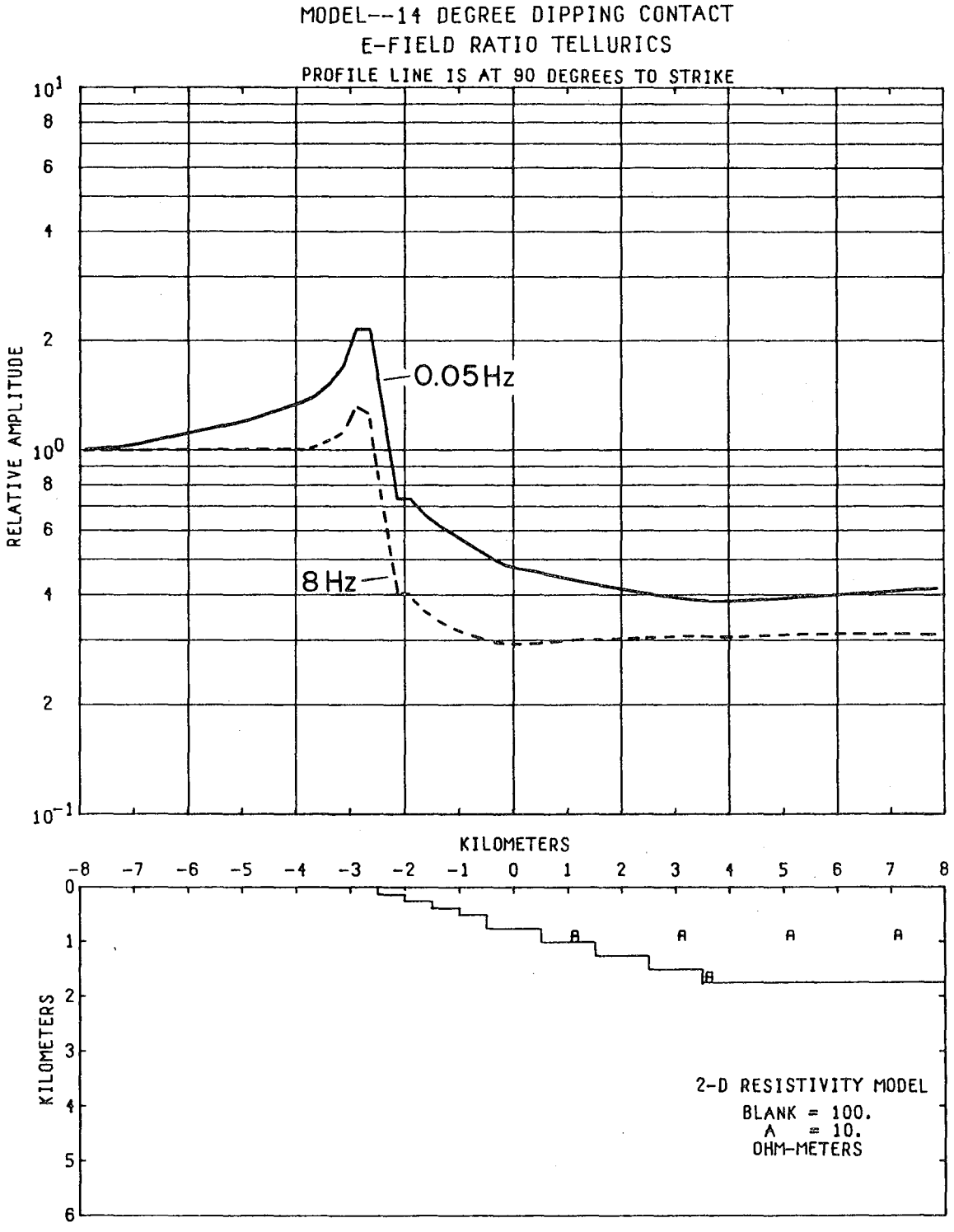
MODEL--14 DEGREE DIPPING CONTACT
E-FIELD RATIO TELLURICS
PROFILE LINE IS AT 90 DEGREES TO STRIKE
RELATIVE AMPLITUDE
0.05Hz
8 Hz
KILOMETERS
KILOMETERS
2-D RESISTIVITY MODEL
BLANK = 100.
A = 10.
OHM-METERS

Figure I-A8

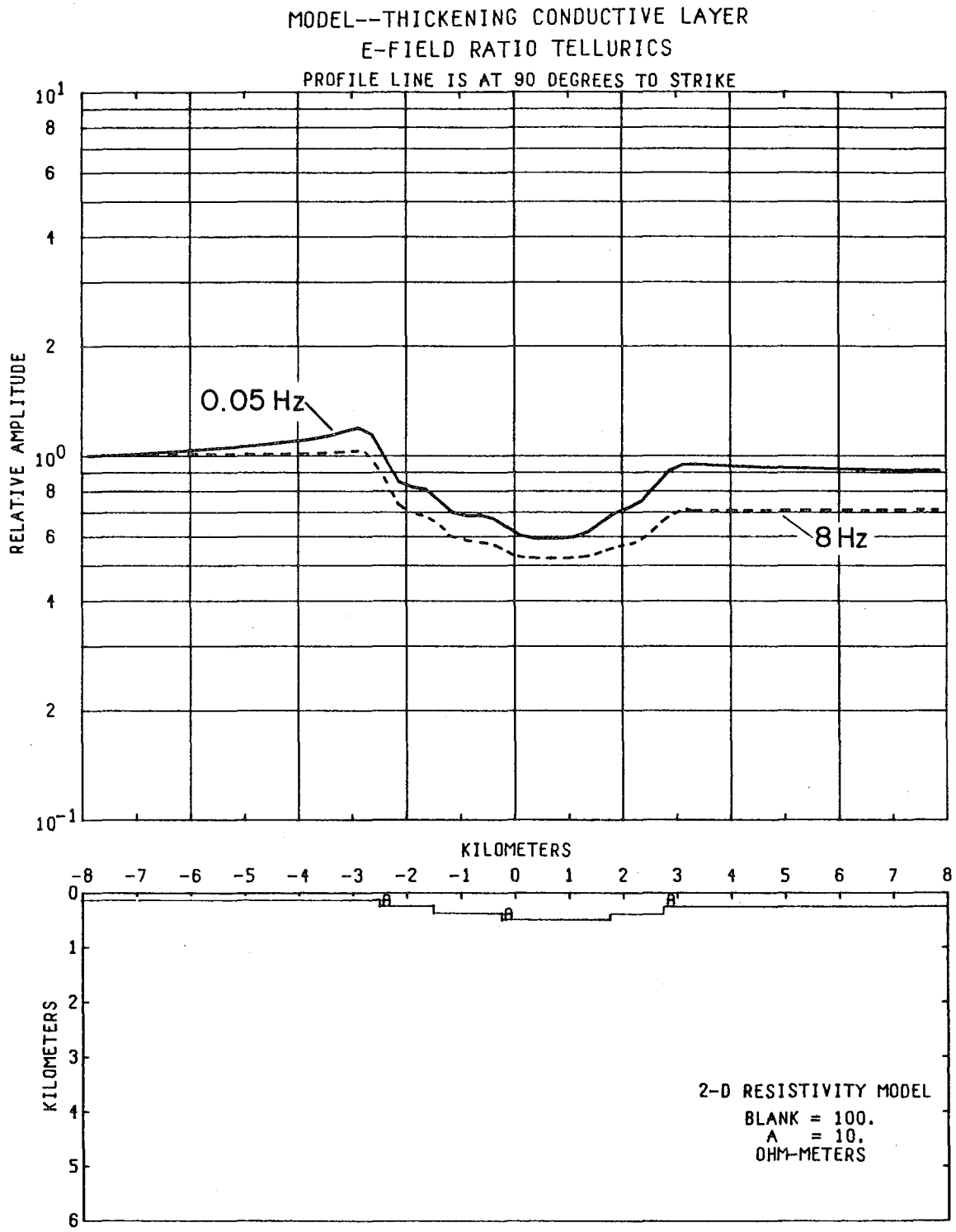
MODEL--THICKENING CONDUCTIVE LAYER
E-FIELD RATIO TELLURICS
PROFILE LINE IS AT 90 DEGREES TO STRIKE
RELATIVE AMPLITUDE
0.05 Hz
8 Hz
KILOMETERS
KILOMETERS
2-D RESISTIVITY MODEL
BLANK = 100.
A = 10.
OHM-METERS

Figure I-A9

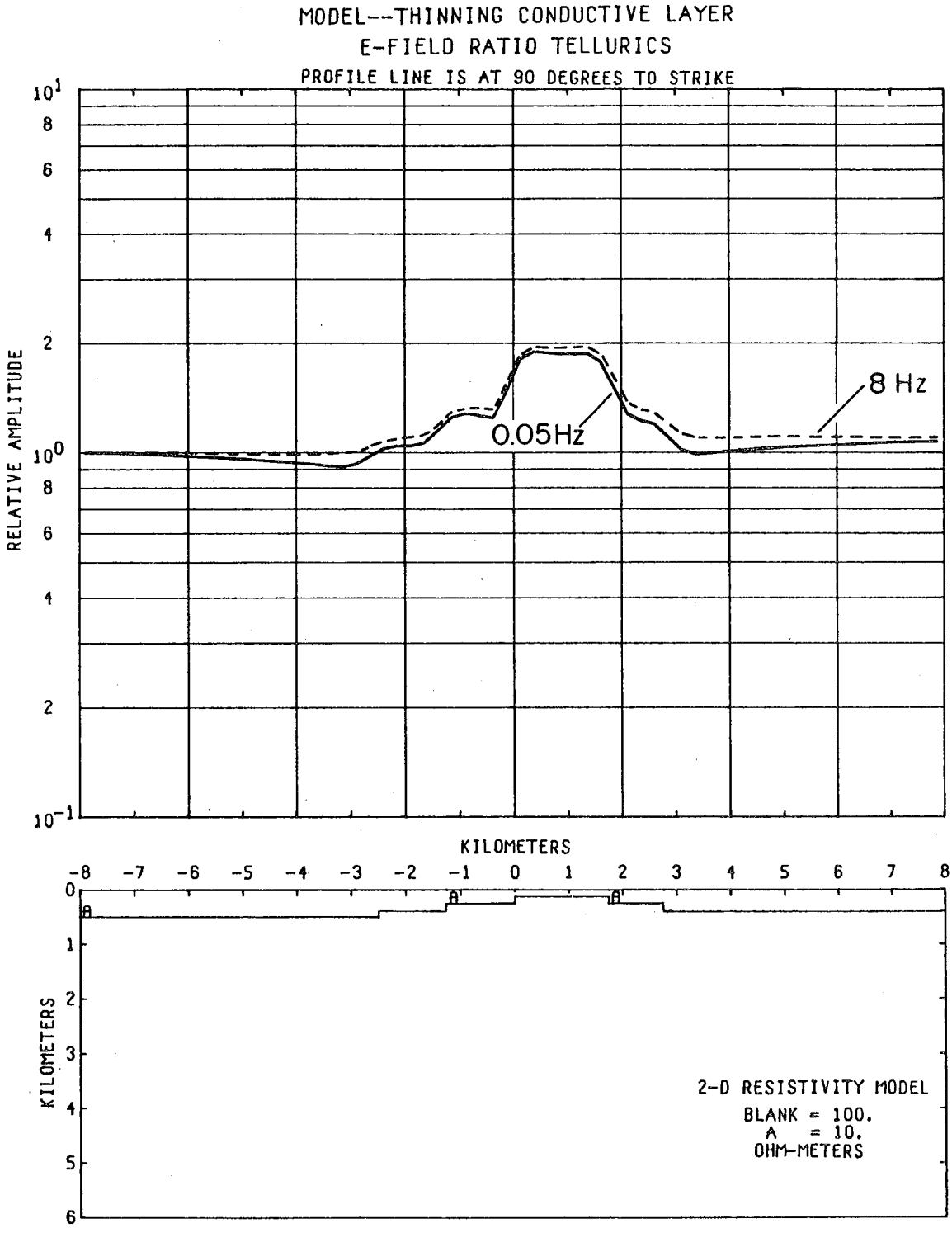

Figure I-A10

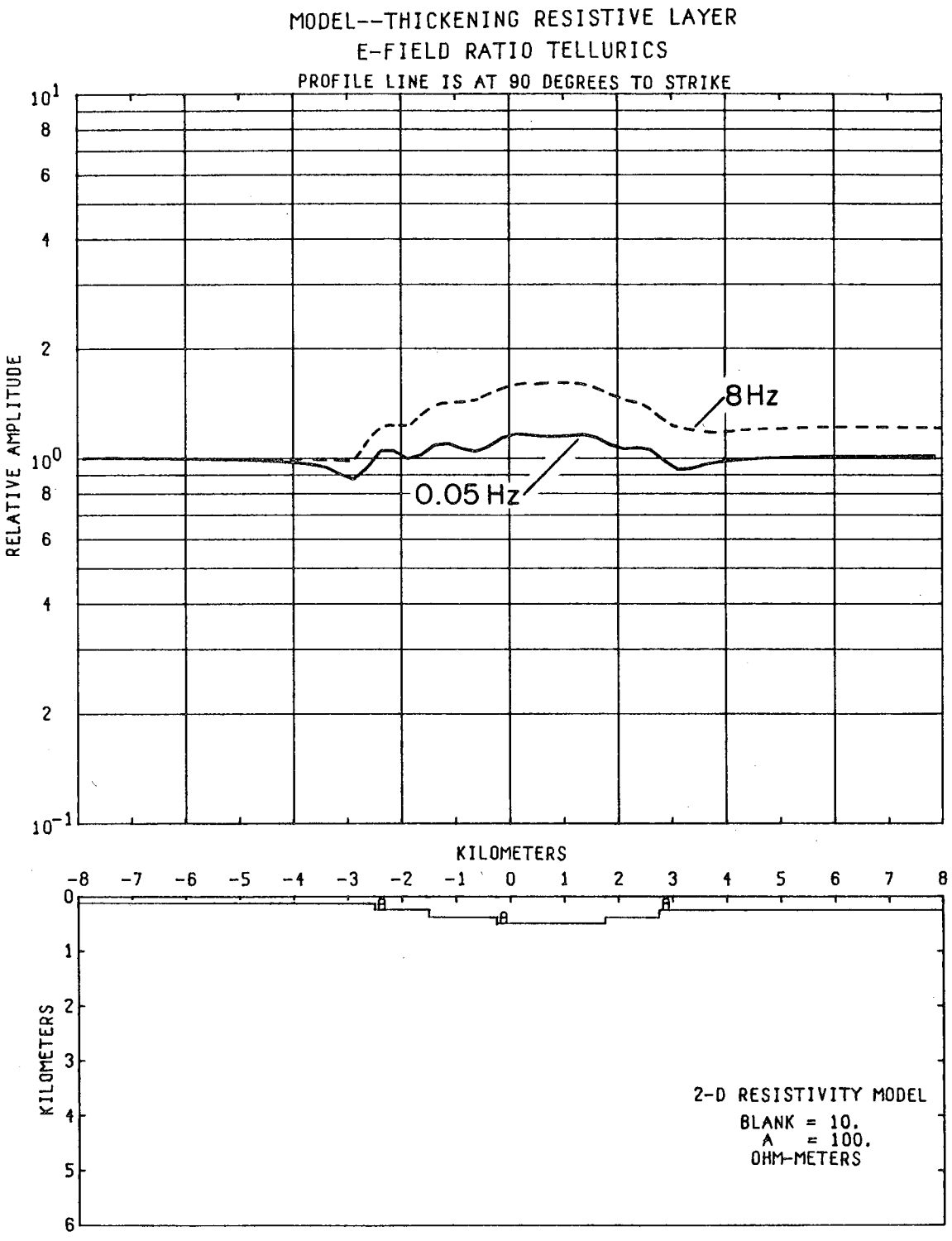
MODEL--THICKENING RESISTIVE LAYER
E-FIELD RATIO TELLURICS
PROFILE LINE IS AT 90 DEGREES TO STRIKE
RELATIVE AMPLITUDE
8Hz
0.05 Hz
KILOMETERS
KILOMETERS
2-D RESISTIVITY MODEL
BLANK = 10.
A = 100.
OHM-METERS

Figure I-A11

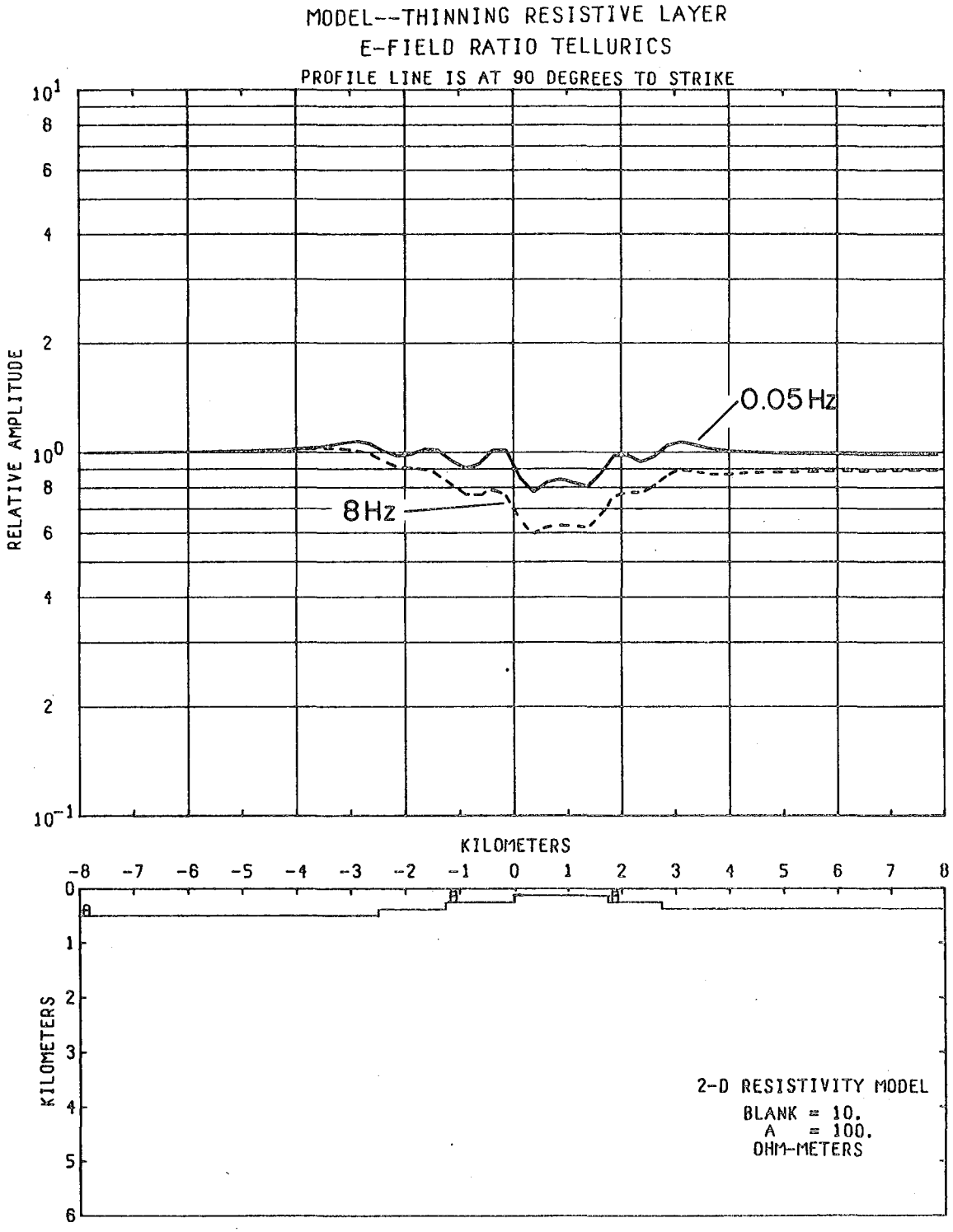

Figure I-A12

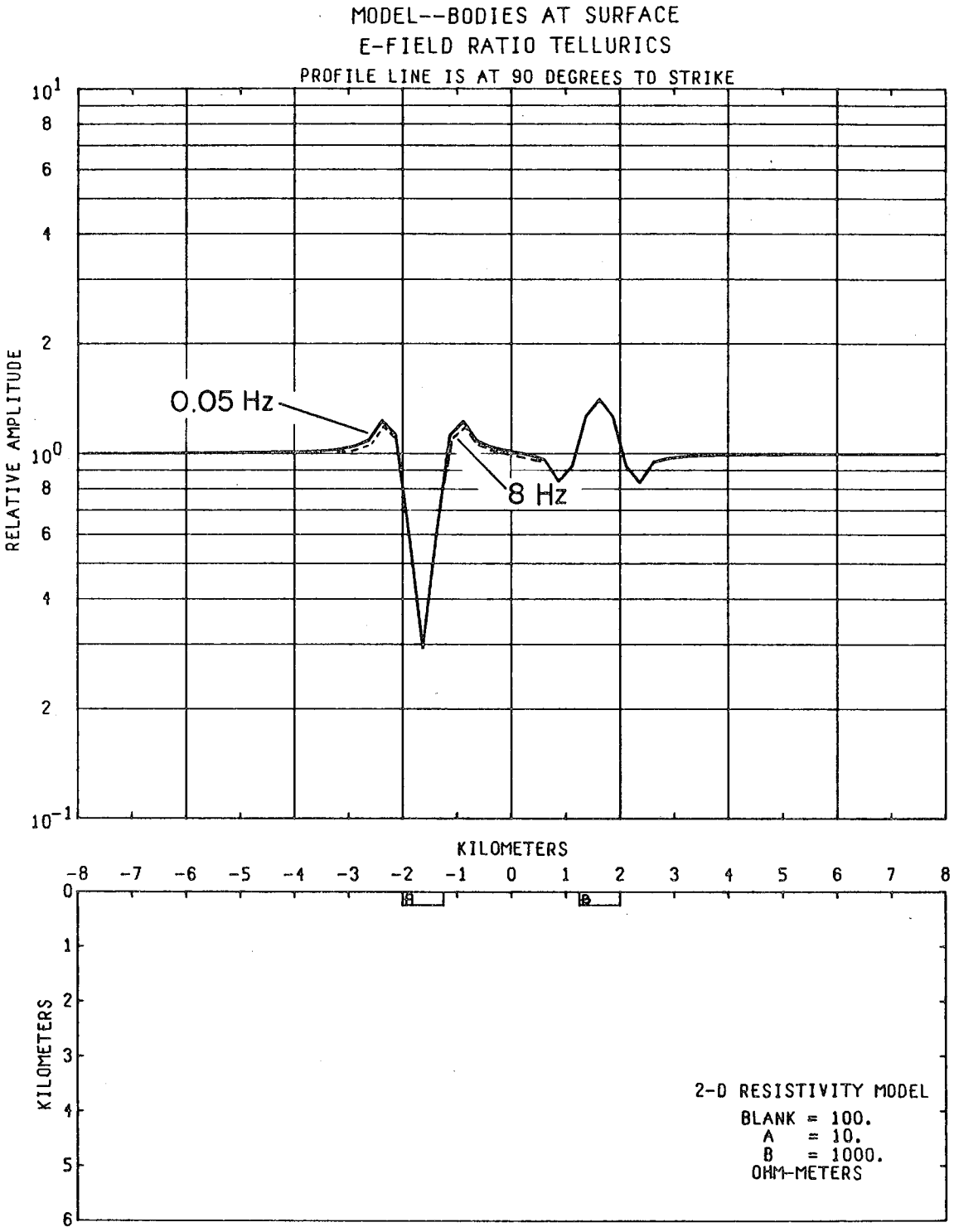
MODEL--BODIES AT SURFACE
E-FIELD RATIO TELLURICS
PROFILE LINE IS AT 90 DEGREES TO STRIKE
RELATIVE AMPLITUDE
0.05 Hz
8 Hz
KILOMETERS
KILOMETERS
2-D RESISTIVITY MODEL
BLANK = 100.
A = 10.
B = 1000.
OHM-METERS

Figure I-A13

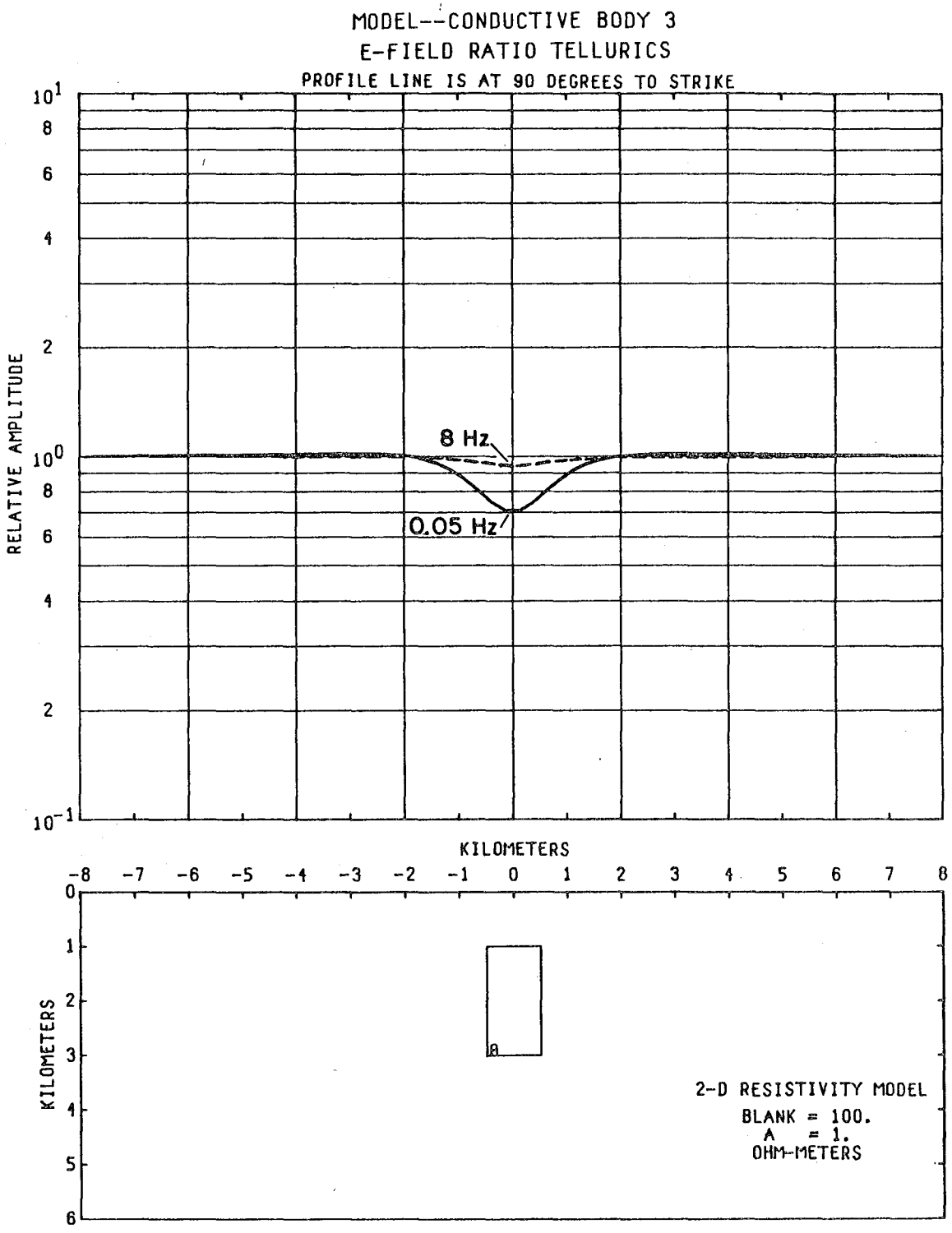

Figure I-A14

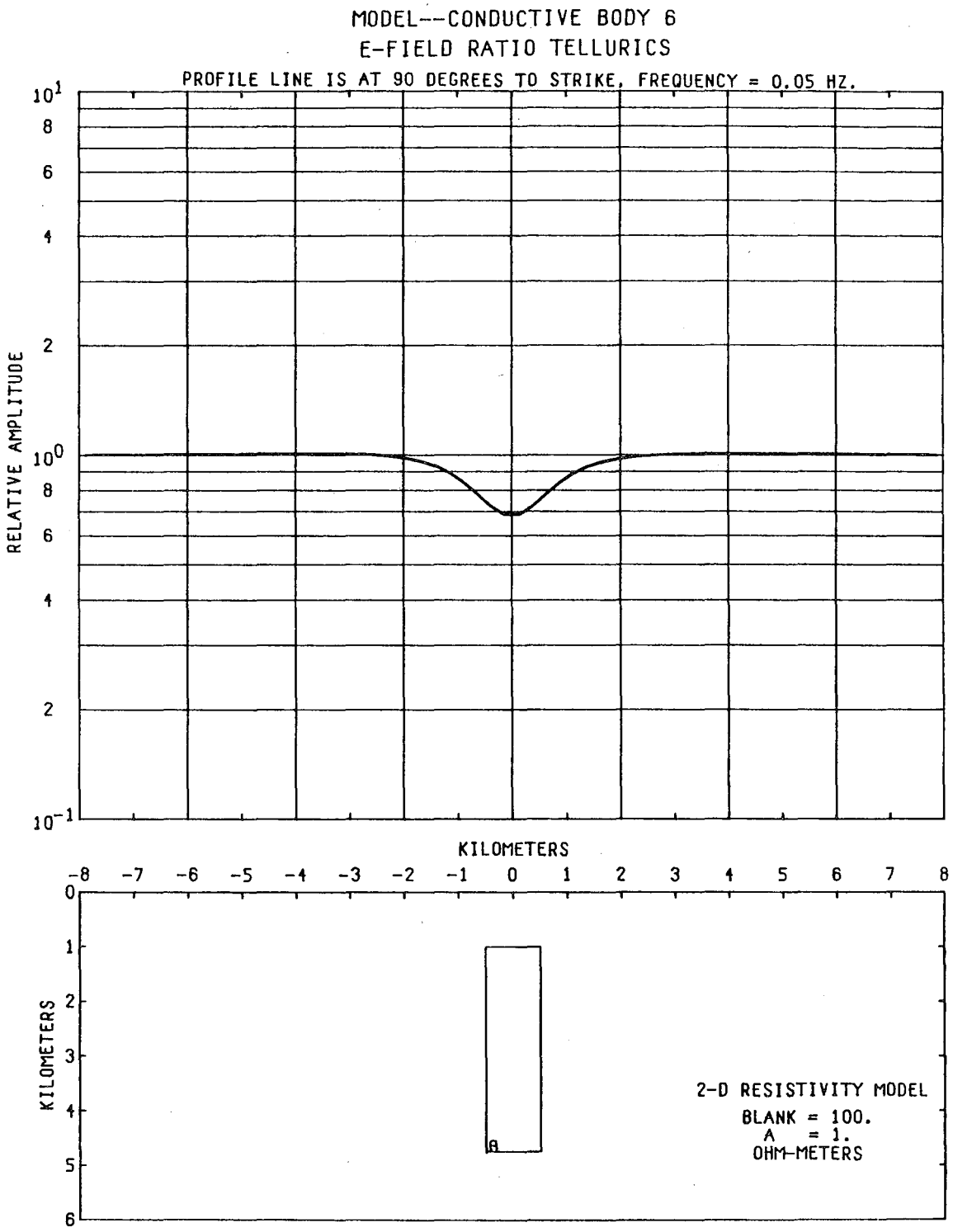
MODEL--CONDUCTIVE BODY 6
E-FIELD RATIO TELLURICS
PROFILE LINE IS AT 90 DEGREES TO STRIKE, FREQUENCY = 0.05 HZ.
RELATIVE AMPLITUDE
10^1
8
6
4
2
10^0
8
6
4
2
10^{-1}
KILOMETERS
-8 -7 -6 -5 -4 -3 -2 -1 0 1 2 3 4 5 6 7 8
KILOMETERS
0
1
2
3
4
5
6
A
2-D RESISTIVITY MODEL
BLANK = 100.
A = 1.
OHM-METERS

Figure I-A15

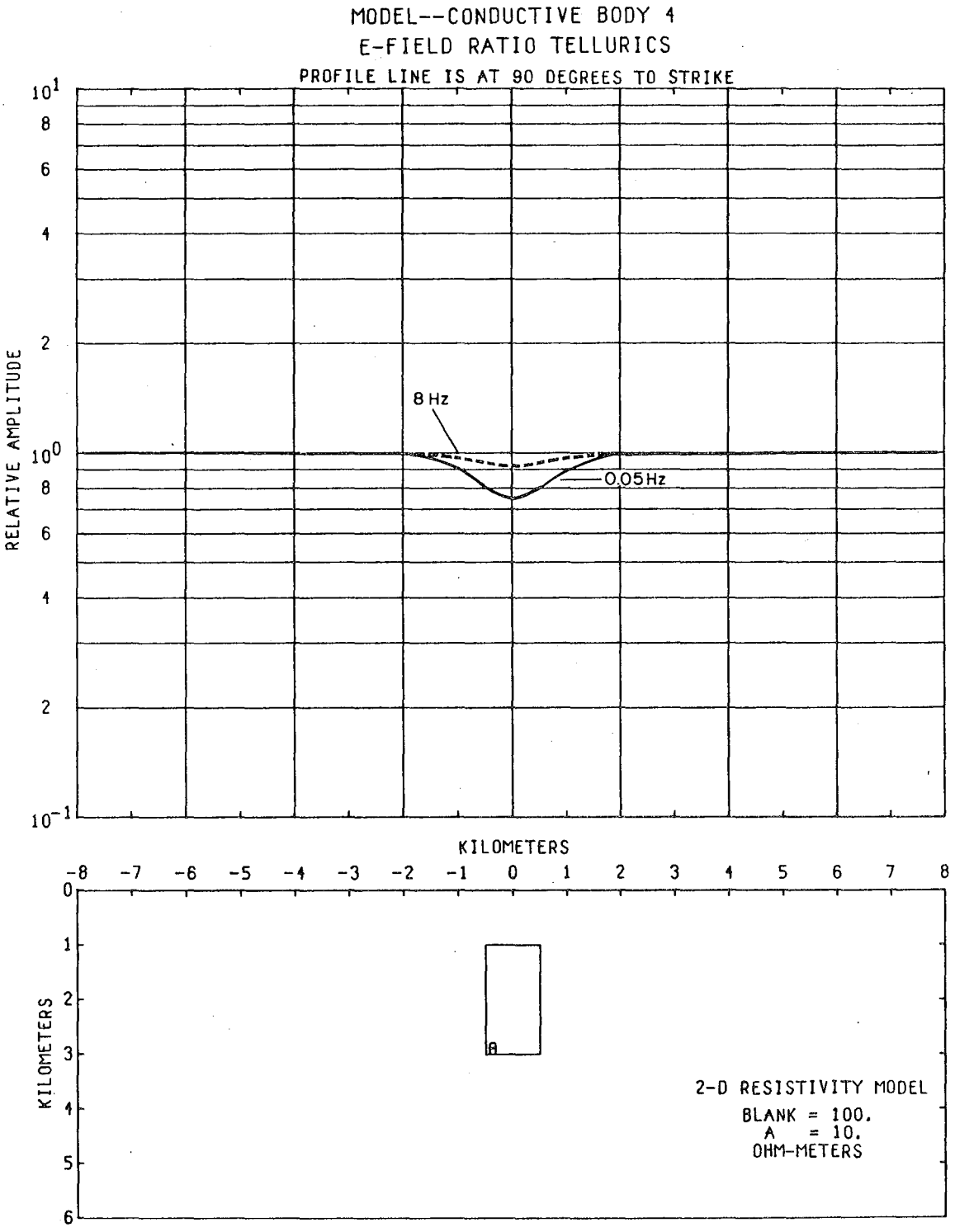

Figure I-A16

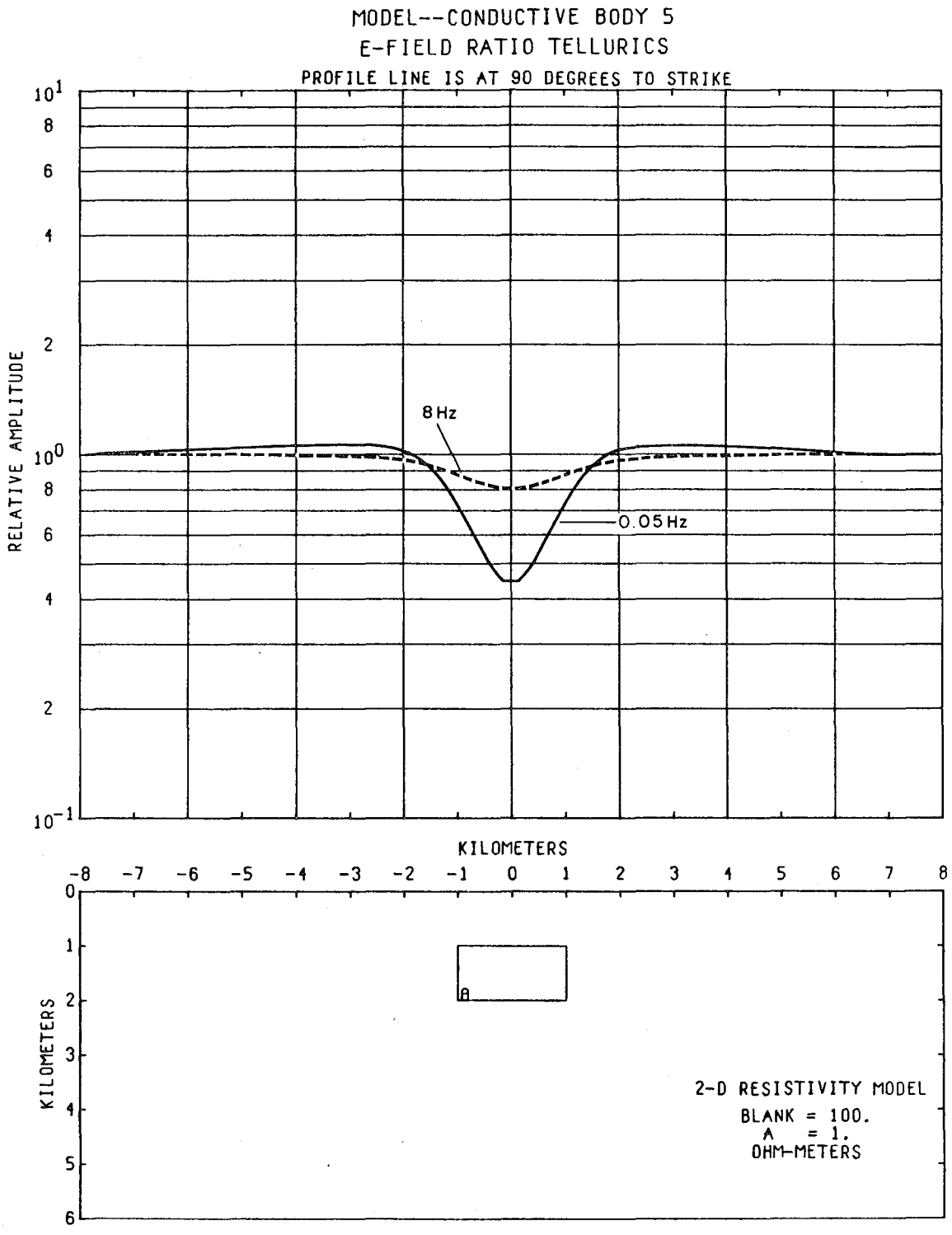
MODEL--CONDUCTIVE BODY 5
E-FIELD RATIO TELLURICS
PROFILE LINE IS AT 90 DEGREES TO STRIKE
RELATIVE AMPLITUDE
8Hz
0.05Hz
KILOMETERS
KILOMETERS
A
2-D RESISTIVITY MODEL
BLANK = 100.
A = 1.
OHM-METERS

Figure I-A17

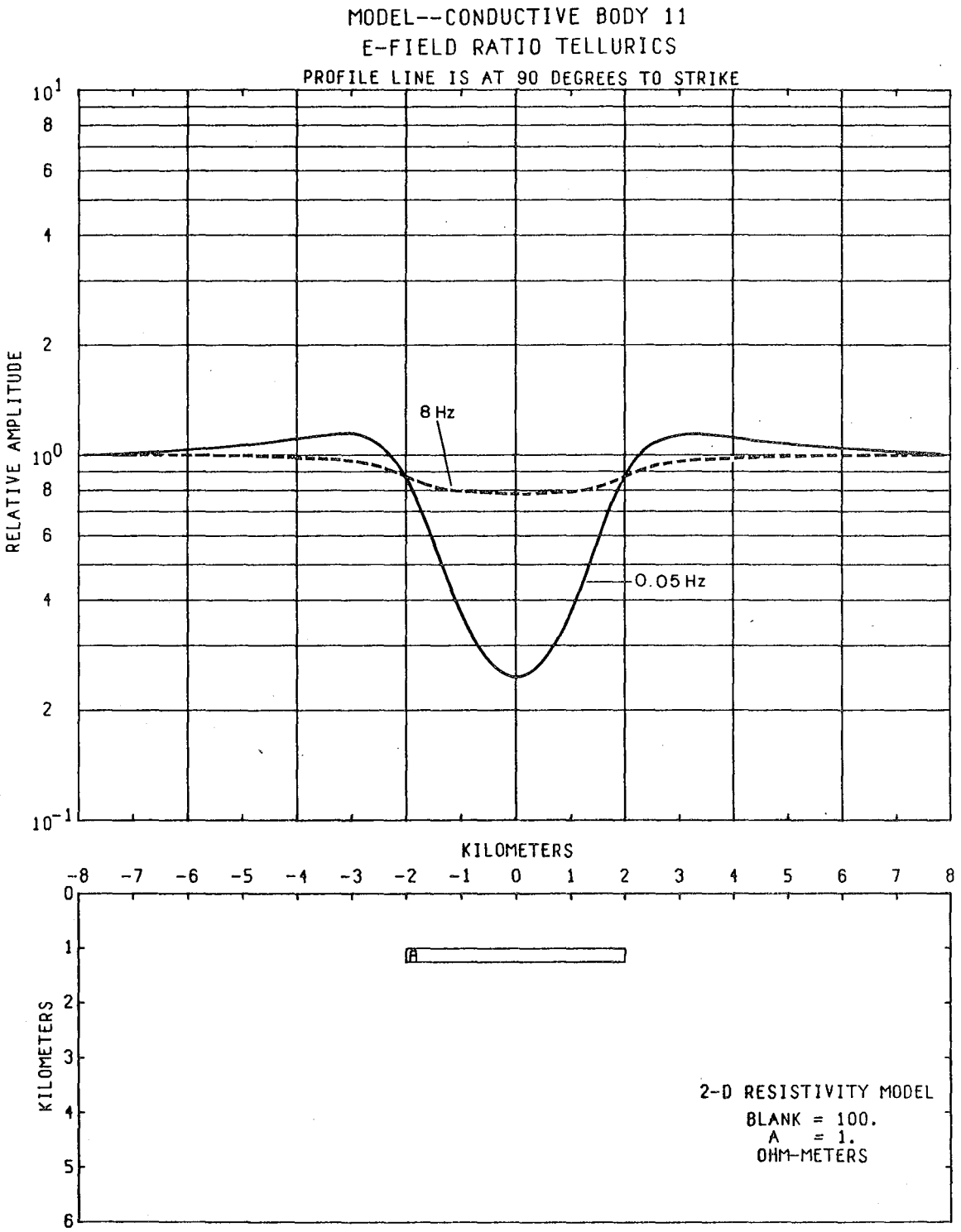

Figure I-A18

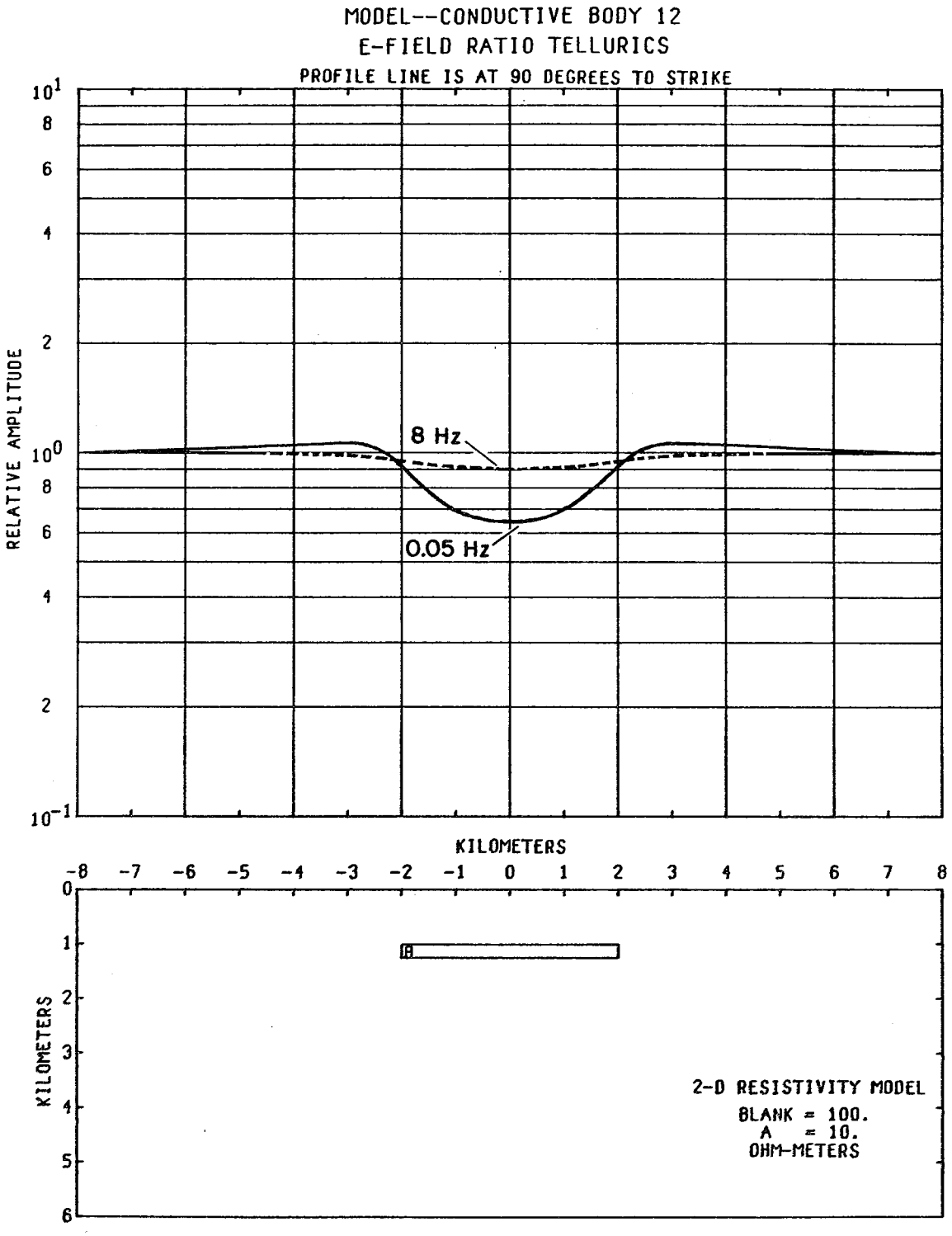
MODEL--CONDUCTIVE BODY 12
E-FIELD RATIO TELLURICS
PROFILE LINE IS AT 90 DEGREES TO STRIKE
RELATIVE AMPLITUDE
8 Hz
0.05 Hz
KILOMETERS
KILOMETERS
2-D RESISTIVITY MODEL
BLANK = 100.
A = 10.
OHM-METERS

Figure I-A19

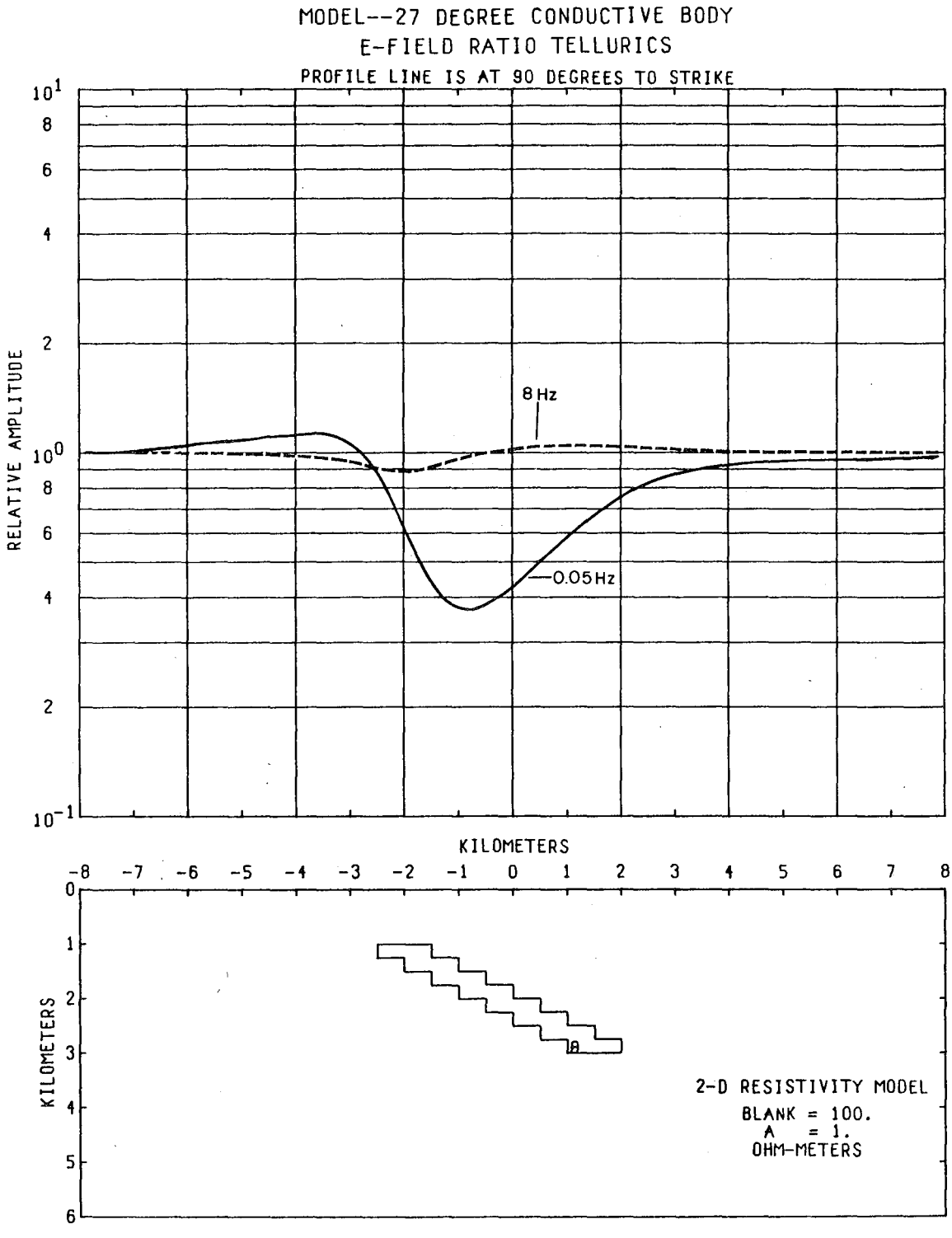

Figure I-A20

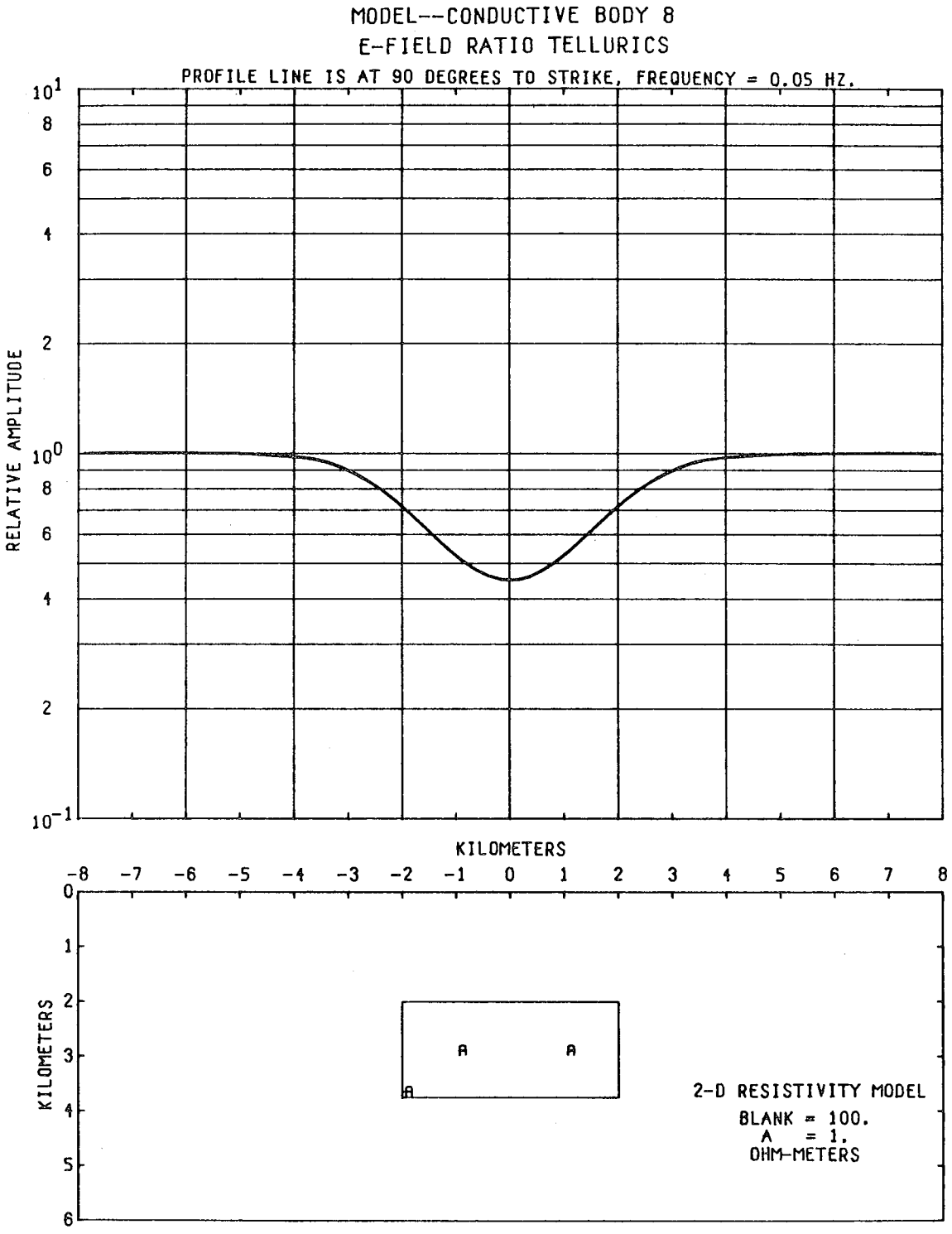
MODEL--CONDUCTIVE BODY 8
E-FIELD RATIO TELLURICS
PROFILE LINE IS AT 90 DEGREES TO STRIKE, FREQUENCY = 0.05 HZ.
RELATIVE AMPLITUDE
KILOMETERS
KILOMETERS
2-D RESISTIVITY MODEL
BLANK = 100.
A = 1.
OHM-METERS

Figure I-A21

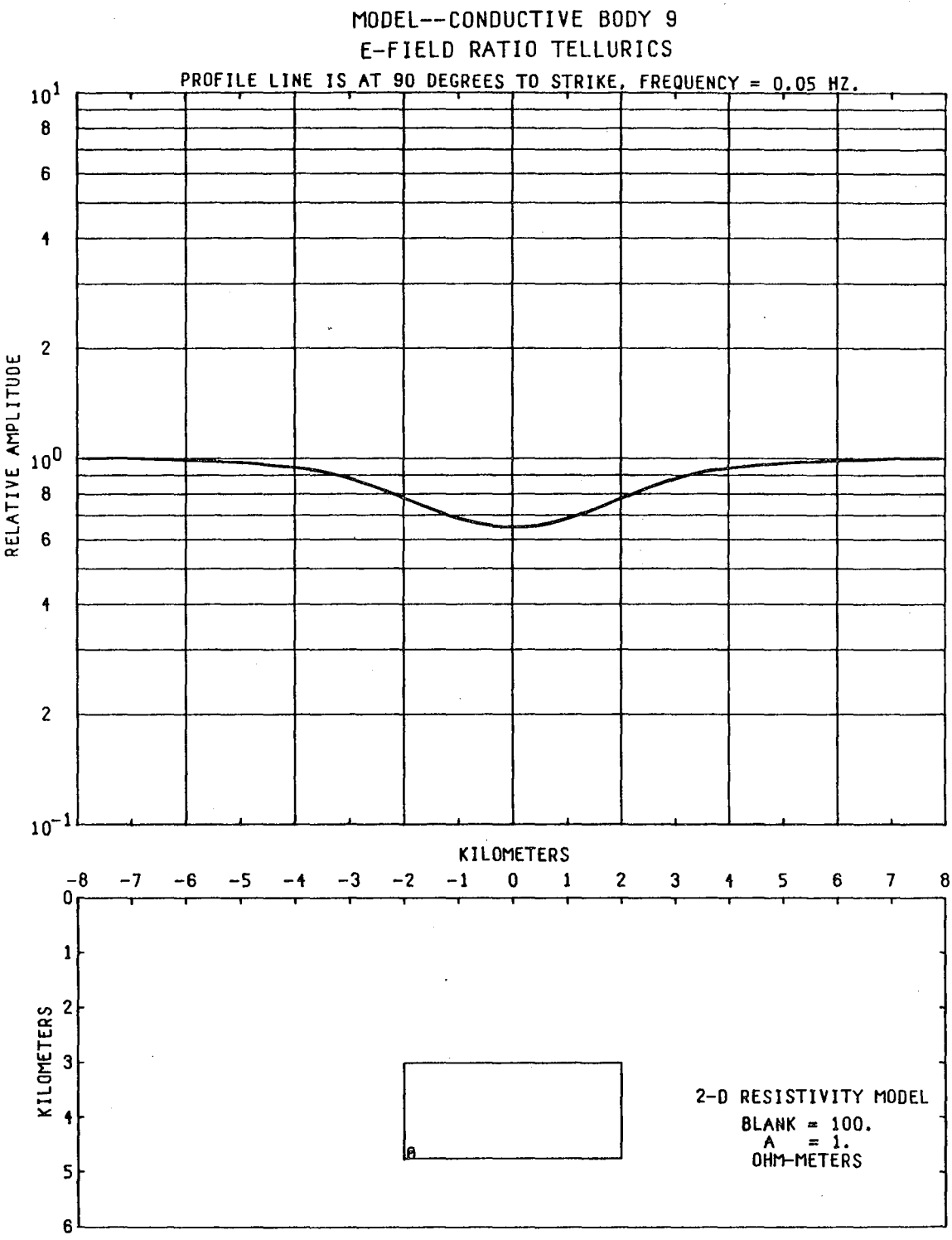
MODEL--CONDUCTIVE BODY 9
E-FIELD RATIO TELLURICS
PROFILE LINE IS AT 90 DEGREES TO STRIKE, FREQUENCY = 0.05 HZ.
RELATIVE AMPLITUDE
10^1
8
6
4
2
10^0
8
6
4
2
10^{-1}
KILOMETERS
-8 -7 -6 -5 -4 -3 -2 -1 0 1 2 3 4 5 6 7 8
KILOMETERS
0
1
2
3
4
5
6
2-D RESISTIVITY MODEL
BLANK = 100.
A = 1.
OHM-METERS

Figure I-A22

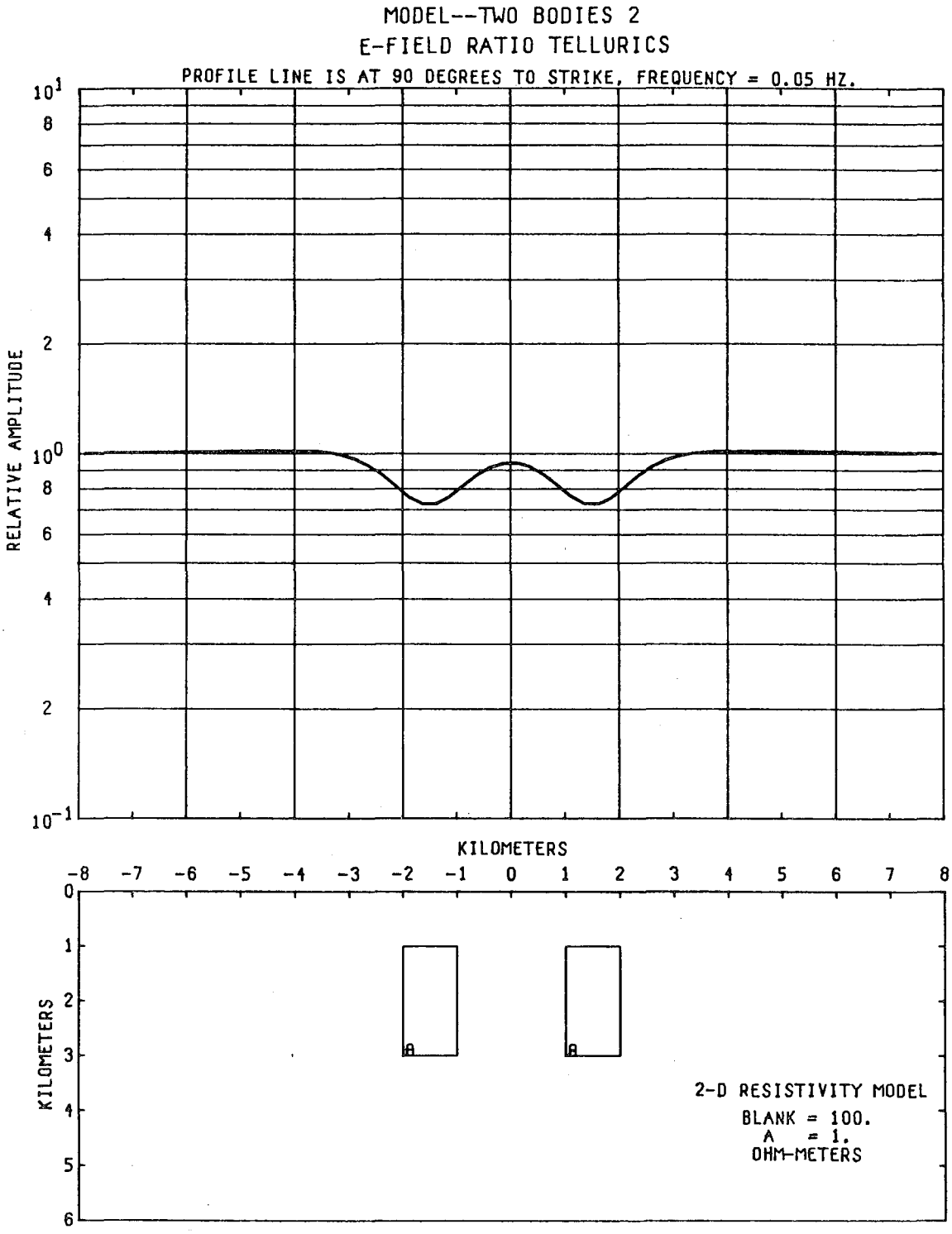
MODEL--TWO BODIES 2
E-FIELD RATIO TELLURICS
PROFILE LINE IS AT 90 DEGREES TO STRIKE, FREQUENCY = 0.05 HZ.
RELATIVE AMPLITUDE
KILOMETERS
KILOMETERS
2-D RESISTIVITY MODEL
BLANK = 100.
A = 1.
OHM-METERS

Figure I-A23

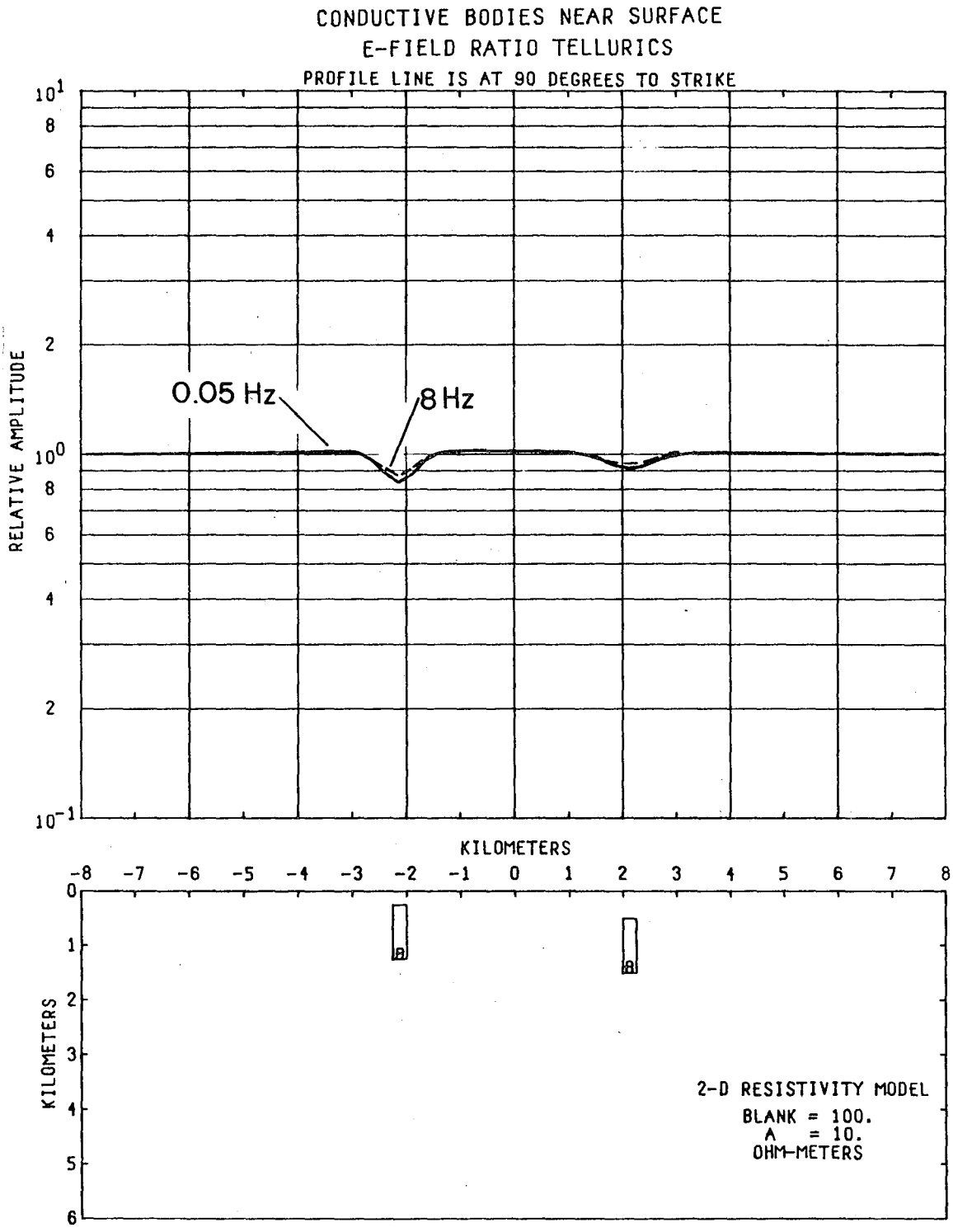

Figure I-A24

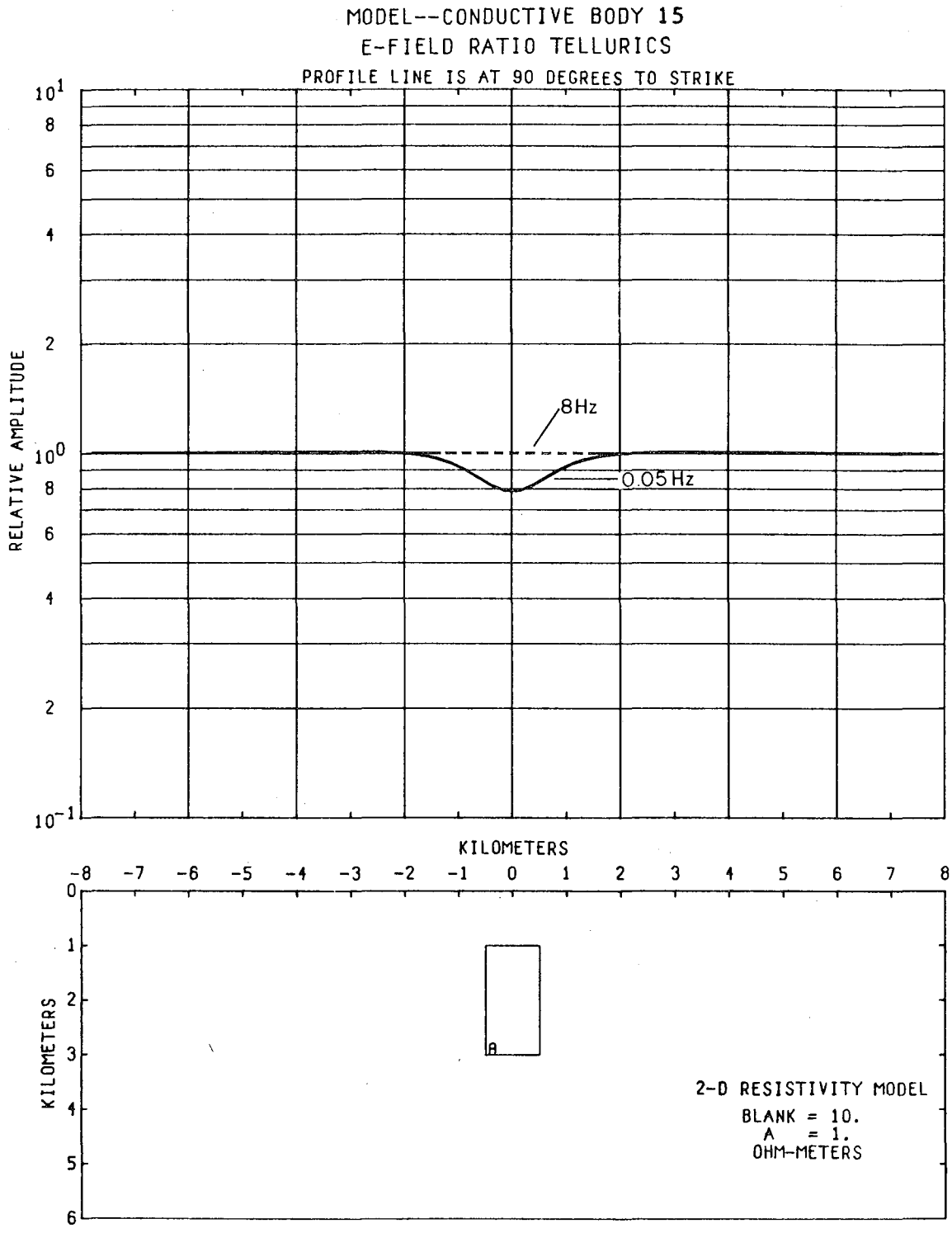
MODEL--CONDUCTIVE BODY 15
E-FIELD RATIO TELLURICS
PROFILE LINE IS AT 90 DEGREES TO STRIKE
RELATIVE AMPLITUDE
8Hz
0.05Hz
KILOMETERS
KILOMETERS
A
2-D RESISTIVITY MODEL
BLANK = 10.
A = 1.
OHM-METERS

Figure I-A25

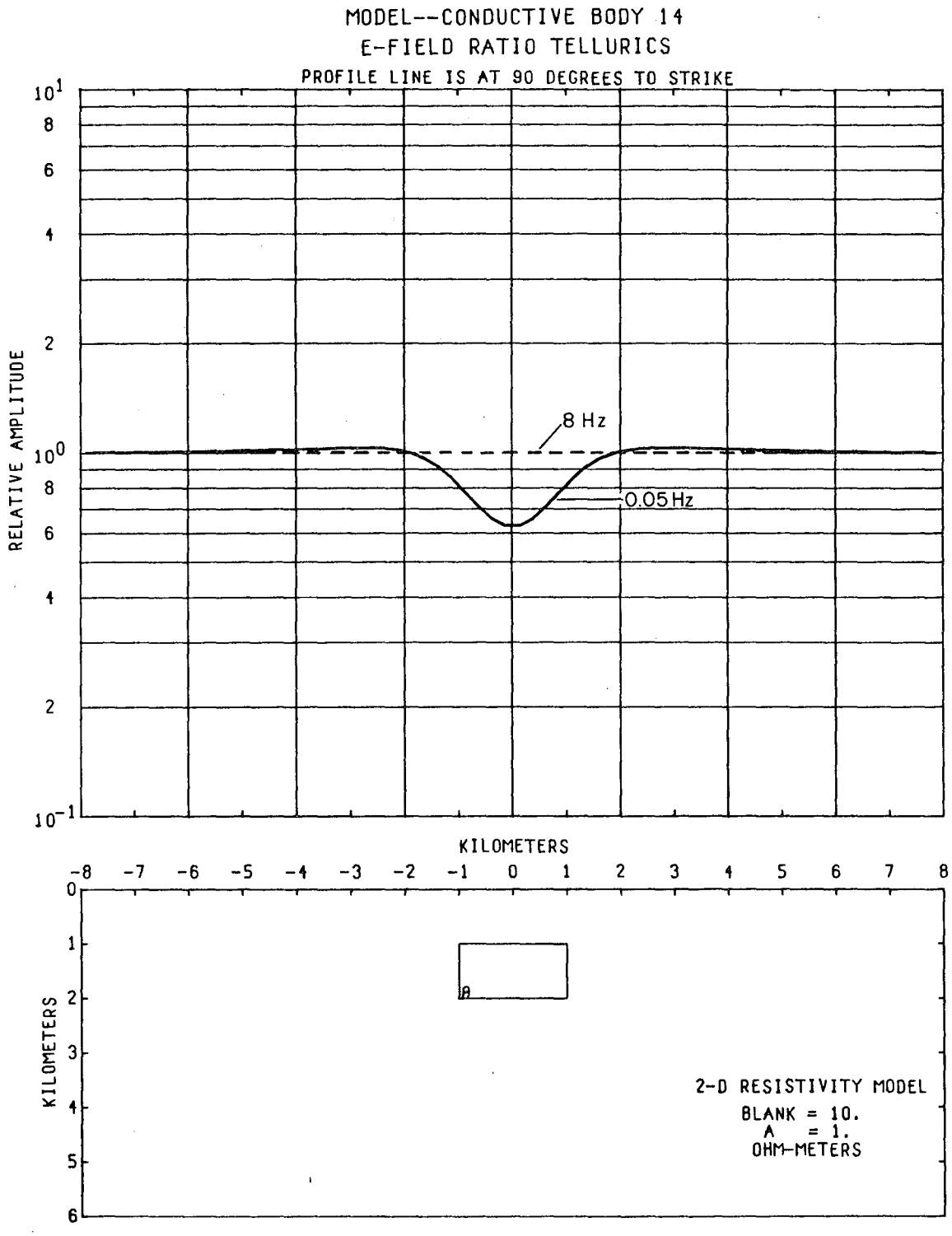

Figure I-A26

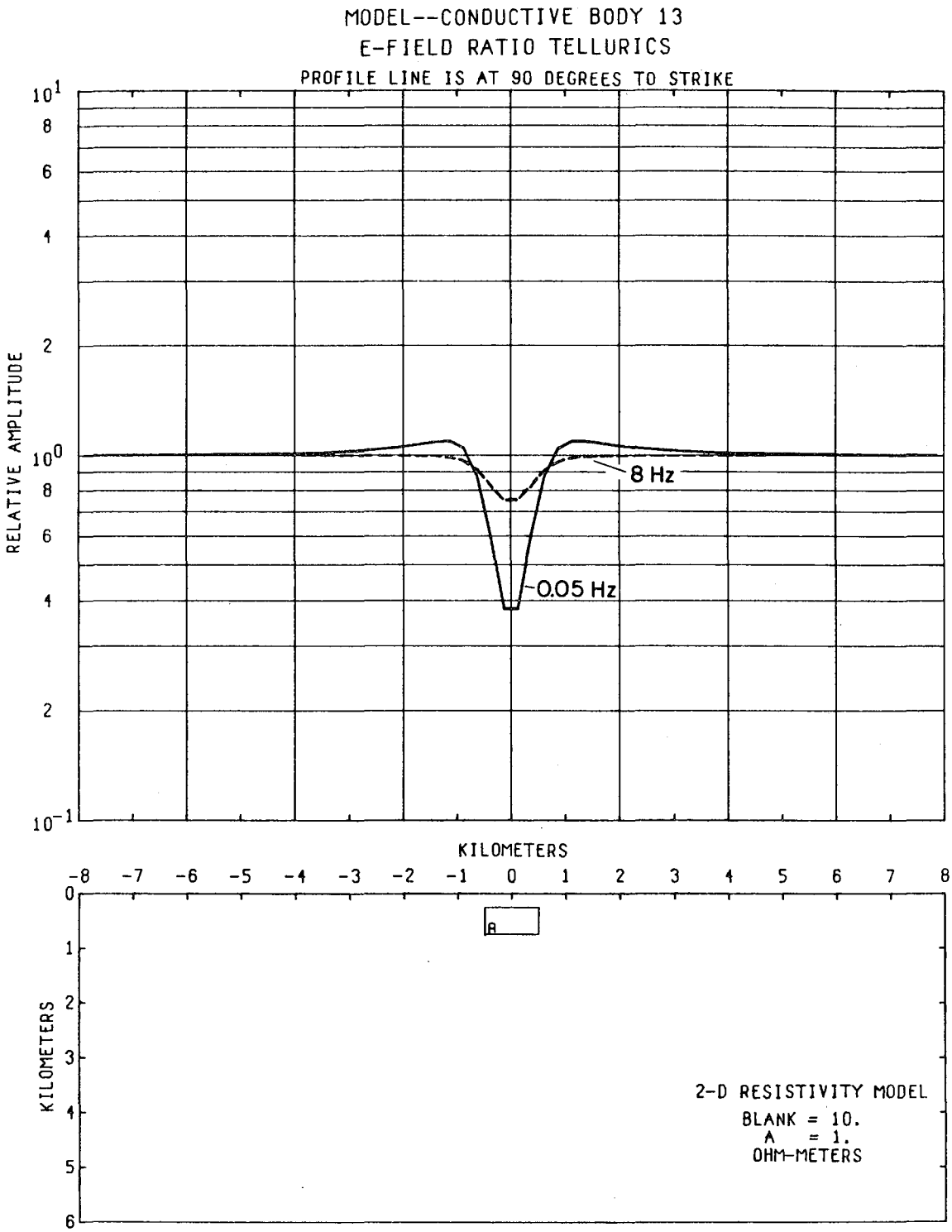
MODEL--CONDUCTIVE BODY 13
E-FIELD RATIO TELLURICS
PROFILE LINE IS AT 90 DEGREES TO STRIKE
RELATIVE AMPLITUDE
8 Hz
0.05 Hz
KILOMETERS
KILOMETERS
2-D RESISTIVITY MODEL
BLANK = 10.
A = 1.
OHM-METERS

Figure I-A27

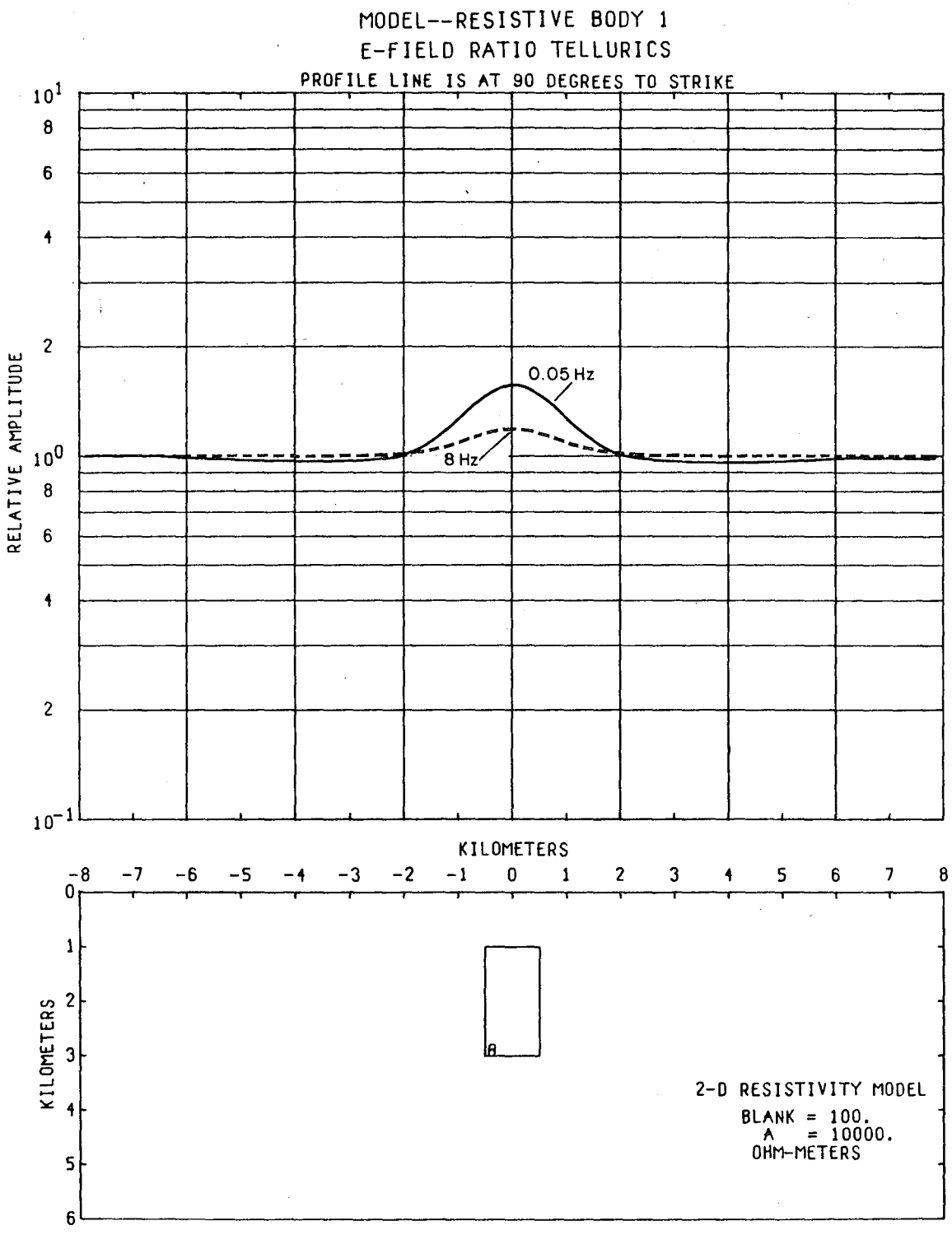
MODEL--RESISTIVE BODY 1
E-FIELD RATIO TELLURICS
PROFILE LINE IS AT 90 DEGREES TO STRIKE
RELATIVE AMPLITUDE
0.05 Hz
8 Hz
KILOMETERS
KILOMETERS
2-D RESISTIVITY MODEL
BLANK = 100.
A = 10000.
OHM-METERS

Figure I-A28

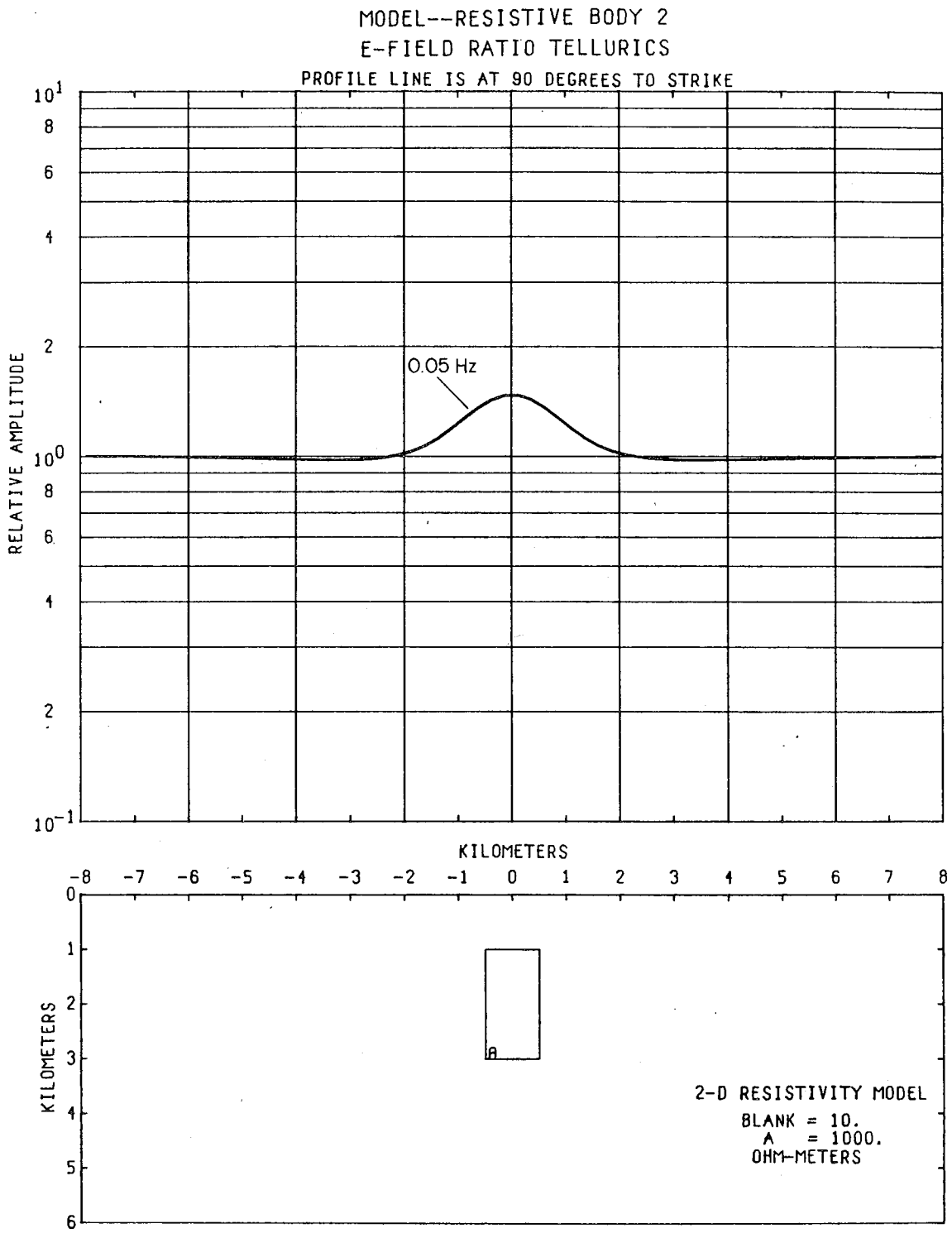
MODEL--RESISTIVE BODY 2
E-FIELD RATIO TELLURICS
PROFILE LINE IS AT 90 DEGREES TO STRIKE
RELATIVE AMPLITUDE
0.05 Hz
KILOMETERS
KILOMETERS
A
2-D RESISTIVITY MODEL
BLANK = 10.
A = 1000.
OHM-METERS

Figure I-A29

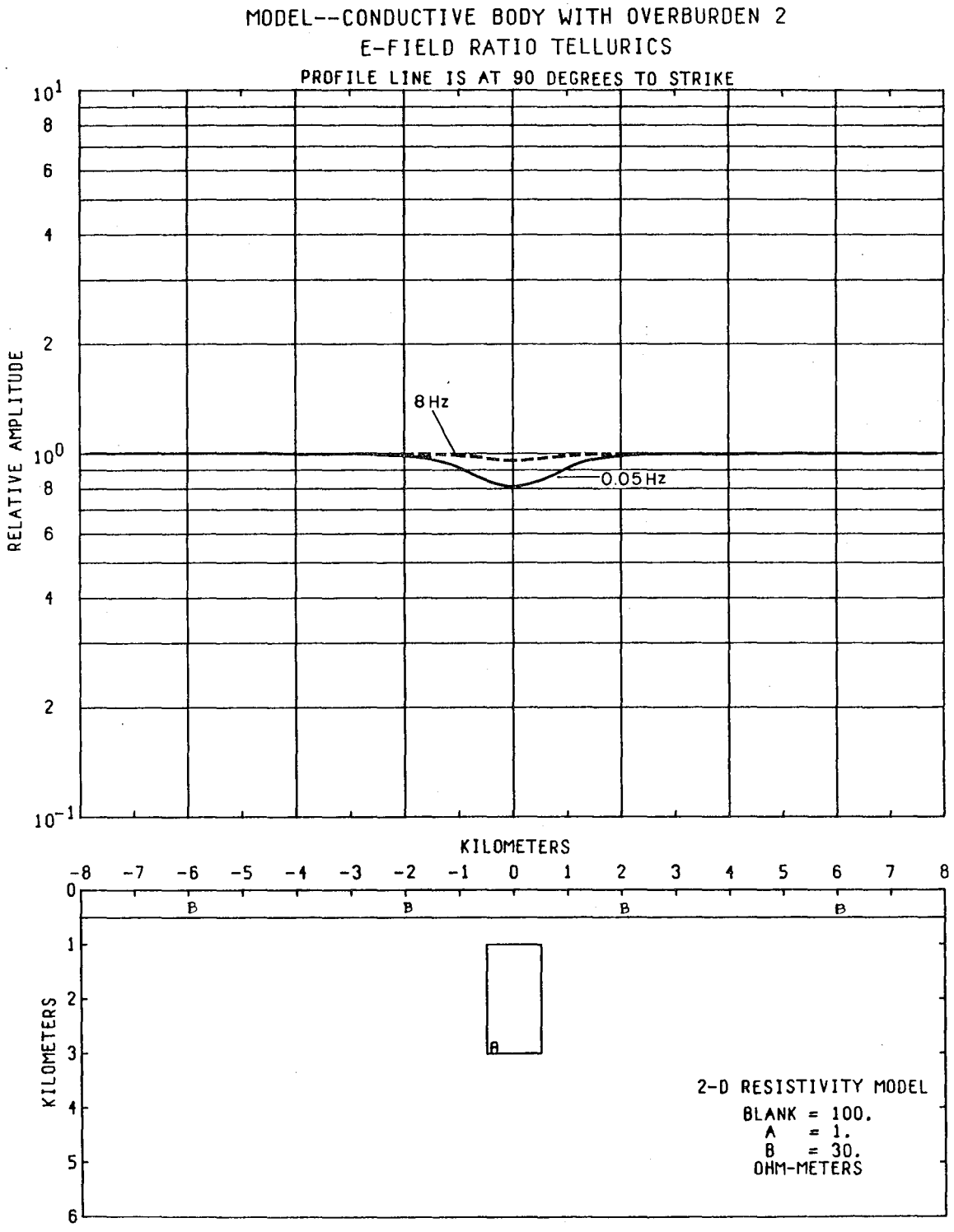

Figure I-A30

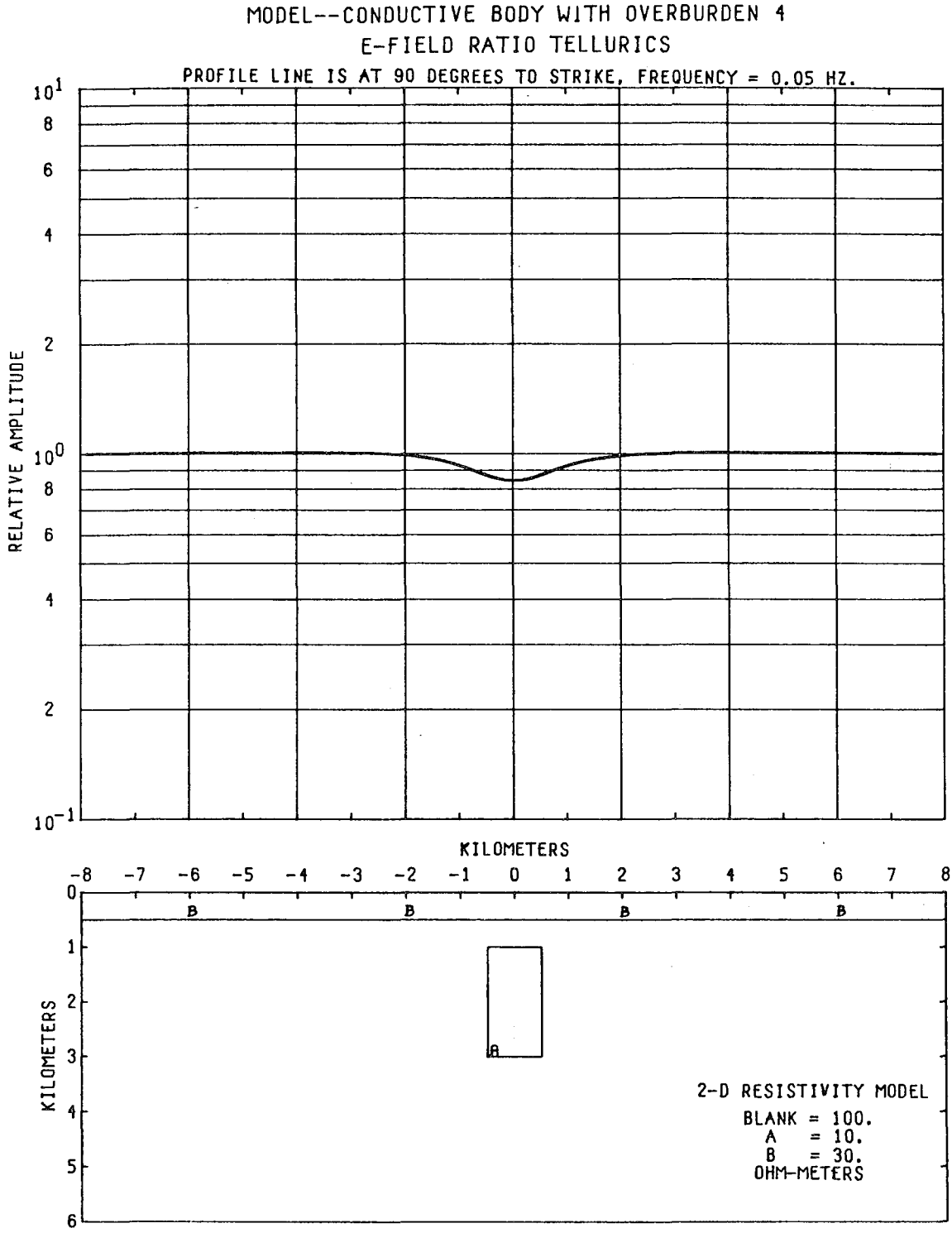
MODEL--CONDUCTIVE BODY WITH OVERBURDEN 4
E-FIELD RATIO TELLURICS
PROFILE LINE IS AT 90 DEGREES TO STRIKE, FREQUENCY = 0.05 HZ.
RELATIVE AMPLITUDE
10^1
8
6
4
2
10^0
8
6
4
2
10^-1
KILOMETERS
-8 -7 -6 -5 -4 -3 -2 -1 0 1 2 3 4 5 6 7 8
B
B
B
B
KILOMETERS
1
2
3
4
5
6
A
2-D RESISTIVITY MODEL
BLANK = 100.
A = 10.
B = 30.
OHM-METERS

Figure I-A31

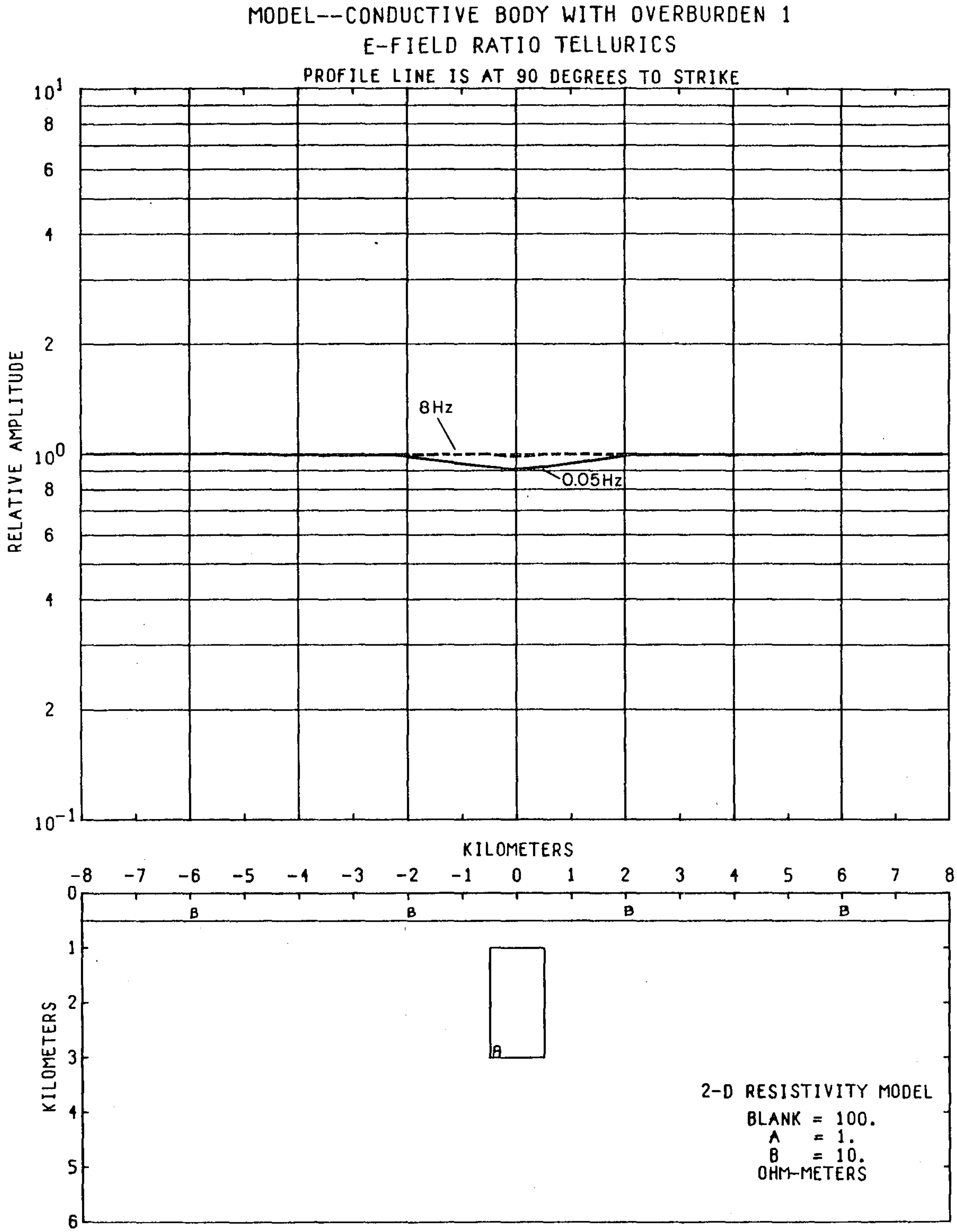

Figure I-A32

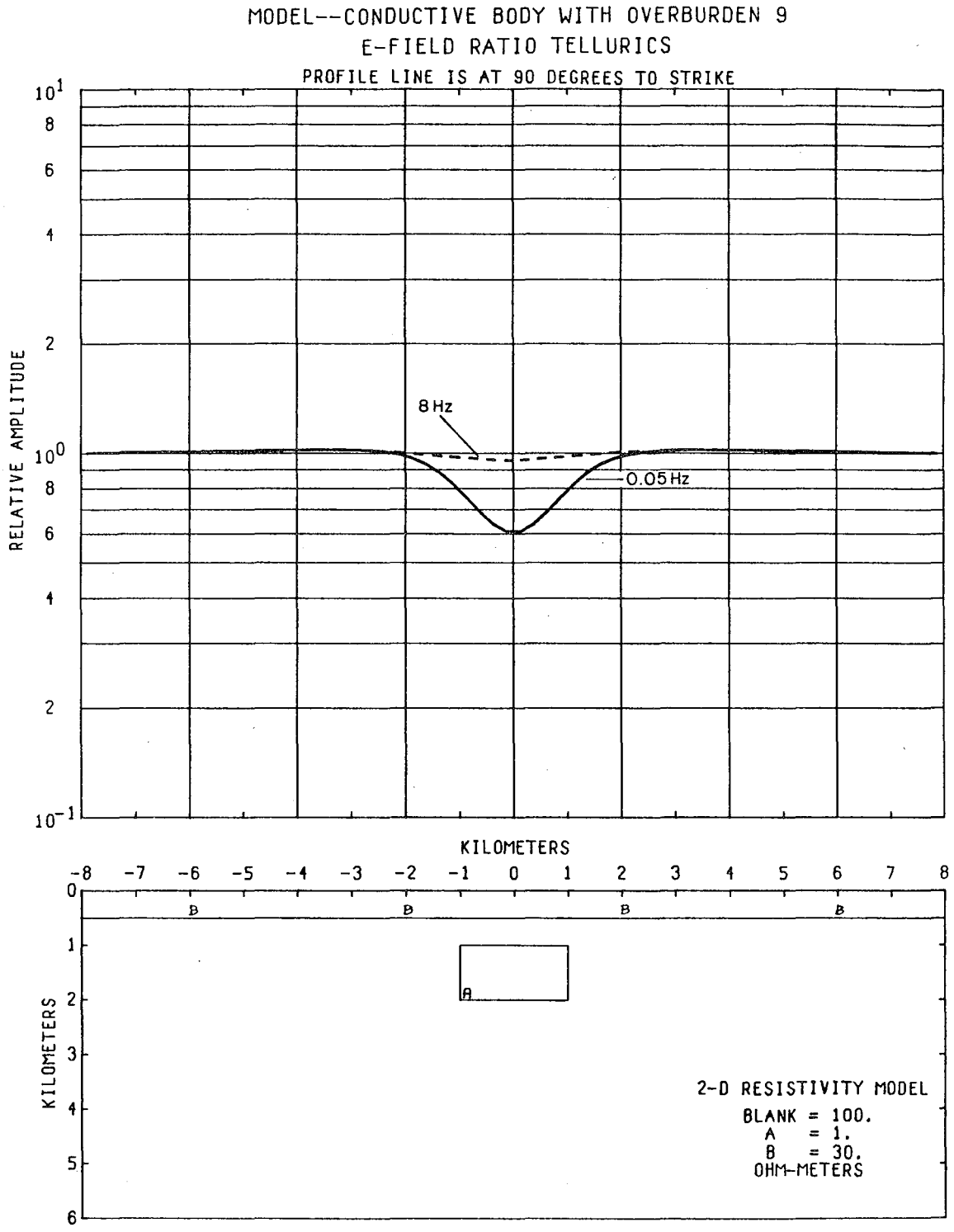
MODEL--CONDUCTIVE BODY WITH OVERBURDEN 9
E-FIELD RATIO TELLURICS
PROFILE LINE IS AT 90 DEGREES TO STRIKE
RELATIVE AMPLITUDE
8 Hz
0.05 Hz
KILOMETERS
KILOMETERS
2-D RESISTIVITY MODEL
BLANK = 100.
A = 1.
B = 30.
OHM-METERS

Figure I-A33

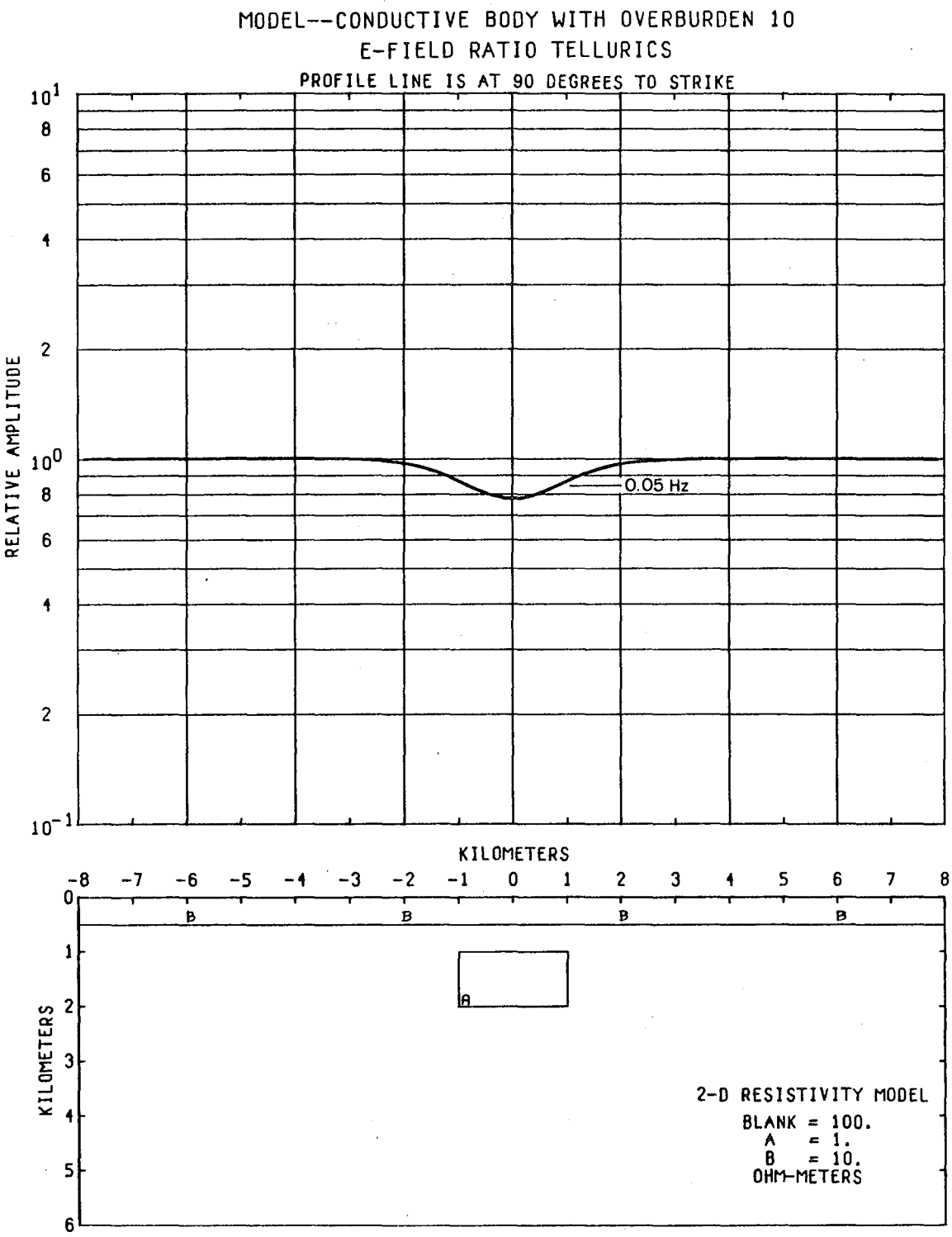

Figure I-A34

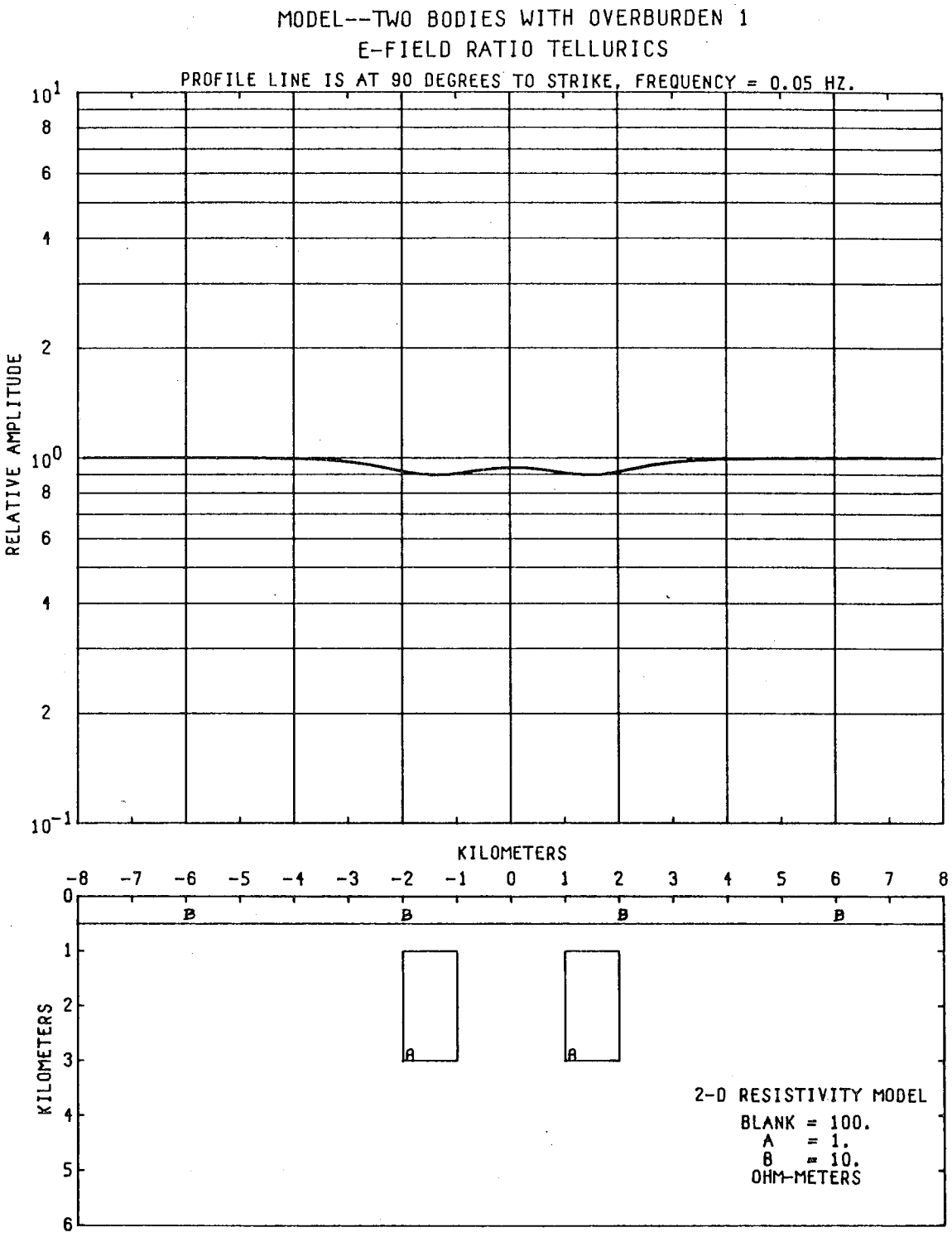
MODEL--TWO BODIES WITH OVERBURDEN 1
E-FIELD RATIO TELLURICS
PROFILE LINE IS AT 90 DEGREES TO STRIKE, FREQUENCY = 0.05 HZ.
RELATIVE AMPLITUDE
KILOMETERS
KILOMETERS
2-D RESISTIVITY MODEL
BLANK = 100.
A = 1.
B = 10.
OHM-METERS

Figure I-A35

APPENDIX I-B

E-Field Ratio Telluric Anomalies at 0.05 and 8 Hz over a Buried Conductive Body Varying the Incident Field Polarization Direction and Ellipticity

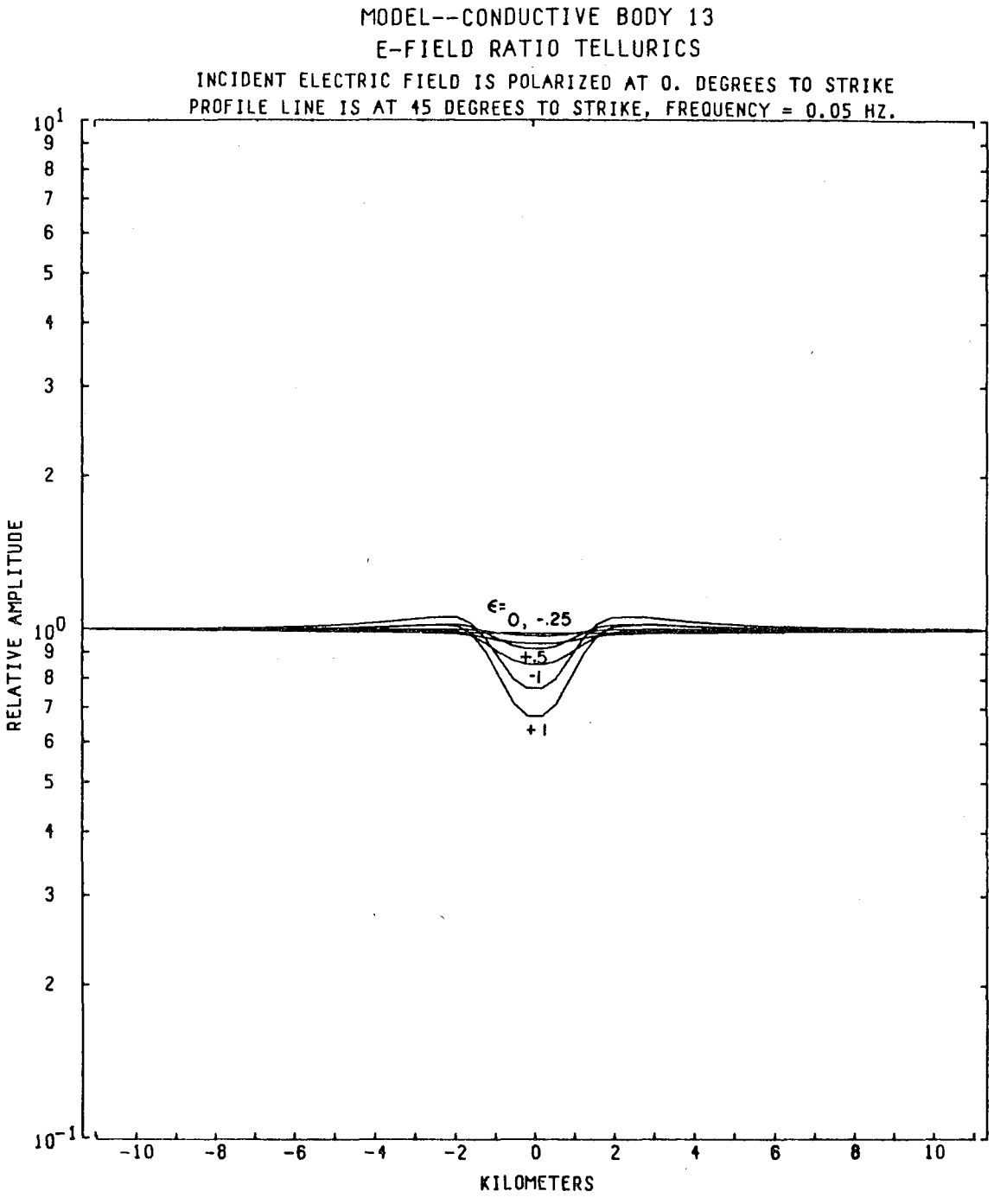
MODEL--CONDUCTIVE BODY 13
E-FIELD RATIO TELLURICS
INCIDENT ELECTRIC FIELD IS POLARIZED AT 0. DEGREES TO STRIKE
PROFILE LINE IS AT 45 DEGREES TO STRIKE, FREQUENCY = 0.05 HZ.
RELATIVE AMPLITUDE
KILOMETERS
ϵ= 0, -.25
+.5
-1
+1

Figure I-B1

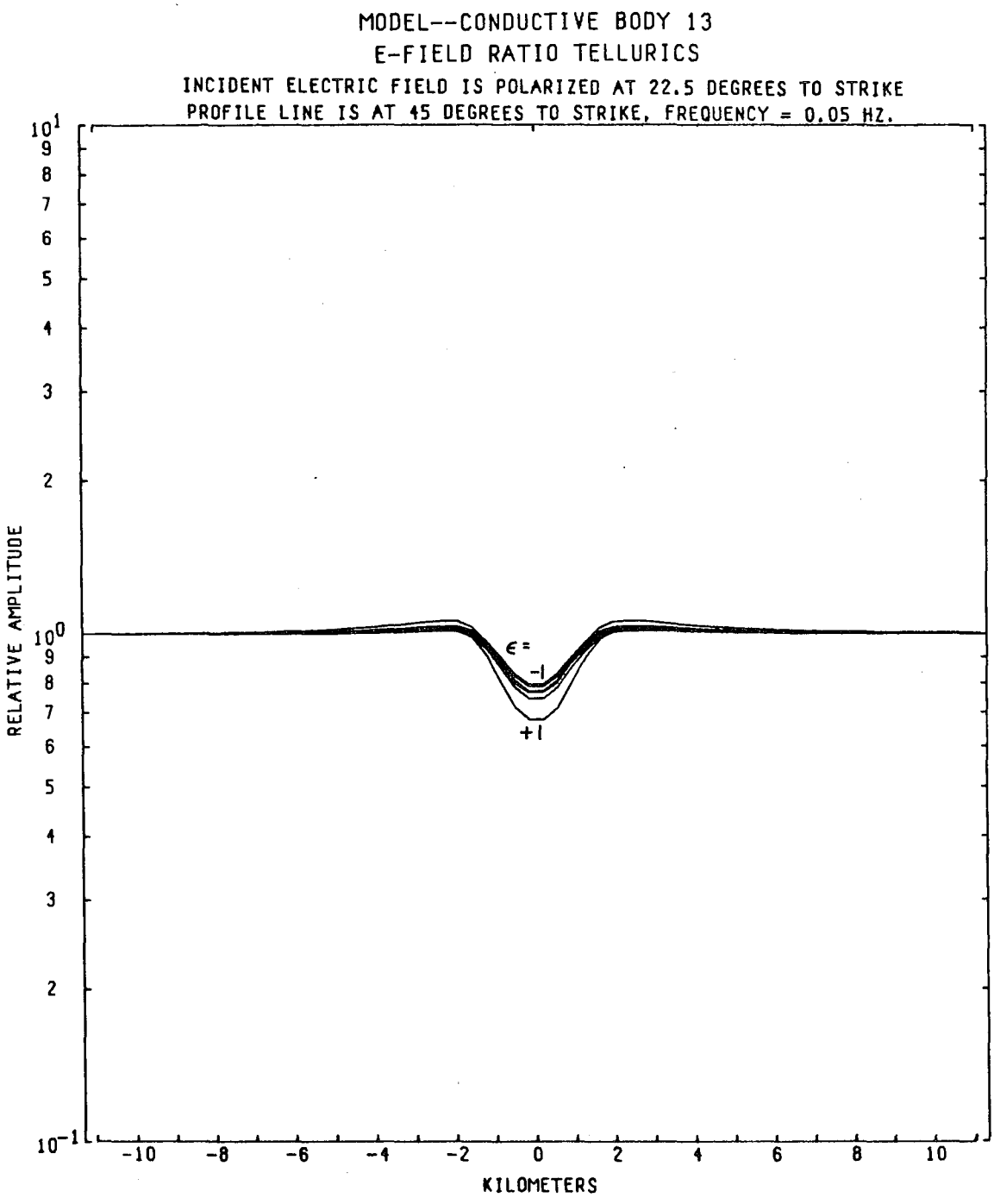

Figure I-B2

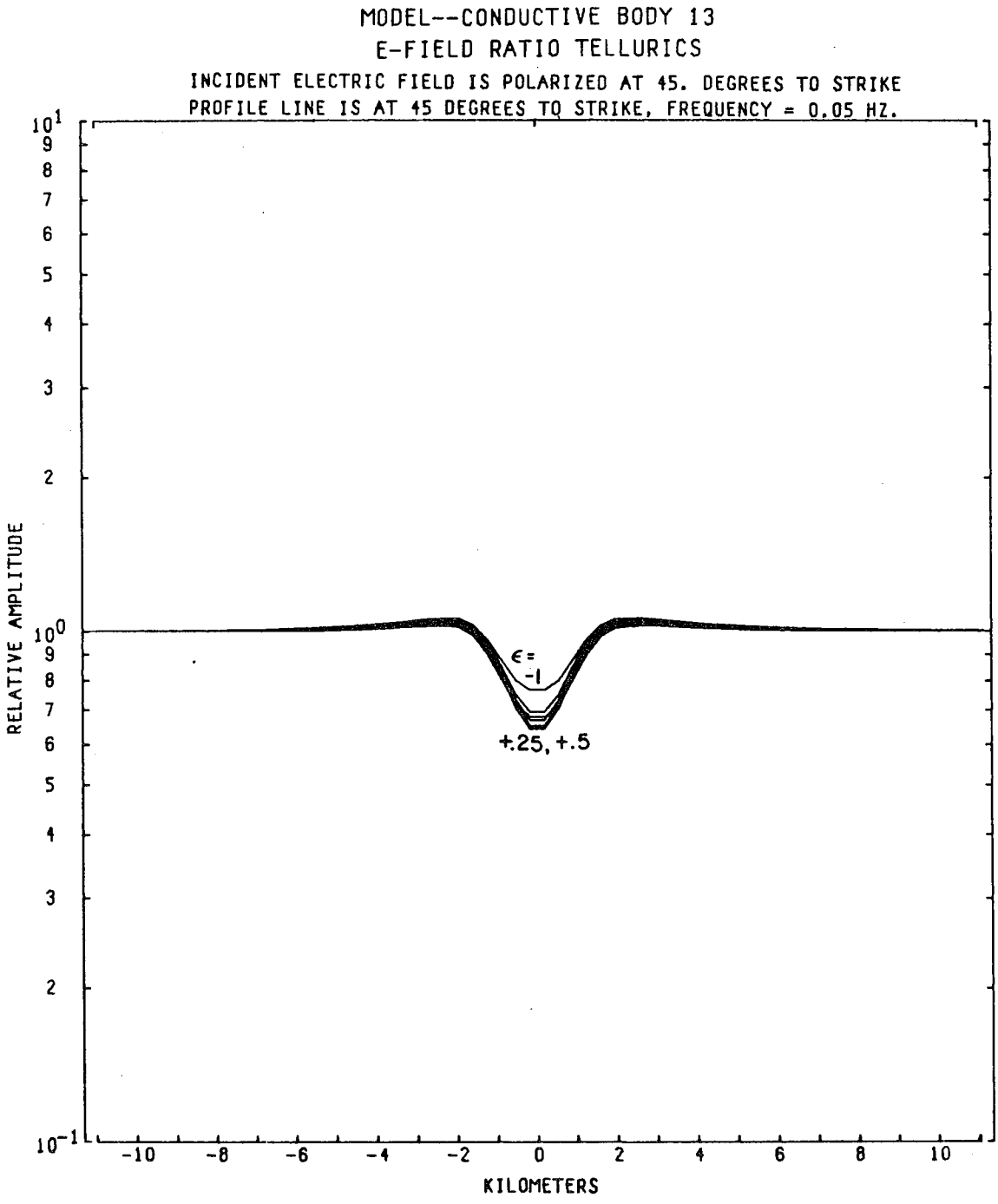
MODEL--CONDUCTIVE BODY 13
E-FIELD RATIO TELLURICS
INCIDENT ELECTRIC FIELD IS POLARIZED AT 45. DEGREES TO STRIKE
PROFILE LINE IS AT 45 DEGREES TO STRIKE, FREQUENCY = 0.05 HZ.
RELATIVE AMPLITUDE
KILOMETERS
ϵ = -1
+.25, +.5

Figure I-B3

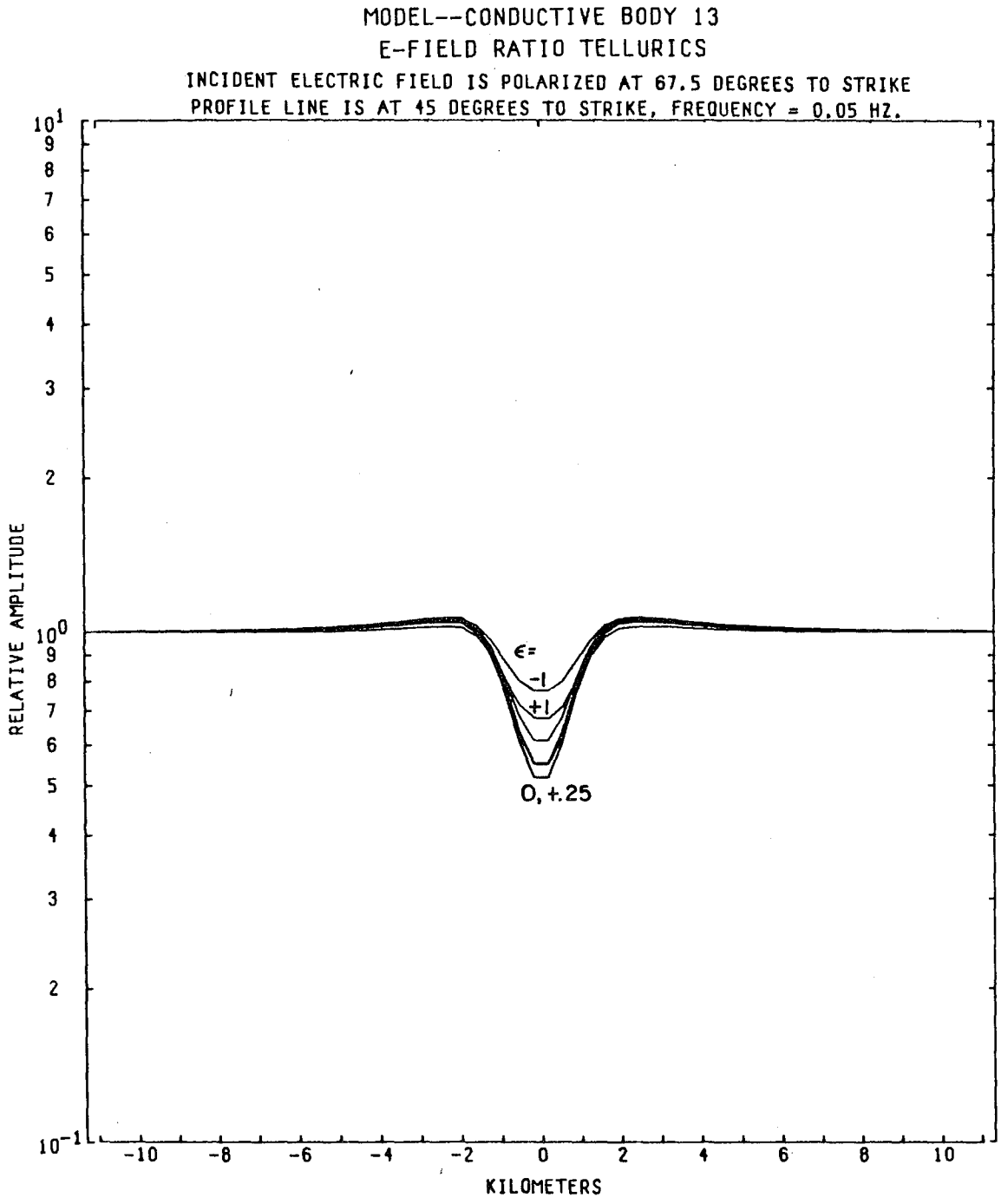

Figure I-B4

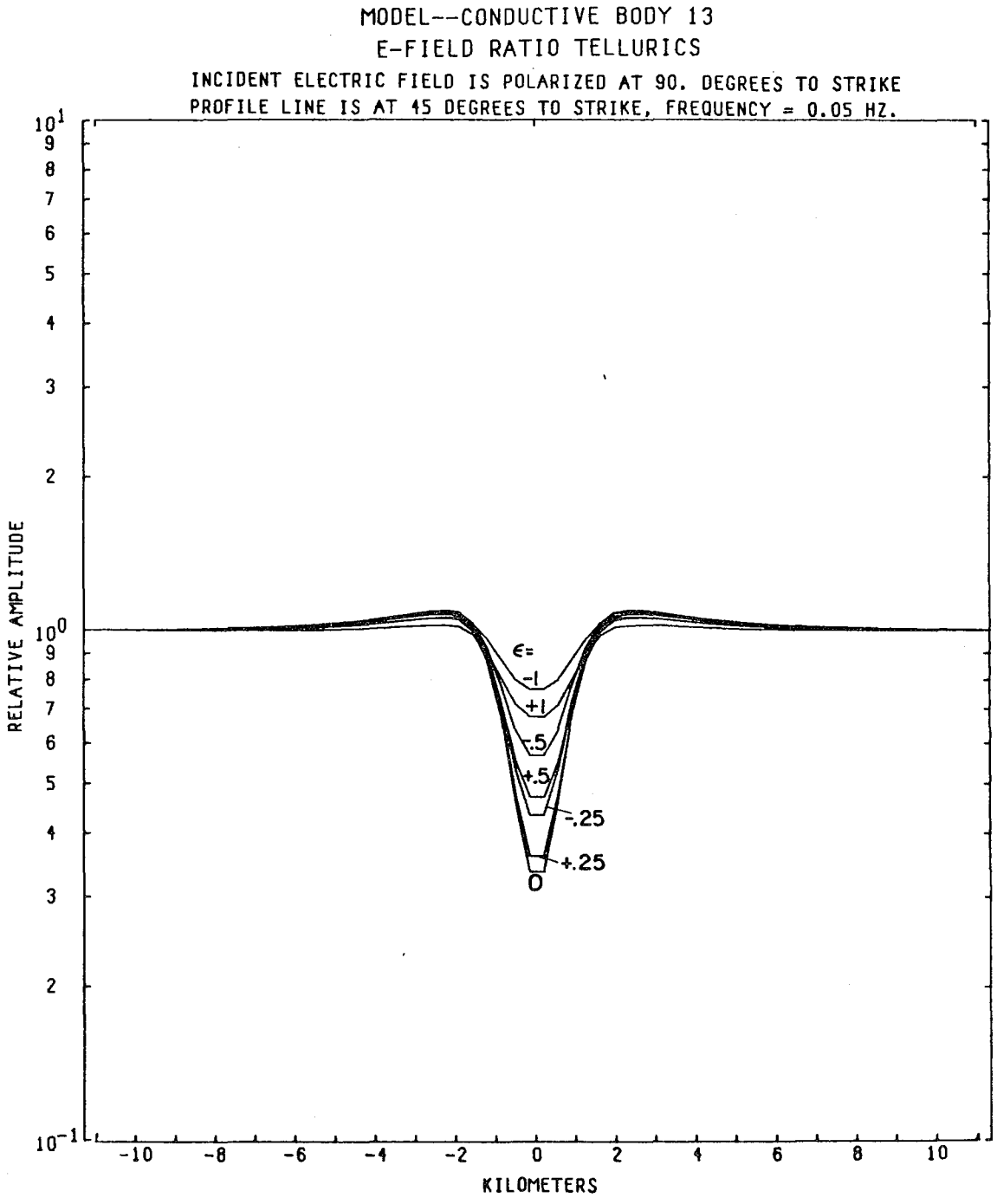
MODEL--CONDUCTIVE BODY 13
E-FIELD RATIO TELLURICS
INCIDENT ELECTRIC FIELD IS POLARIZED AT 90. DEGREES TO STRIKE
PROFILE LINE IS AT 45 DEGREES TO STRIKE, FREQUENCY = 0.05 HZ.
RELATIVE AMPLITUDE
KILOMETERS
ϵ=
-1
+1
-.5
+.5
-.25
+.25
0

Figure I-B5

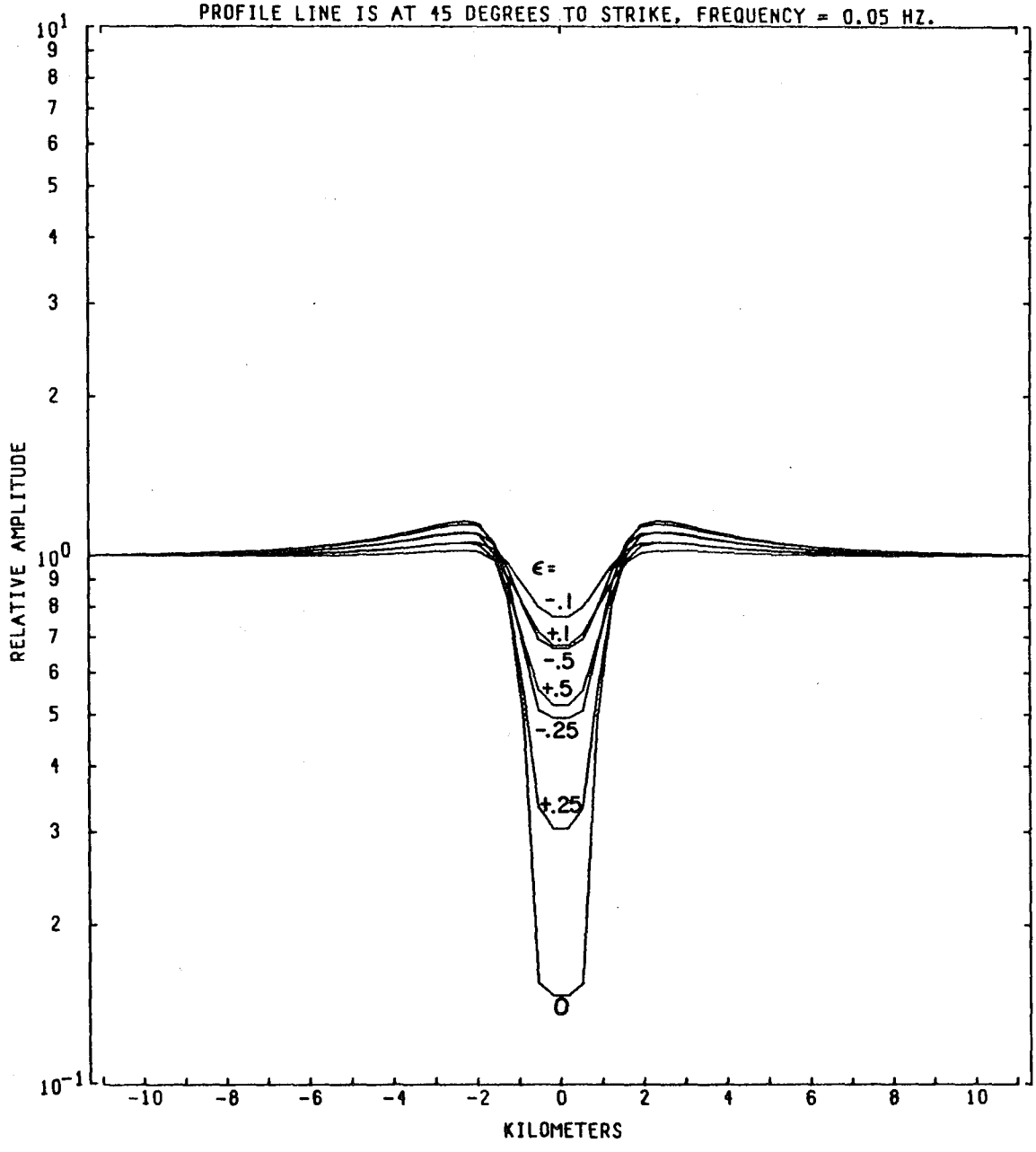
MODEL--CONDUCTIVE BODY 13
E-FIELD RATIO TELLURICS
INCIDENT ELECTRIC FIELD IS POLARIZED AT 112.5 DEGREES TO STRIKE
PROFILE LINE IS AT 45 DEGREES TO STRIKE, FREQUENCY = 0.05 HZ.
RELATIVE AMPLITUDE
KILOMETERS
ε=
-.1
+.1
-.5
+.5
-.25
+.25
0

Figure I-B6

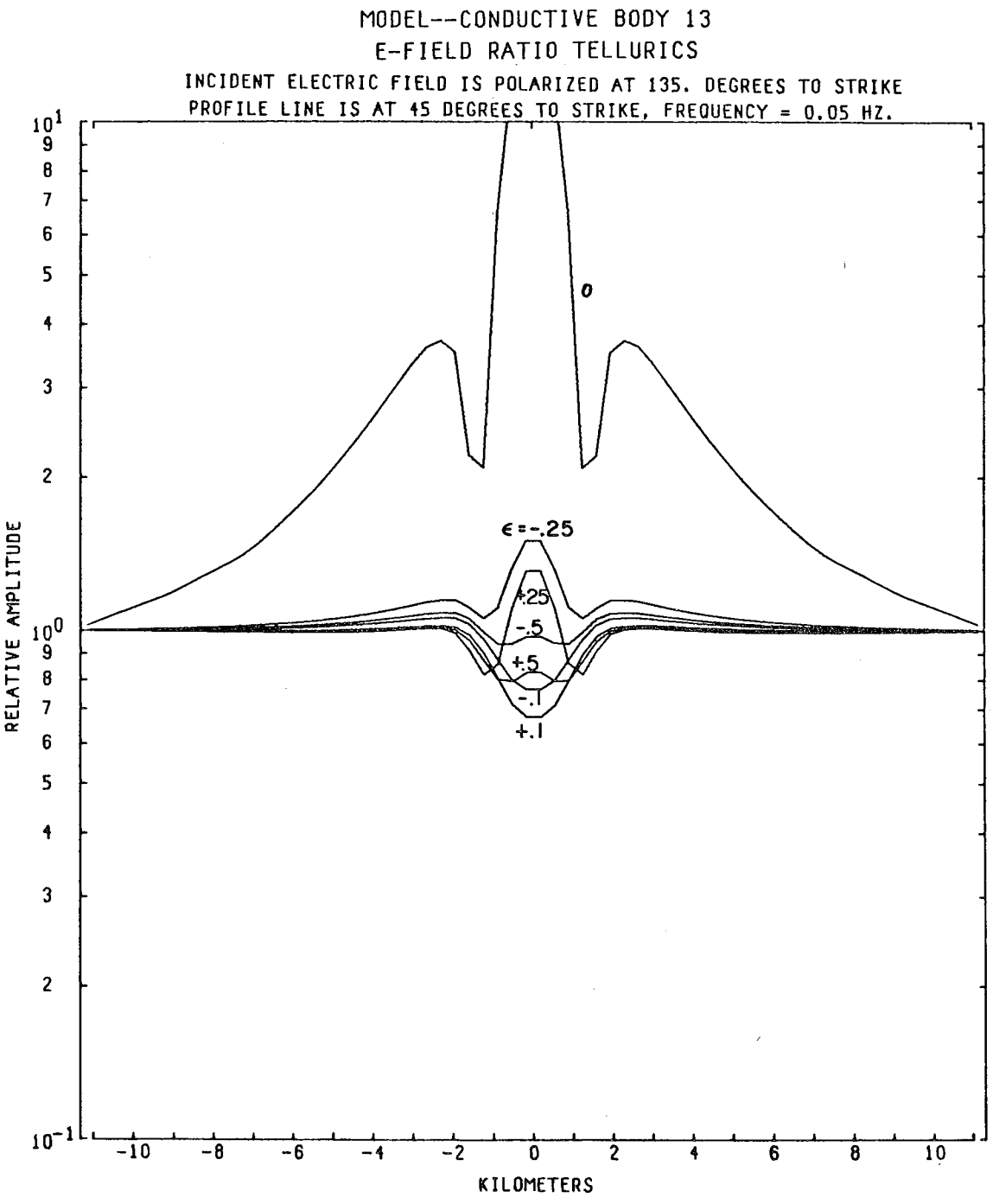
MODEL--CONDUCTIVE BODY 13
E-FIELD RATIO TELLURICS
INCIDENT ELECTRIC FIELD IS POLARIZED AT 135. DEGREES TO STRIKE
PROFILE LINE IS AT 45 DEGREES TO STRIKE, FREQUENCY = 0.05 HZ.
RELATIVE AMPLITUDE
KILOMETERS
0
ϵ=-.25
+.25
-.5
+.5
-.1
+.1

Figure I-B7

MODEL--CONDUCTIVE BODY 13
E-FIELD RATIO TELLURICS
INCIDENT ELECTRIC FIELD IS POLARIZED AT 157.5 DEGREES TO STRIKE
PROFILE LINE IS AT 45 DEGREES TO STRIKE, FREQUENCY = 0.05 HZ.

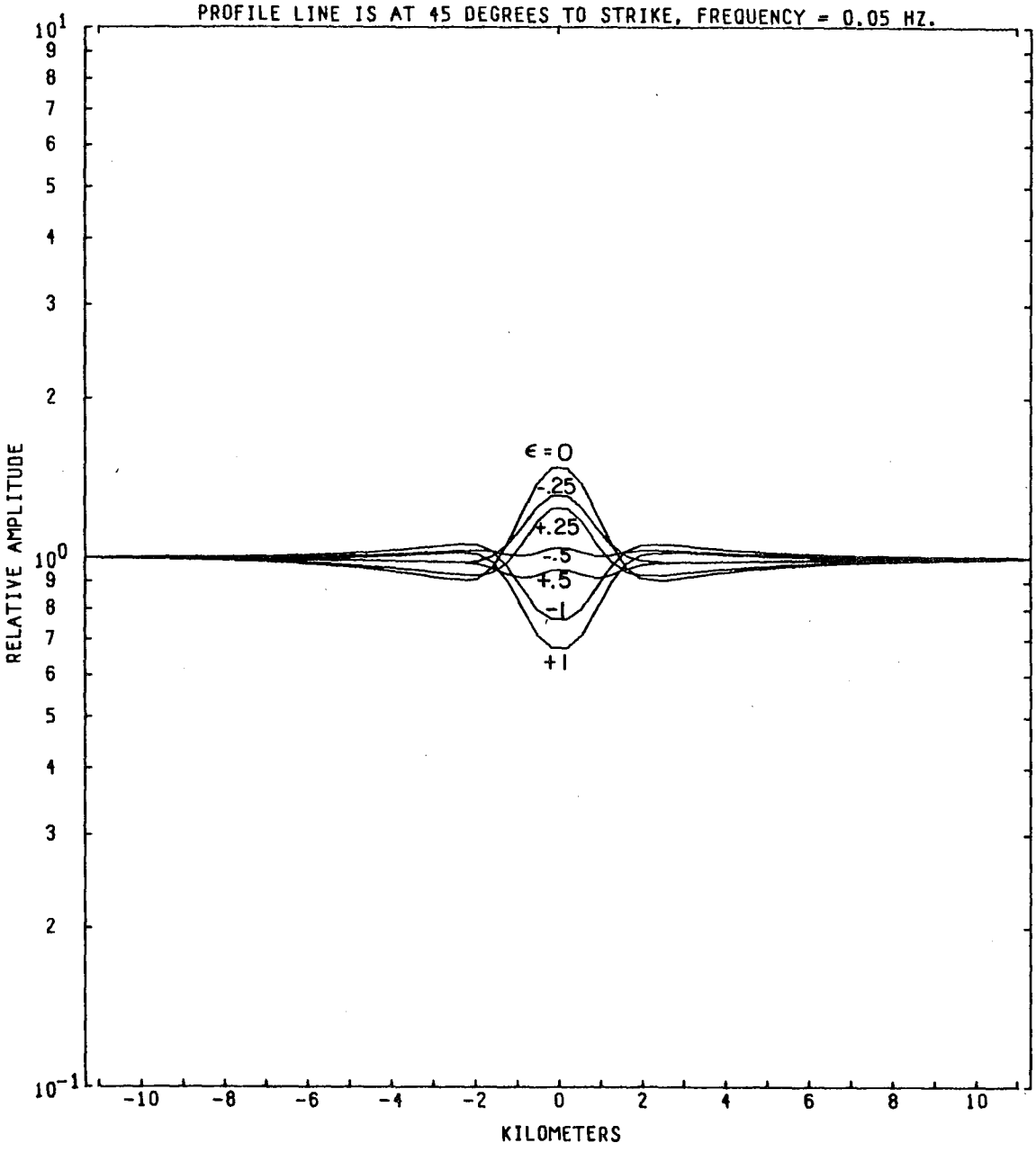

Figure I-B8

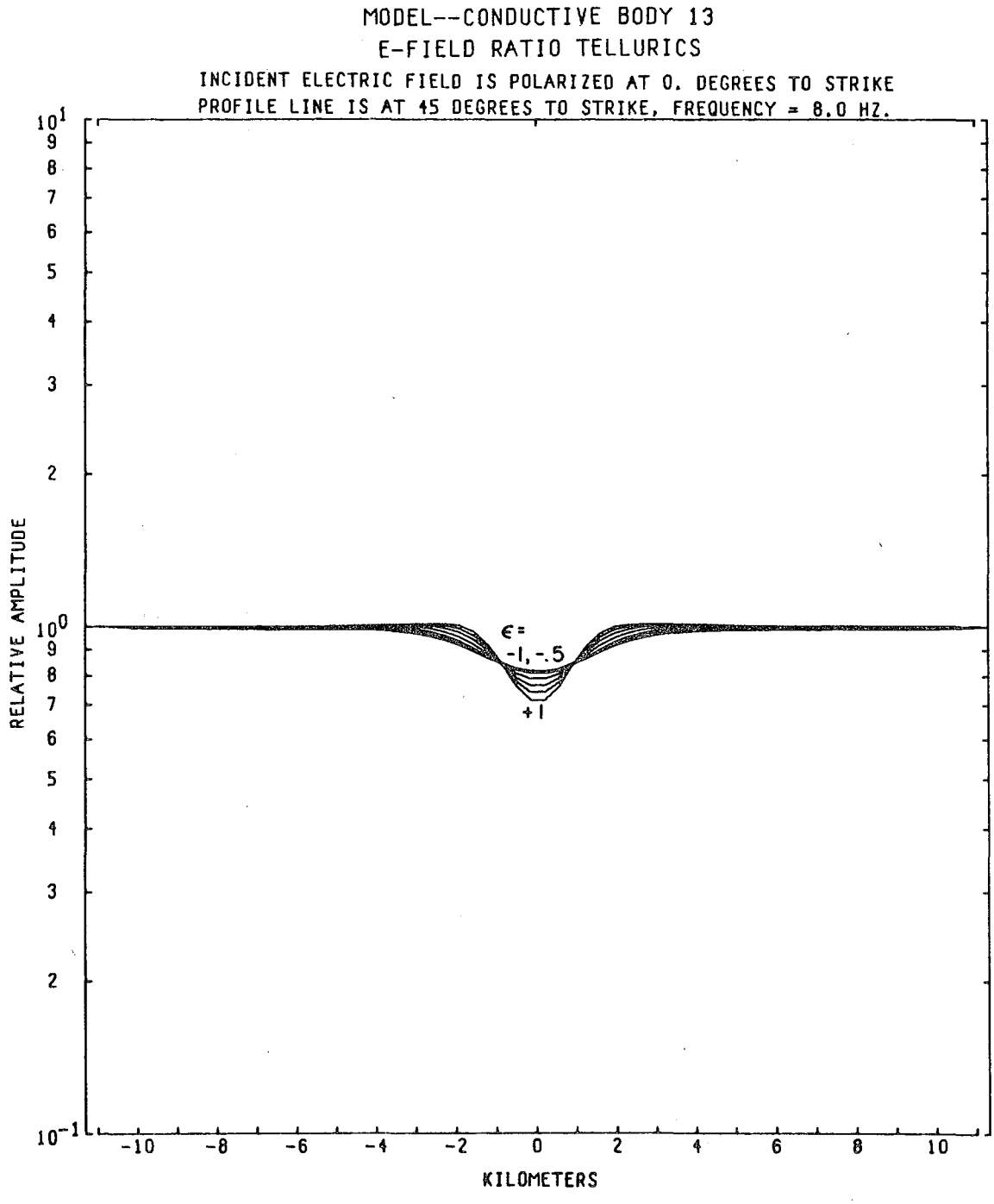
MODEL--CONDUCTIVE BODY 13
E-FIELD RATIO TELLURICS
INCIDENT ELECTRIC FIELD IS POLARIZED AT 0. DEGREES TO STRIKE
PROFILE LINE IS AT 45 DEGREES TO STRIKE, FREQUENCY = 8.0 HZ.
RELATIVE AMPLITUDE
KILOMETERS
ε =
-1, -.5
+1

Figure I-B9

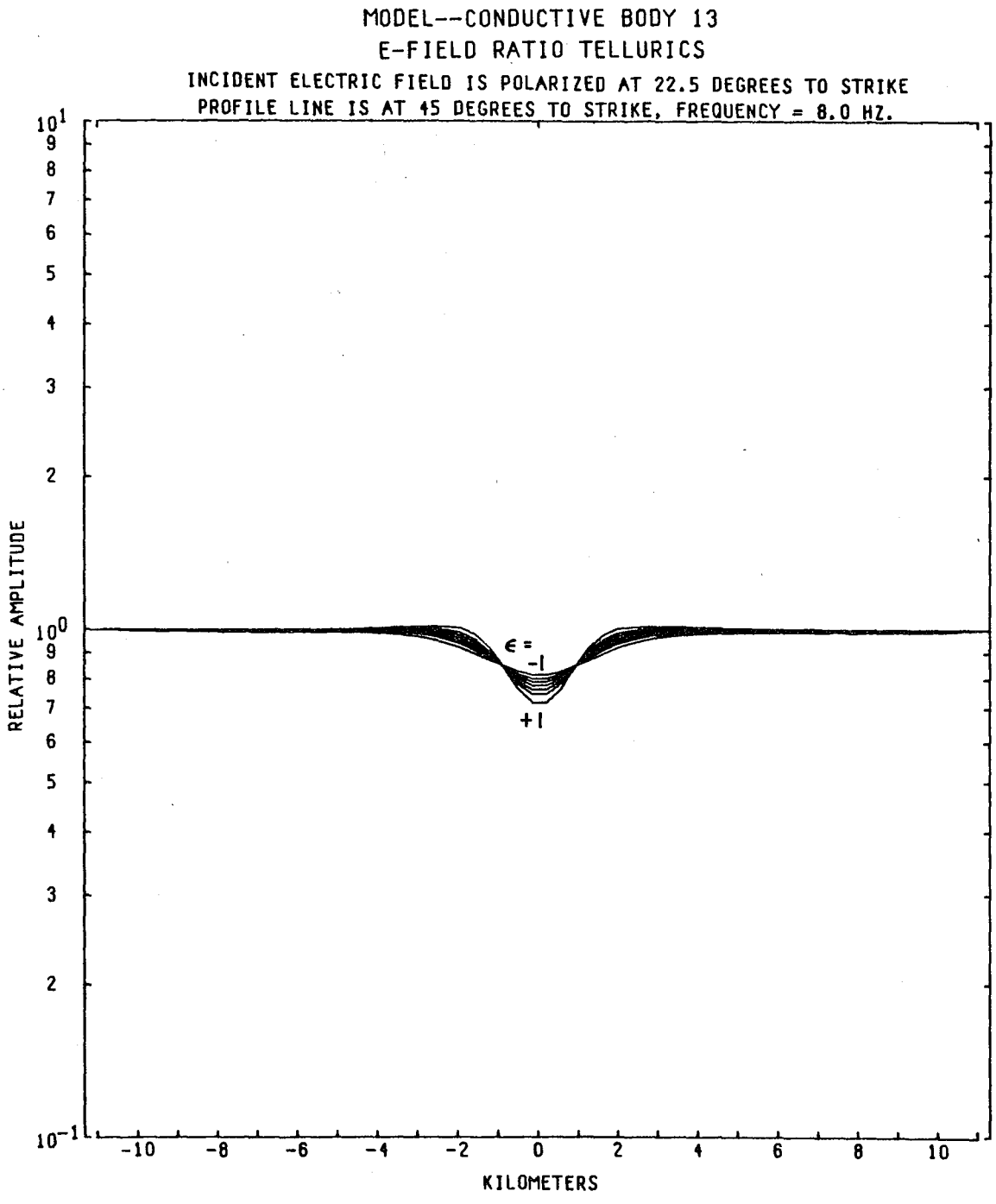

Figure I-B10

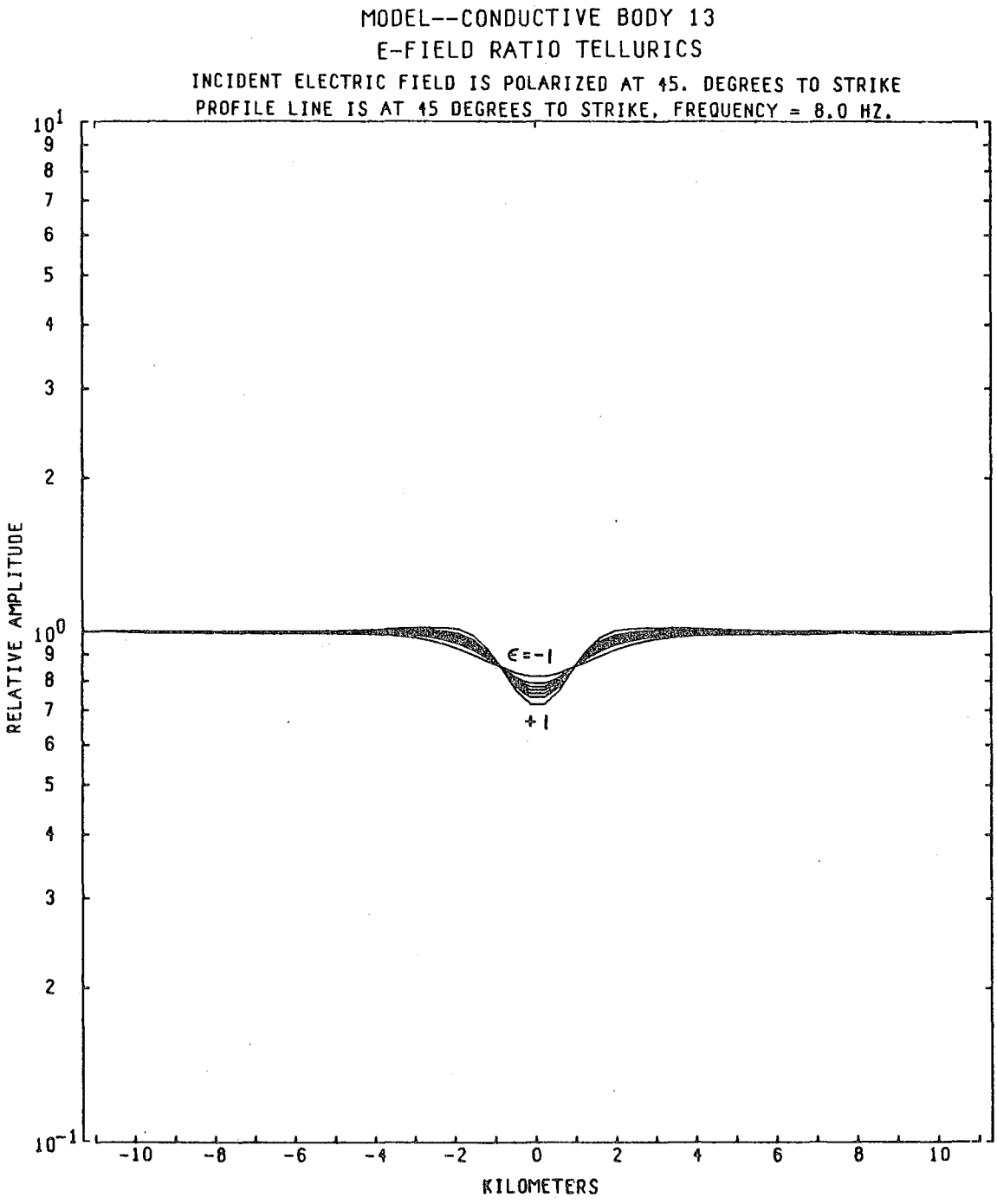
MODEL--CONDUCTIVE BODY 13
E-FIELD RATIO TELLURICS
INCIDENT ELECTRIC FIELD IS POLARIZED AT 45. DEGREES TO STRIKE
PROFILE LINE IS AT 45 DEGREES TO STRIKE, FREQUENCY = 8.0 HZ.
RELATIVE AMPLITUDE
10^1
9
8
7
6
5
4
3
2
10^0
9
8
7
6
5
4
3
2
10^{-1}
ϵ=-1
+1
-10
-8
-6
-4
-2
0
2
4
6
8
10
KILOMETERS

Figure I-B11

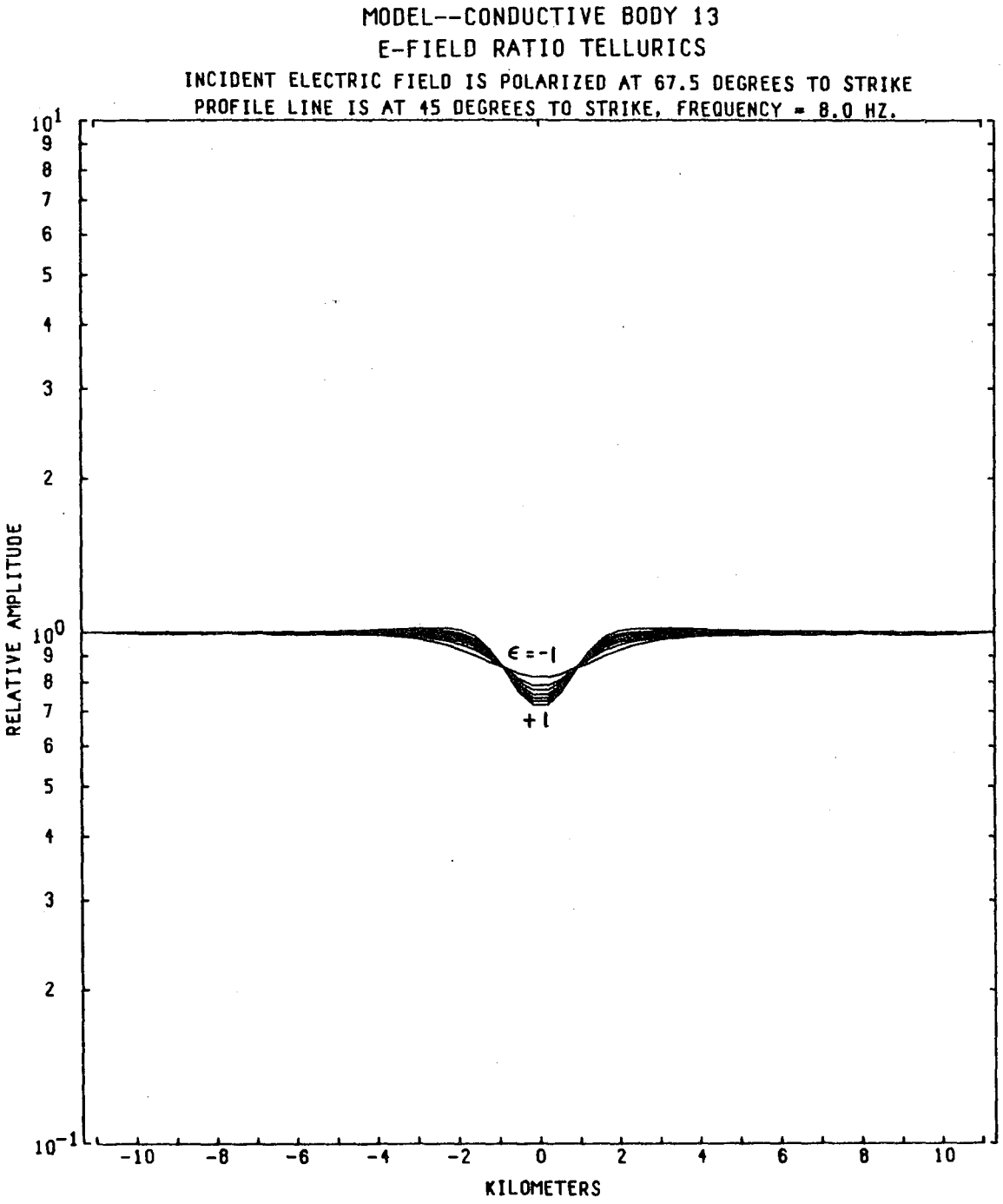
MODEL--CONDUCTIVE BODY 13
E-FIELD RATIO TELLURICS
INCIDENT ELECTRIC FIELD IS POLARIZED AT 67.5 DEGREES TO STRIKE
PROFILE LINE IS AT 45 DEGREES TO STRIKE, FREQUENCY = 8.0 HZ.
RELATIVE AMPLITUDE
10^1
9
8
7
6
5
4
3
2
10^0
9
8
7
6
5
4
3
2
10^{-1}
$\epsilon = -1$
$+1$
-10
-8
-6
-4
-2
0
2
4
6
8
10
KILOMETERS

Figure I-B12

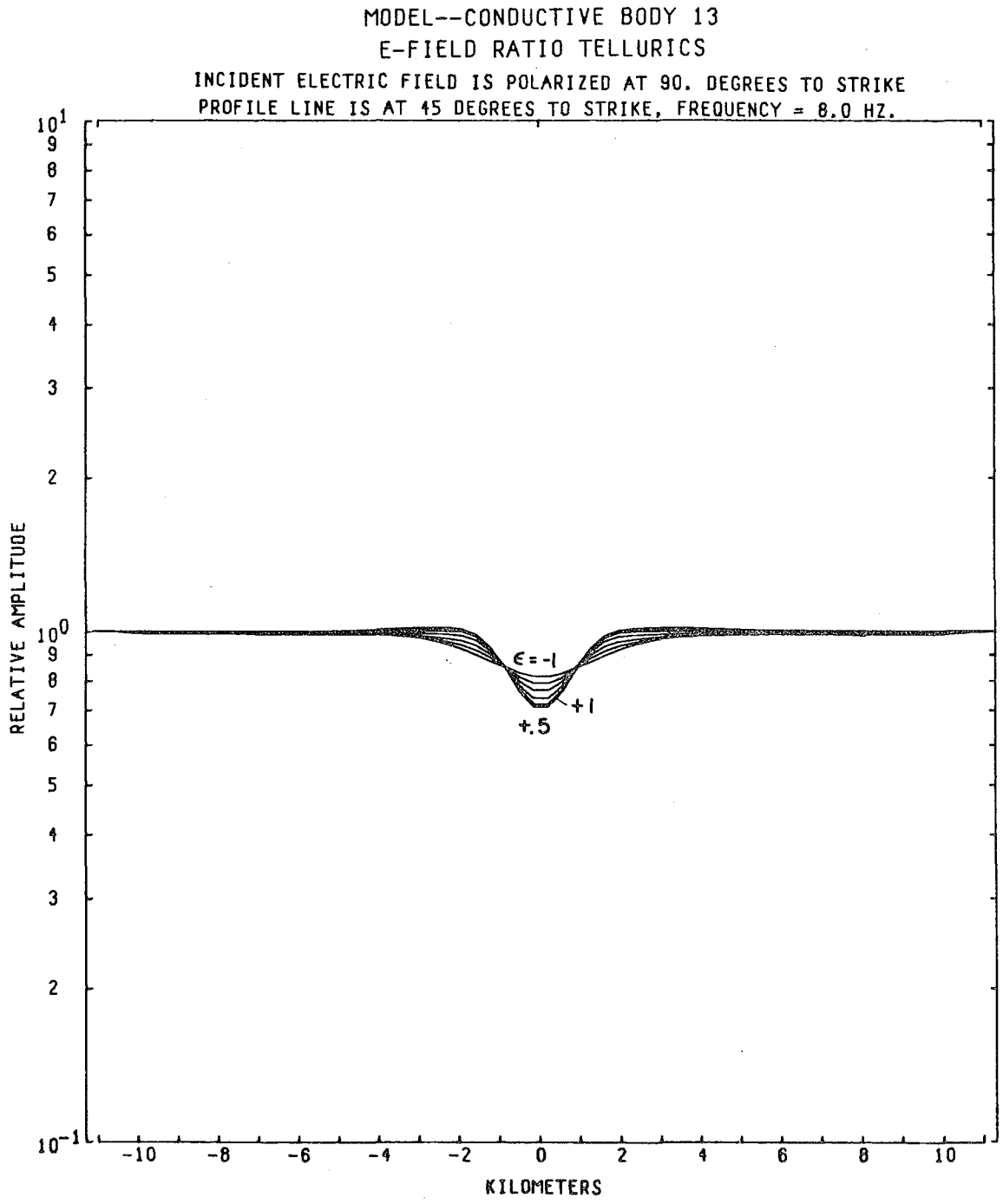
MODEL--CONDUCTIVE BODY 13
E-FIELD RATIO TELLURICS
INCIDENT ELECTRIC FIELD IS POLARIZED AT 90. DEGREES TO STRIKE
PROFILE LINE IS AT 45 DEGREES TO STRIKE, FREQUENCY = 8.0 HZ.
RELATIVE AMPLITUDE
KILOMETERS
ϵ = -1
+1
+.5

Figure I-B13

MODEL--CONDUCTIVE BODY 13
E-FIELD RATIO TELLURICS
INCIDENT ELECTRIC FIELD IS POLARIZED AT 112.5 DEGREES TO STRIKE
PROFILE LINE IS AT 45 DEGREES TO STRIKE, FREQUENCY = 8.0 HZ.

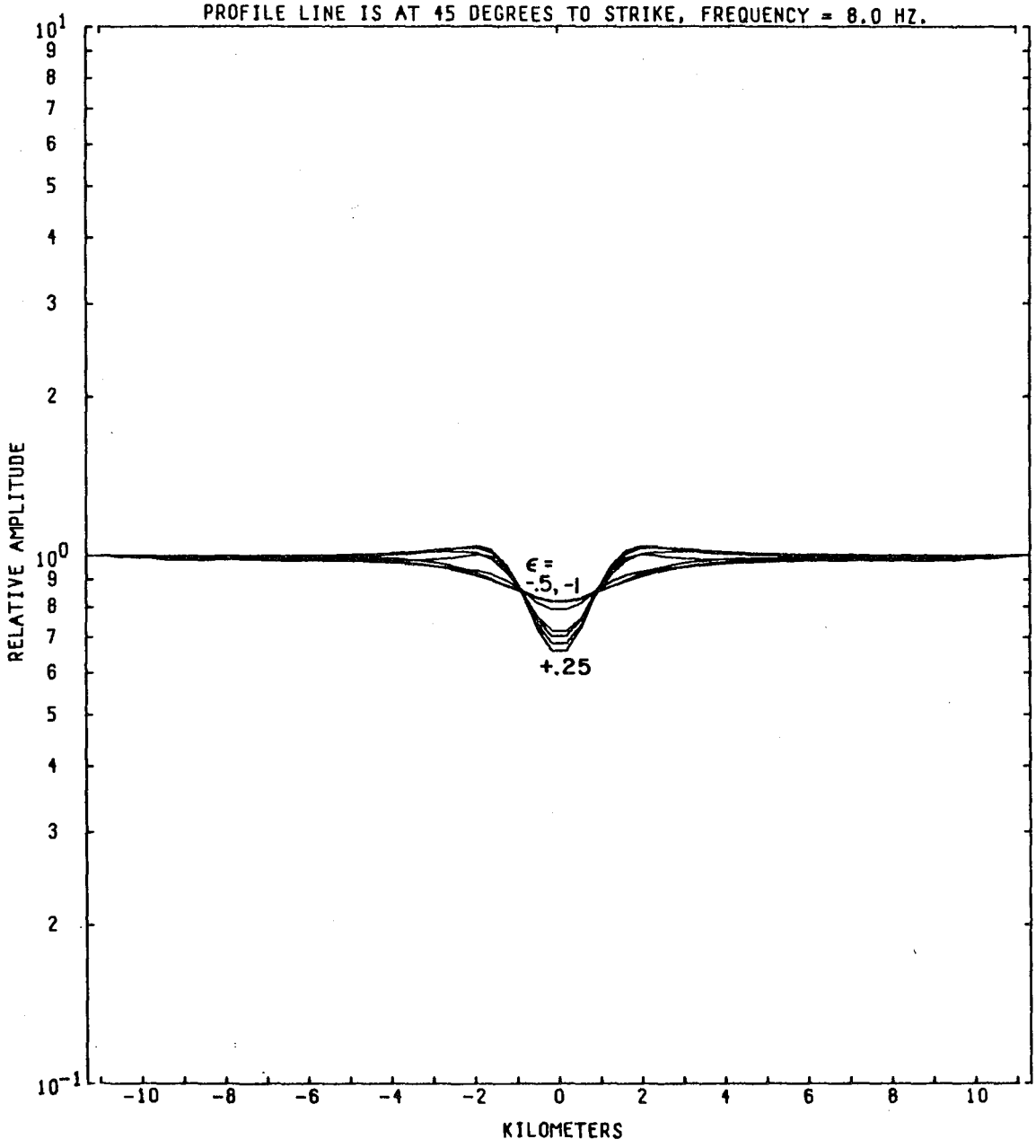

Figure I-B14

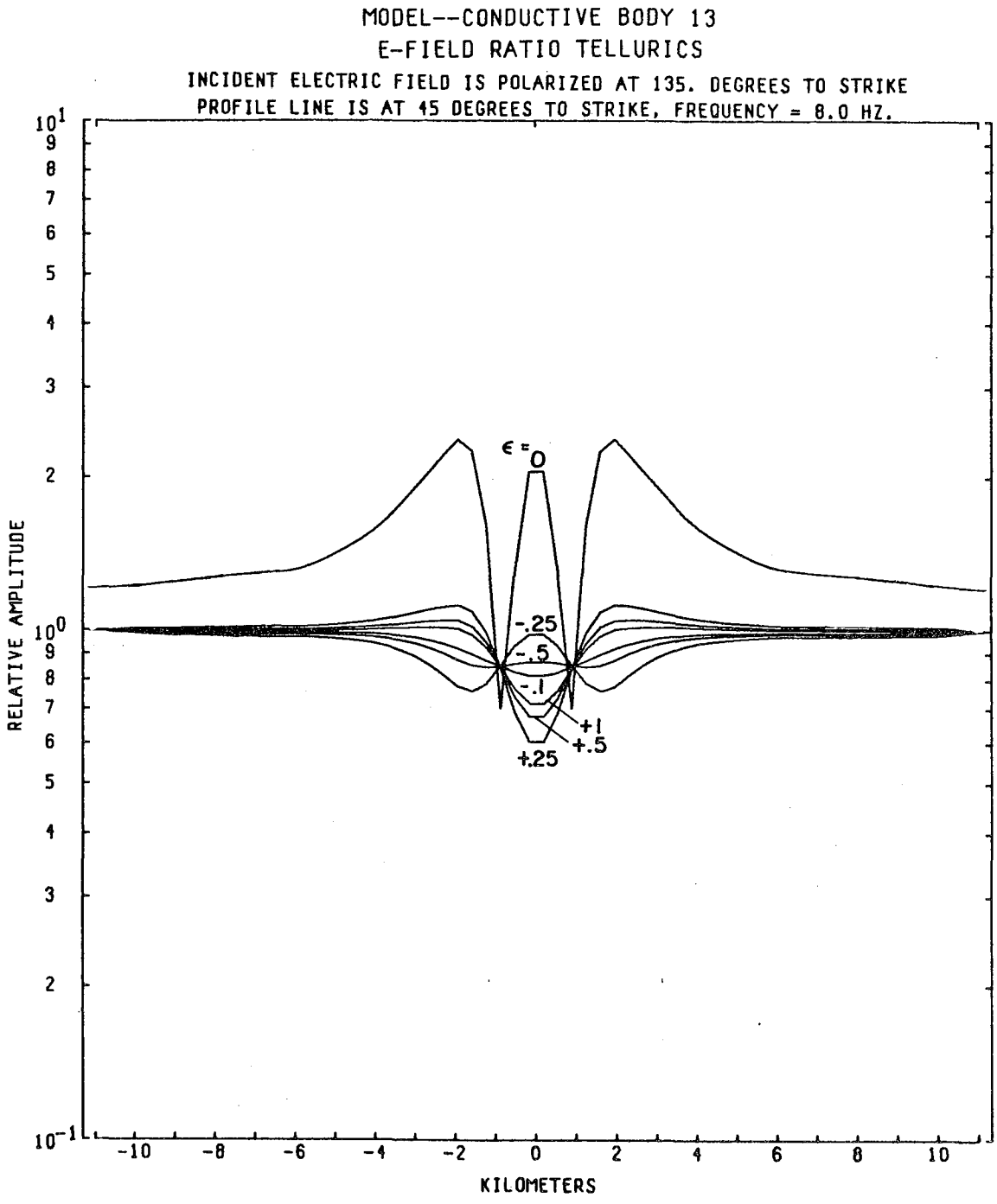
MODEL--CONDUCTIVE BODY 13
E-FIELD RATIO TELLURICS
INCIDENT ELECTRIC FIELD IS POLARIZED AT 135. DEGREES TO STRIKE
PROFILE LINE IS AT 45 DEGREES TO STRIKE, FREQUENCY = 8.0 HZ.
RELATIVE AMPLITUDE
KILOMETERS
ε = 0
-.25
-.5
-.1
+1
+.5
+.25

Figure I-B15

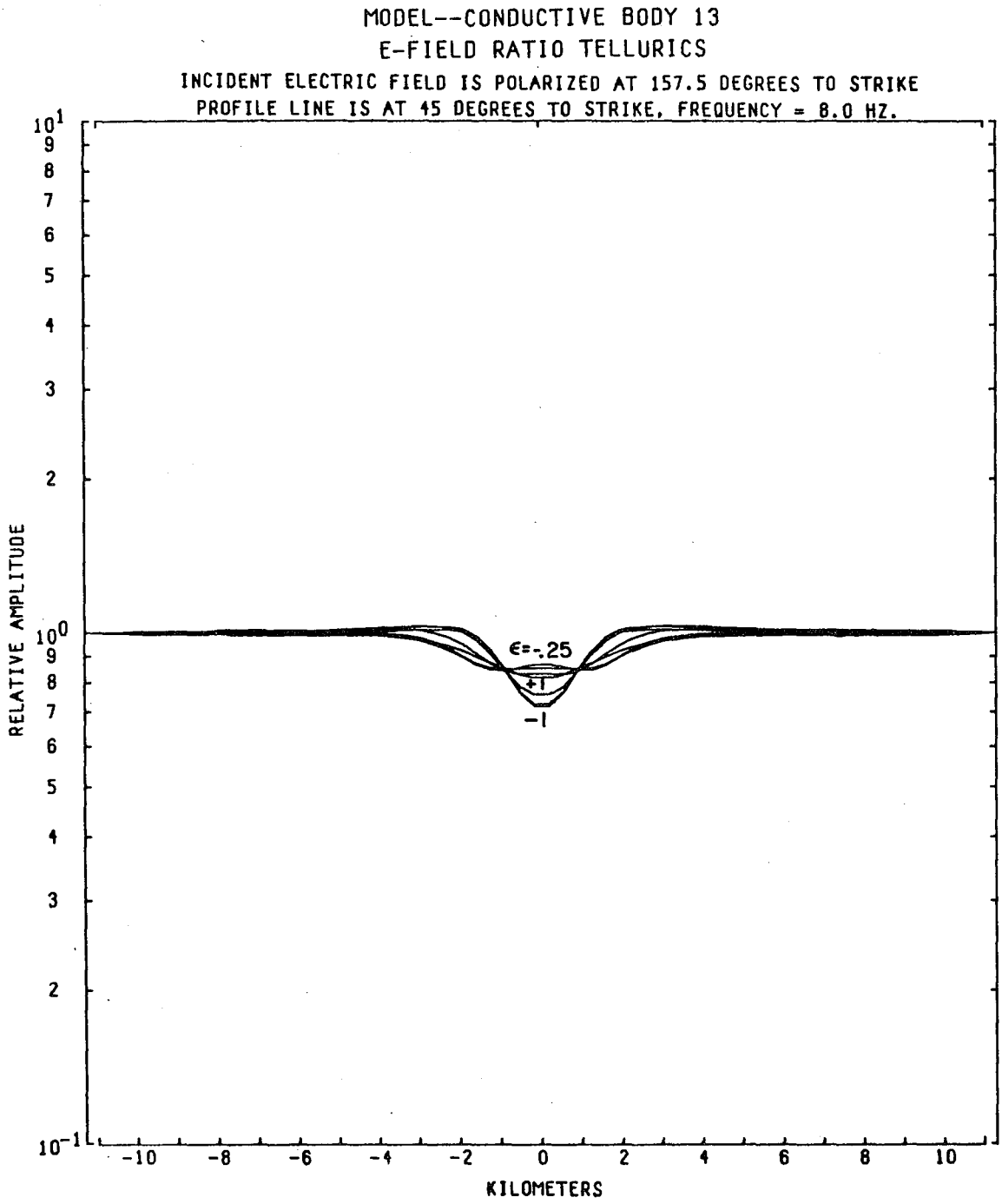

Figure I-B16

(for numbering sequence only)

APPENDIX I-C

E-Field Ratio Telluric Anomalies at 0.05 and 8 Hz over a Vertical Contact Varying the Incident Field Polarization Direction and Ellipticity

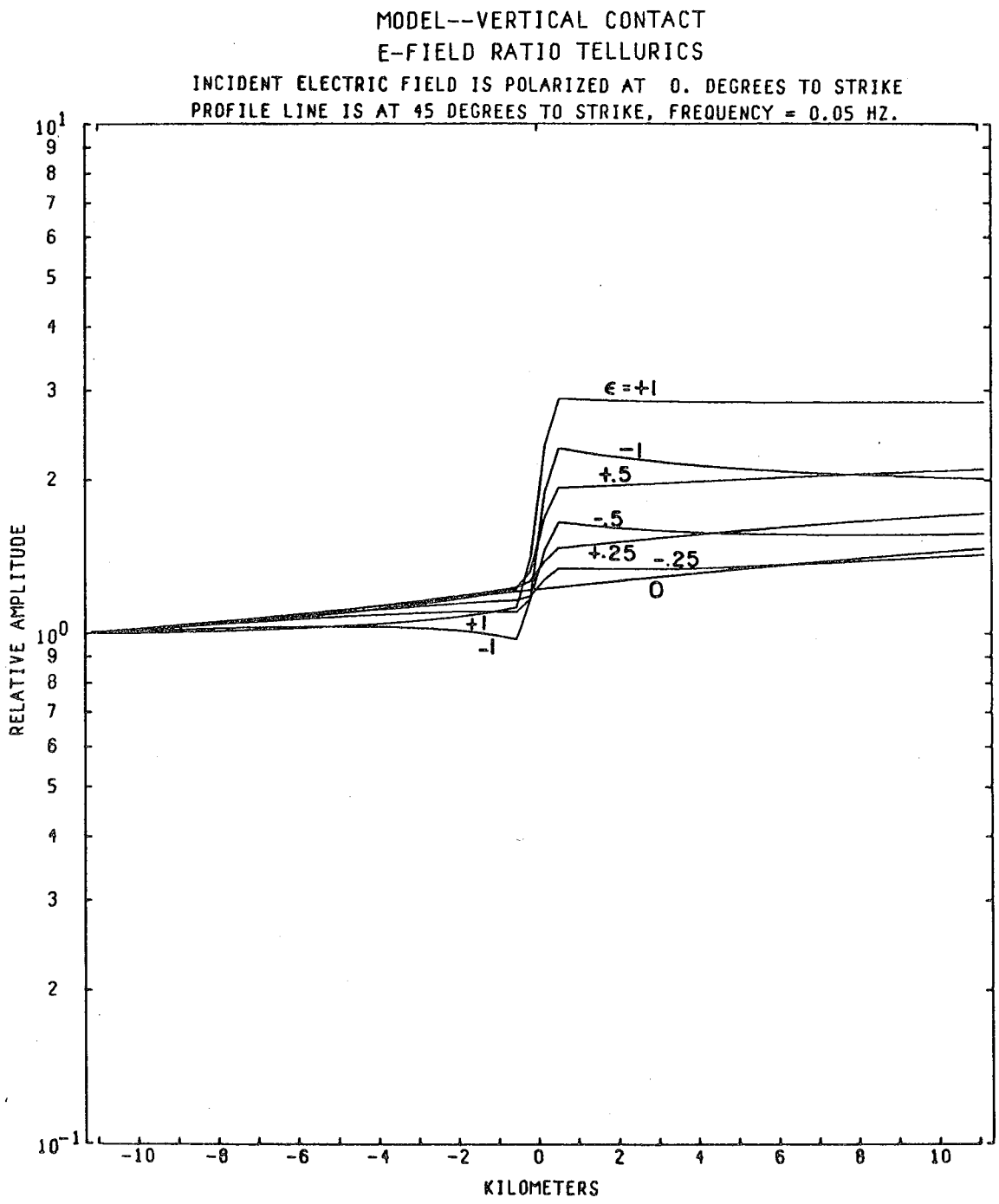
MODEL--VERTICAL CONTACT
E-FIELD RATIO TELLURICS
INCIDENT ELECTRIC FIELD IS POLARIZED AT 0. DEGREES TO STRIKE
PROFILE LINE IS AT 45 DEGREES TO STRIKE, FREQUENCY = 0.05 HZ.
RELATIVE AMPLITUDE
KILOMETERS
ϵ = +1
-1
+.5
-.5
+.25
-.25
0
+1
-1

Figure I-C1

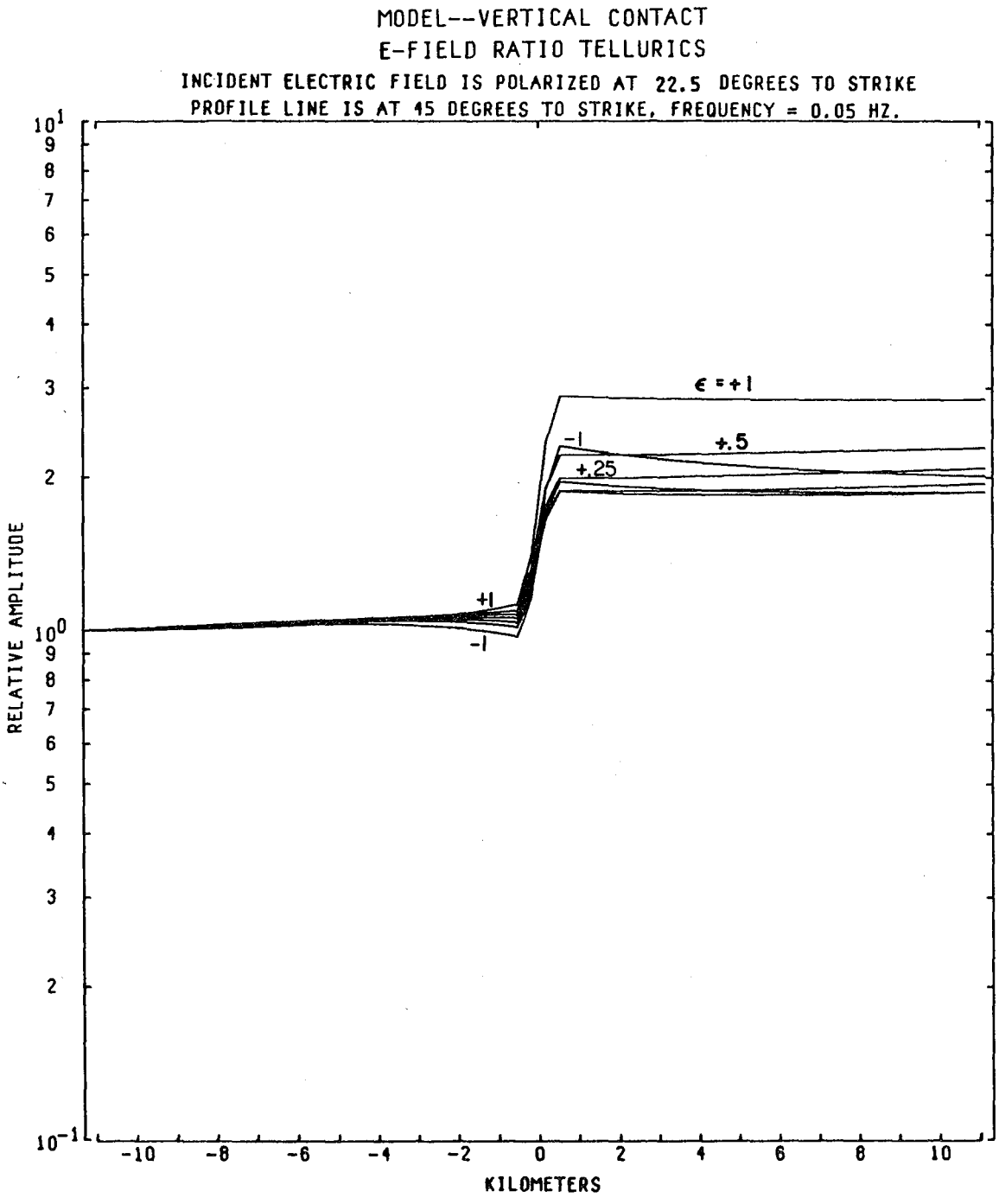

Figure I-C2

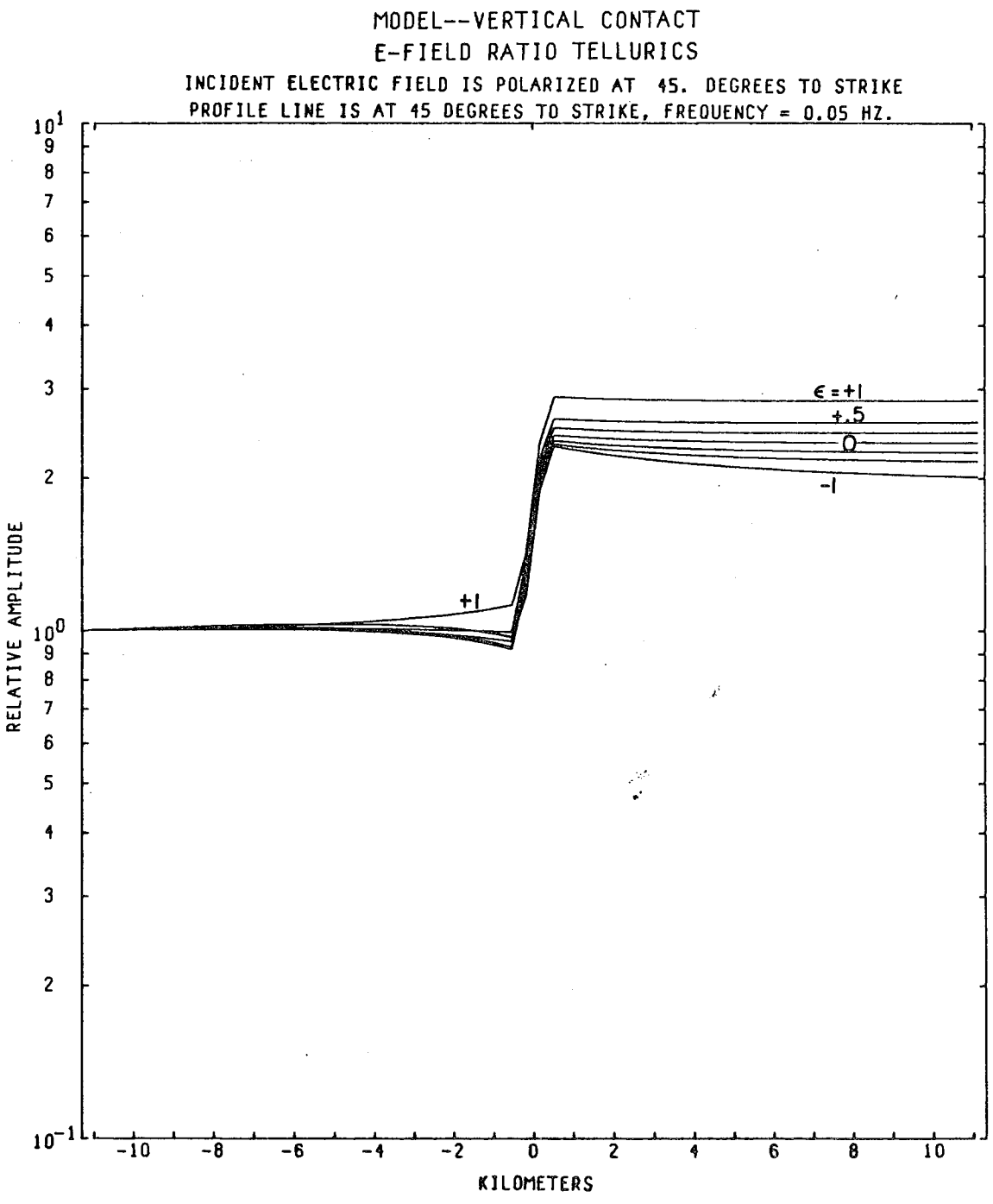
MODEL--VERTICAL CONTACT
E-FIELD RATIO TELLURICS
INCIDENT ELECTRIC FIELD IS POLARIZED AT 45. DEGREES TO STRIKE
PROFILE LINE IS AT 45 DEGREES TO STRIKE, FREQUENCY = 0.05 HZ.
RELATIVE AMPLITUDE
KILOMETERS
ϵ=+1
+.5
0
-1
+1
10^1
10^0
10^-1
-10
-8
-6
-4
-2
0
2
4
6
8
10

Figure I-C3

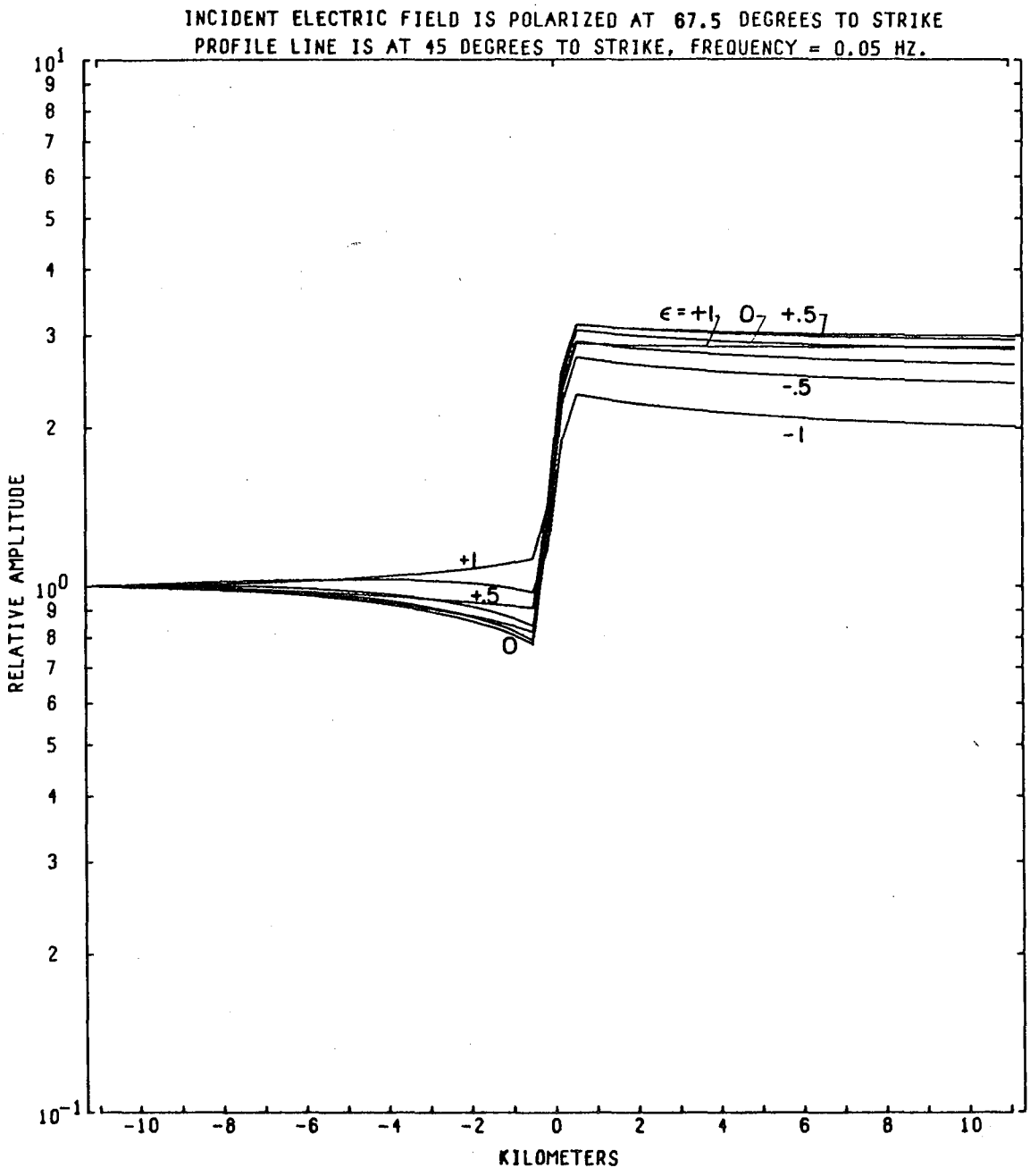
MODEL--VERTICAL CONTACT
E-FIELD RATIO TELLURICS
INCIDENT ELECTRIC FIELD IS POLARIZED AT 67.5 DEGREES TO STRIKE
PROFILE LINE IS AT 45 DEGREES TO STRIKE, FREQUENCY = 0.05 HZ.
RELATIVE AMPLITUDE
KILOMETERS
ϵ=+1, 0, +.5
-.5
-1
+1
+.5
0

Figure I-C4

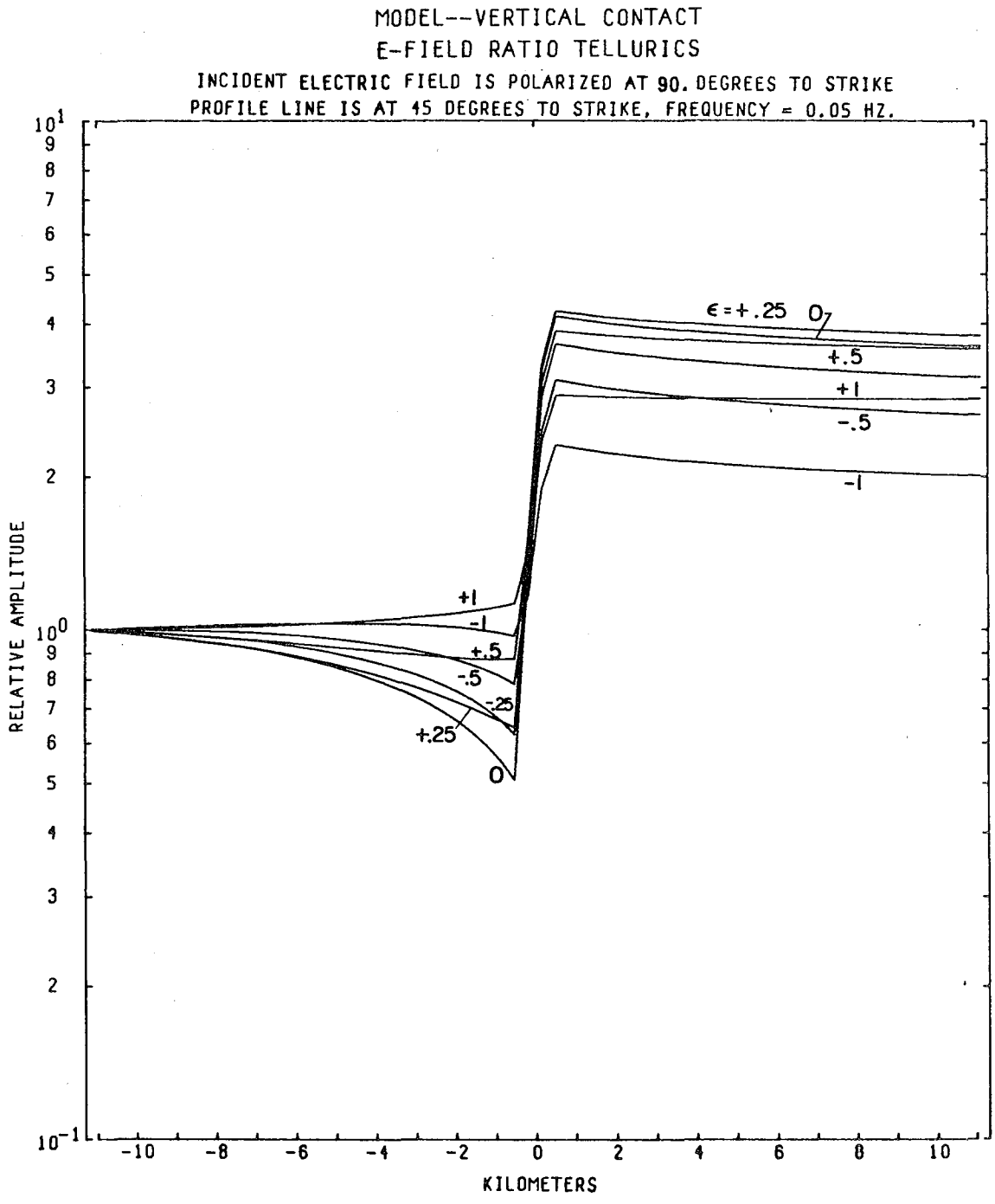
MODEL--VERTICAL CONTACT
E-FIELD RATIO TELLURICS
INCIDENT ELECTRIC FIELD IS POLARIZED AT 90. DEGREES TO STRIKE
PROFILE LINE IS AT 45 DEGREES TO STRIKE, FREQUENCY = 0.05 HZ.
RELATIVE AMPLITUDE
KILOMETERS
ϵ=+.25
0
+.5
+1
-.5
-1
+1
-1
+.5
-.5
-.25
+.25
0

Figure I-C5

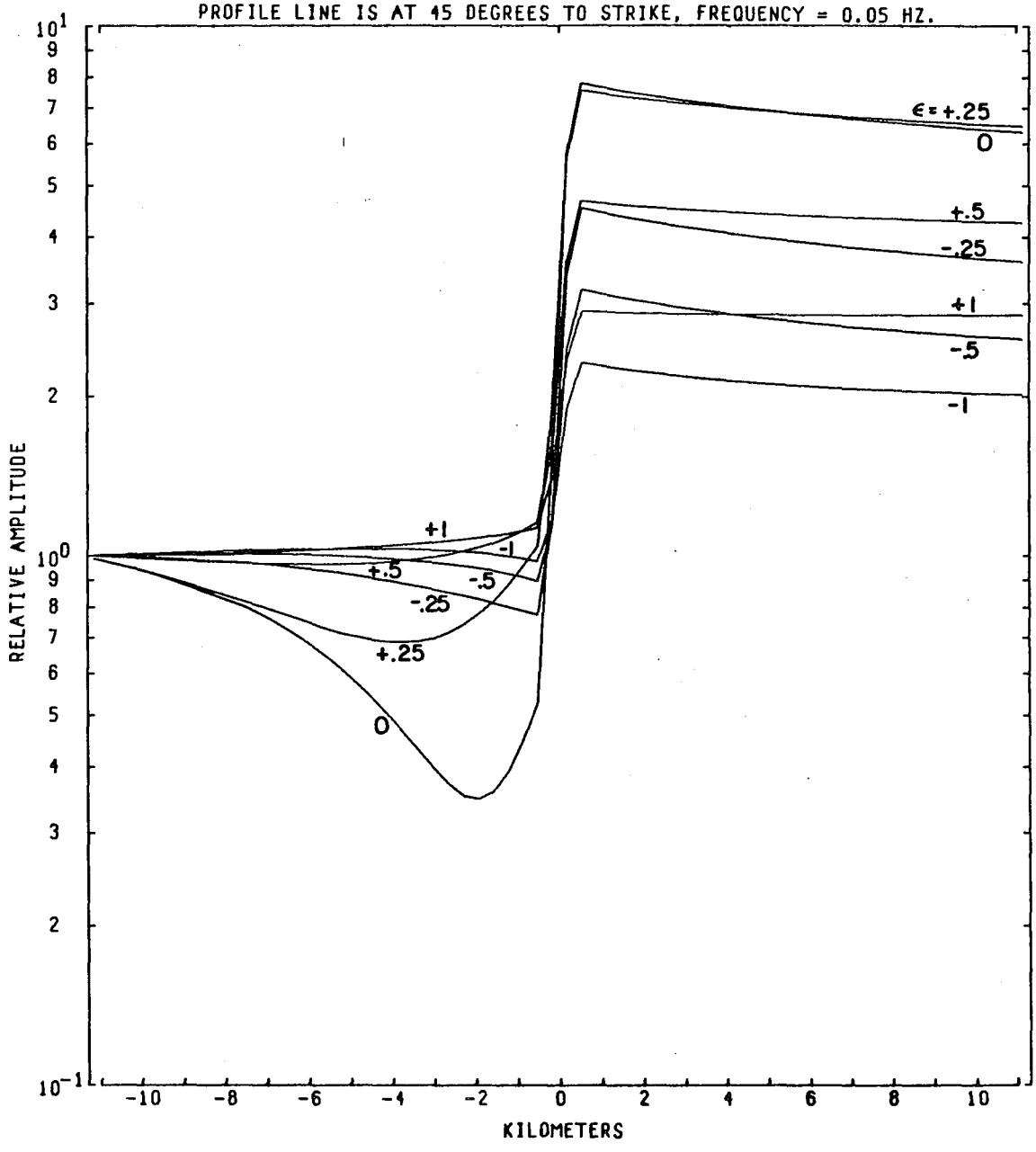
MODEL--VERTICAL CONTACT
E-FIELD RATIO TELLURICS
INCIDENT ELECTRIC FIELD IS POLARIZED AT 112.5 DEGREES TO STRIKE
PROFILE LINE IS AT 45 DEGREES TO STRIKE, FREQUENCY = 0.05 HZ.
RELATIVE AMPLITUDE
KILOMETERS
ε=+.25
0
+.5
-.25
+1
-.5
-1
+1
-1
+.5
-.5
-.25
+.25
0

Figure I-C6

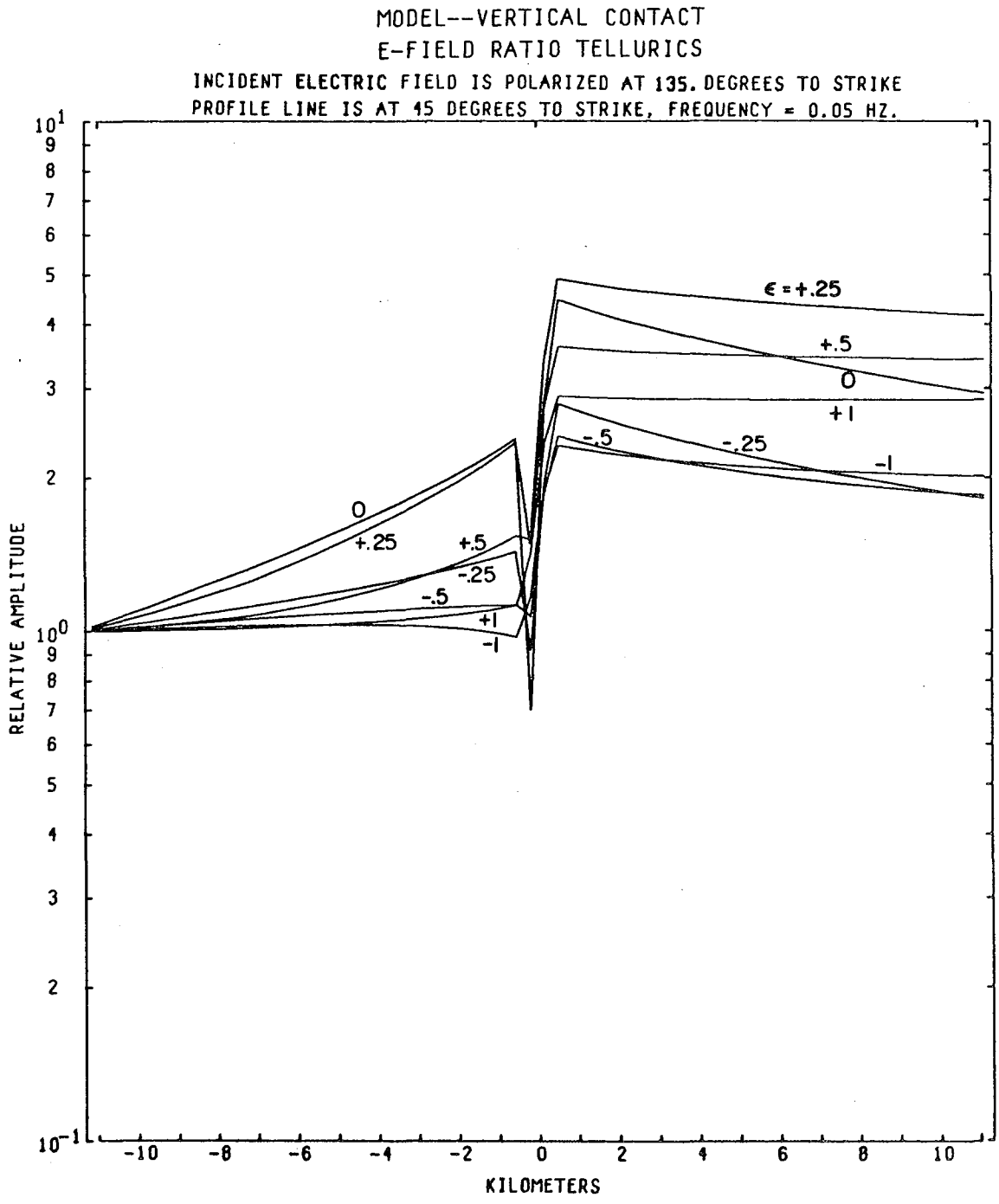
MODEL--VERTICAL CONTACT
E-FIELD RATIO TELLURICS
INCIDENT ELECTRIC FIELD IS POLARIZED AT 135. DEGREES TO STRIKE
PROFILE LINE IS AT 45 DEGREES TO STRIKE, FREQUENCY = 0.05 HZ.
RELATIVE AMPLITUDE
KILOMETERS
ε=+.25
+.5
0
+1
-.5
-.25
-1
0
+.25
+.5
-.25
-.5
+1
-1

Figure I-C7

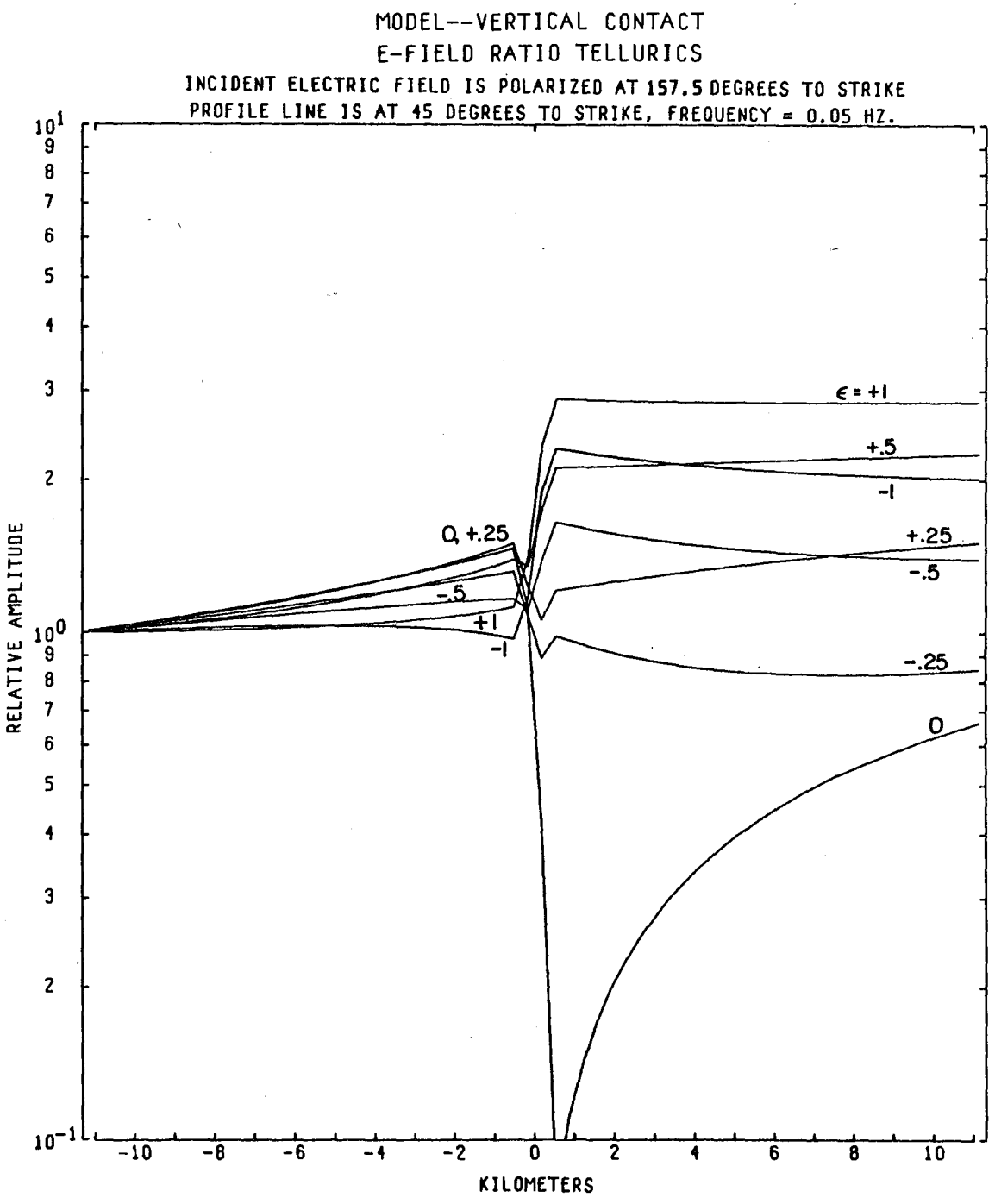

Figure I-C8

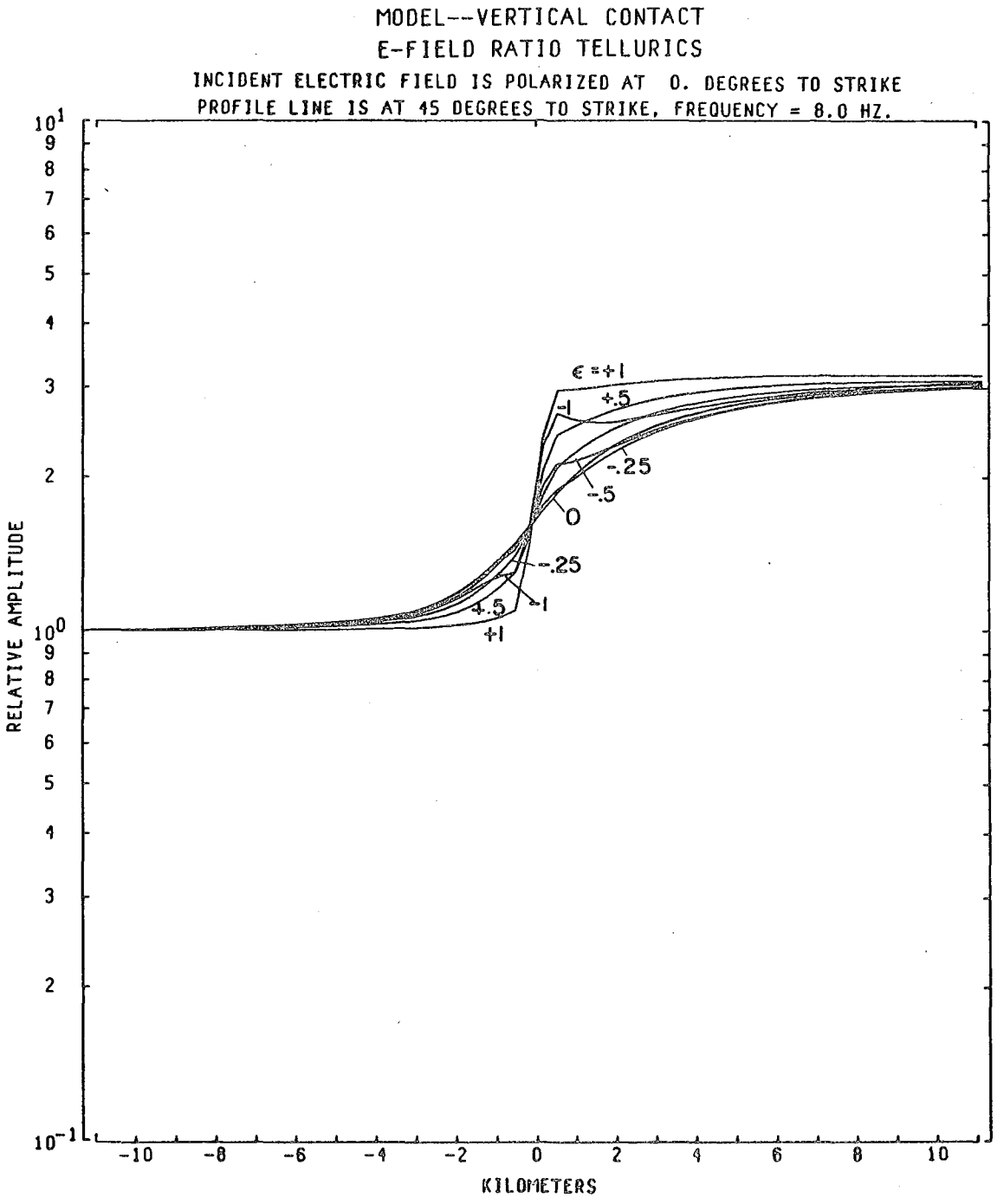
MODEL--VERTICAL CONTACT
E-FIELD RATIO TELLURICS
INCIDENT ELECTRIC FIELD IS POLARIZED AT 0. DEGREES TO STRIKE
PROFILE LINE IS AT 45 DEGREES TO STRIKE, FREQUENCY = 8.0 HZ.
RELATIVE AMPLITUDE
KILOMETERS
ε = +1
+.5
-1
-.25
-.5
0
-.25
+.5
-1
+1

Figure I-C9

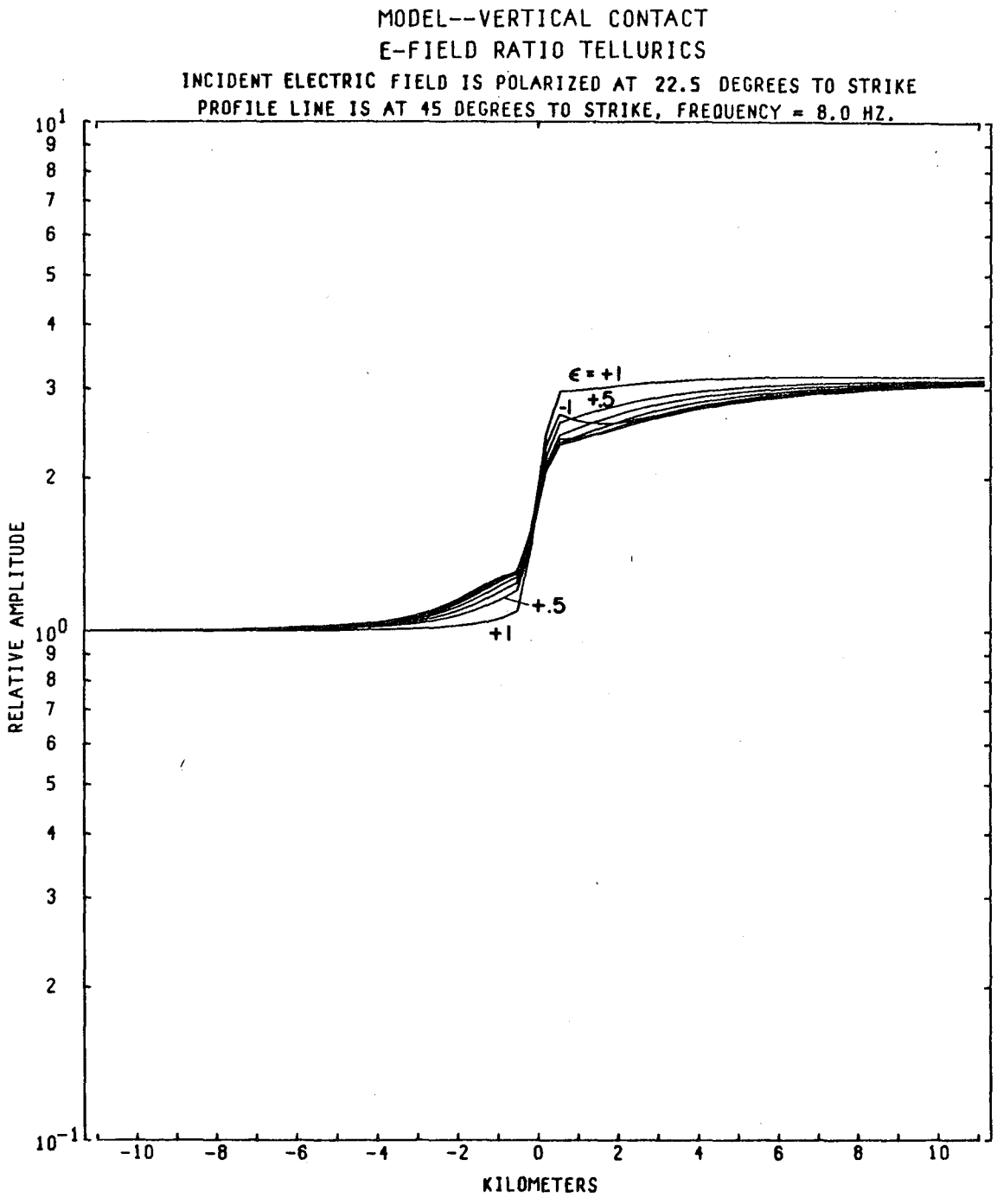

Figure I-C10

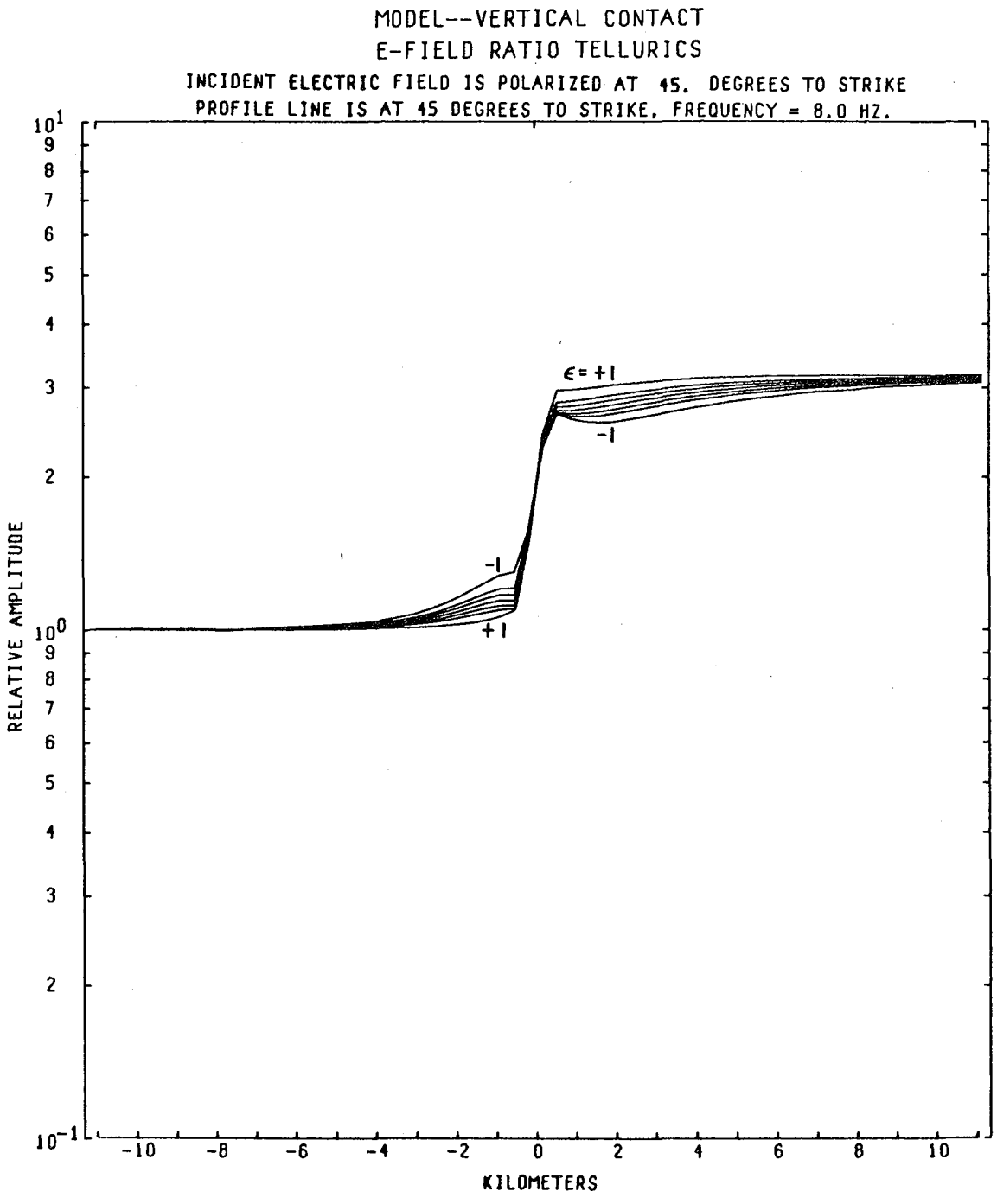
MODEL--VERTICAL CONTACT
E-FIELD RATIO TELLURICS
INCIDENT ELECTRIC FIELD IS POLARIZED AT 45. DEGREES TO STRIKE
PROFILE LINE IS AT 45 DEGREES TO STRIKE, FREQUENCY = 8.0 HZ.
RELATIVE AMPLITUDE
KILOMETERS
ε = +1
-1
-1
+1

Figure I-C11

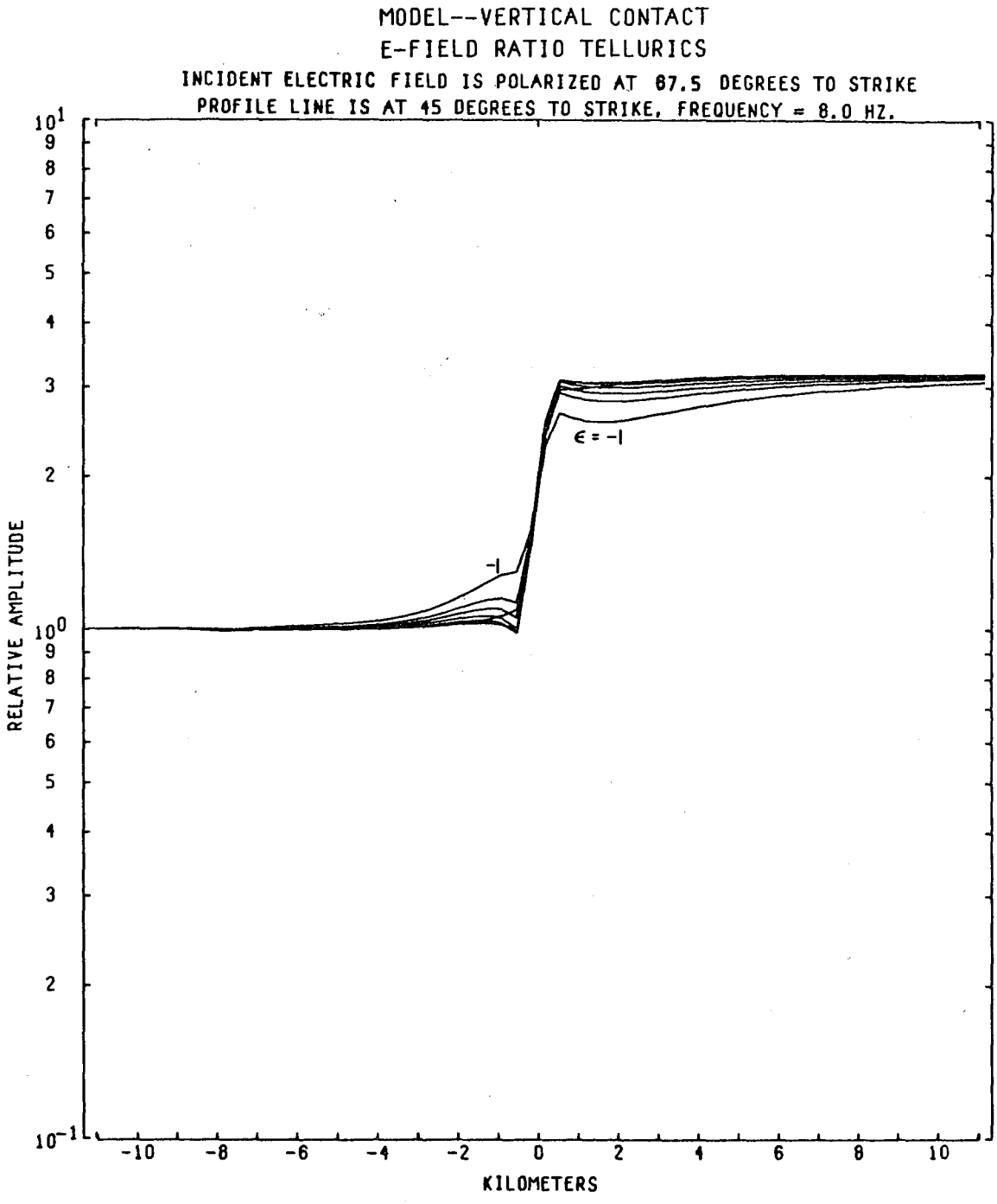

Figure I-C12

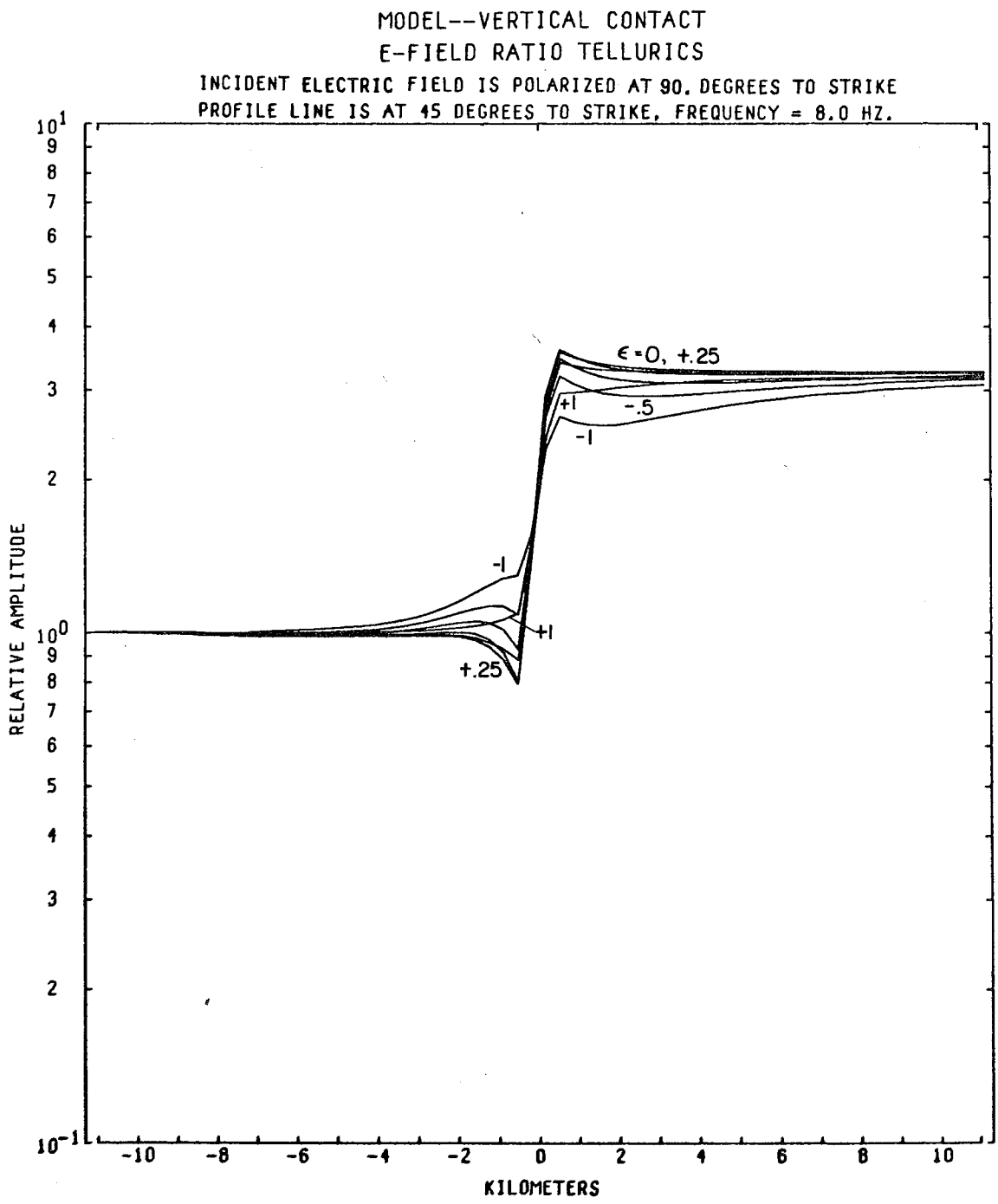
MODEL--VERTICAL CONTACT
E-FIELD RATIO TELLURICS
INCIDENT ELECTRIC FIELD IS POLARIZED AT 90. DEGREES TO STRIKE
PROFILE LINE IS AT 45 DEGREES TO STRIKE, FREQUENCY = 8.0 HZ.
RELATIVE AMPLITUDE
KILOMETERS
ϵ=0, +.25
+1
-.5
-1
-1
+1
+.25

Figure I-C13

MODEL--VERTICAL CONTACT
E-FIELD RATIO TELLURICS
INCIDENT ELECTRIC FIELD IS POLARIZED AT 112.5 DEGREES TO STRIKE
PROFILE LINE IS AT 45 DEGREES TO STRIKE, FREQUENCY = 8.0 HZ.

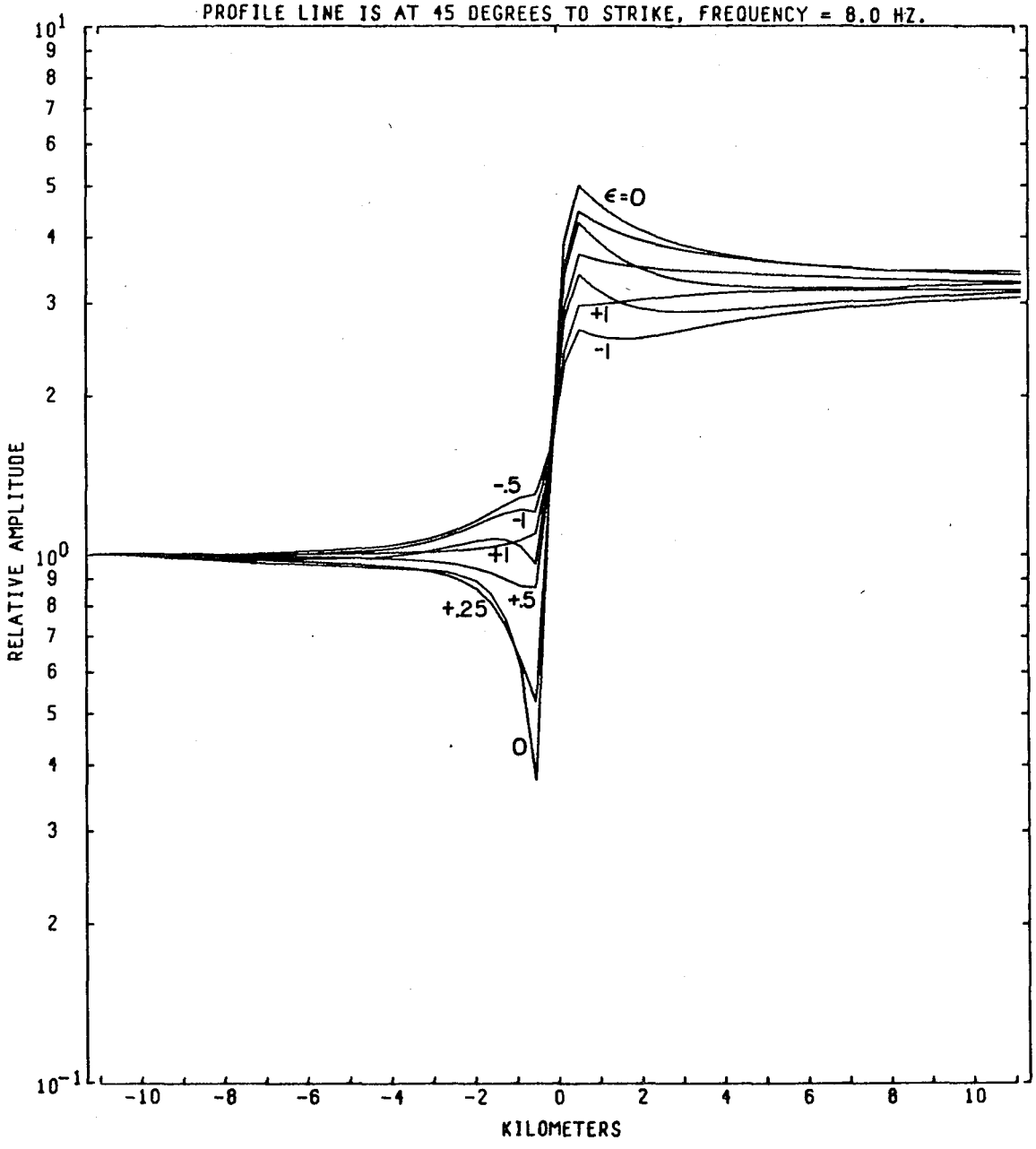

Figure I-C14

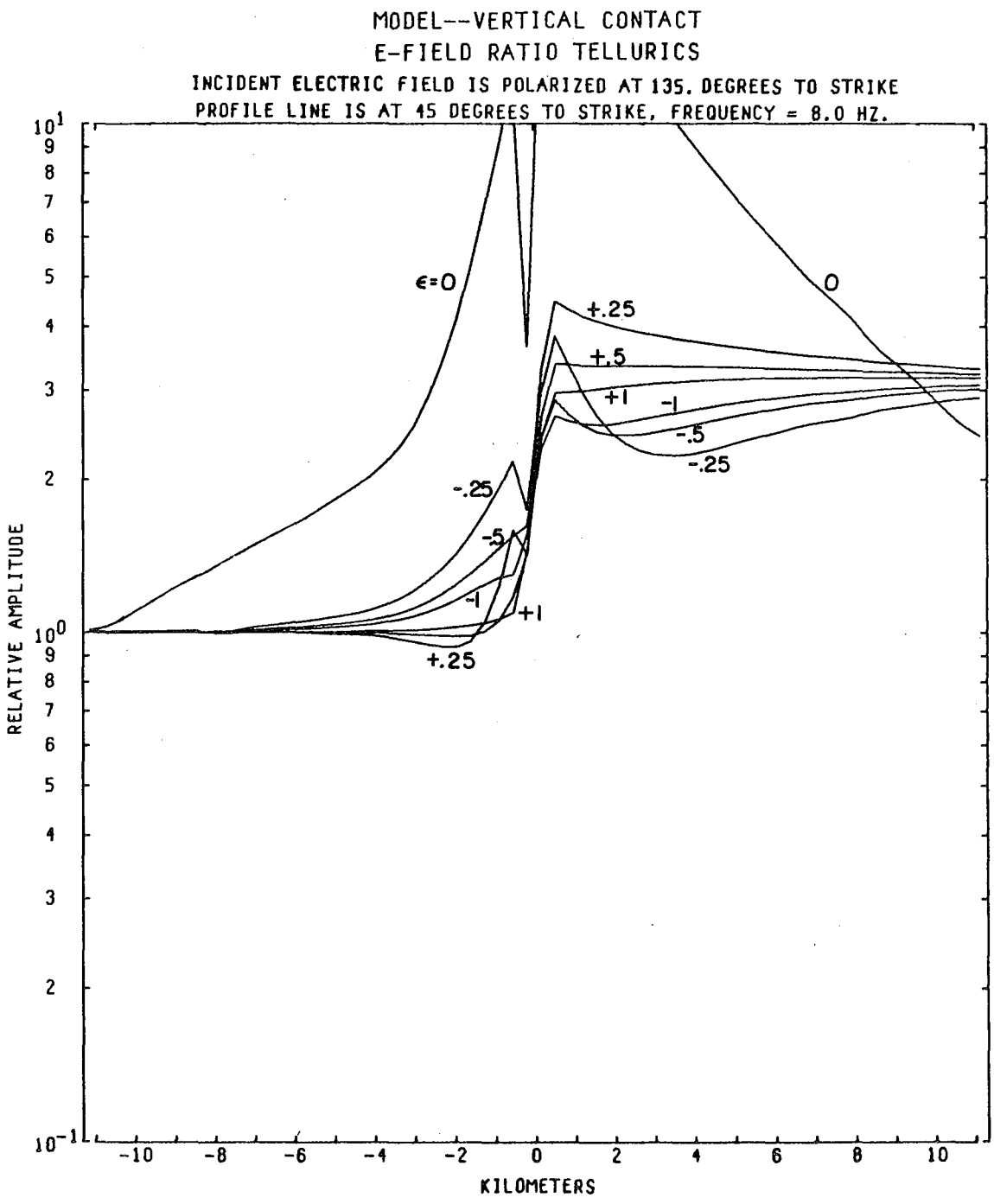
MODEL--VERTICAL CONTACT
E-FIELD RATIO TELLURICS
INCIDENT ELECTRIC FIELD IS POLARIZED AT 135. DEGREES TO STRIKE
PROFILE LINE IS AT 45 DEGREES TO STRIKE, FREQUENCY = 8.0 HZ.
RELATIVE AMPLITUDE
KILOMETERS
ϵ=0
0
+.25
+.5
+1
-1
-.5
-.25
-.25
-.5
-1
+1
+.25

Figure I-C15

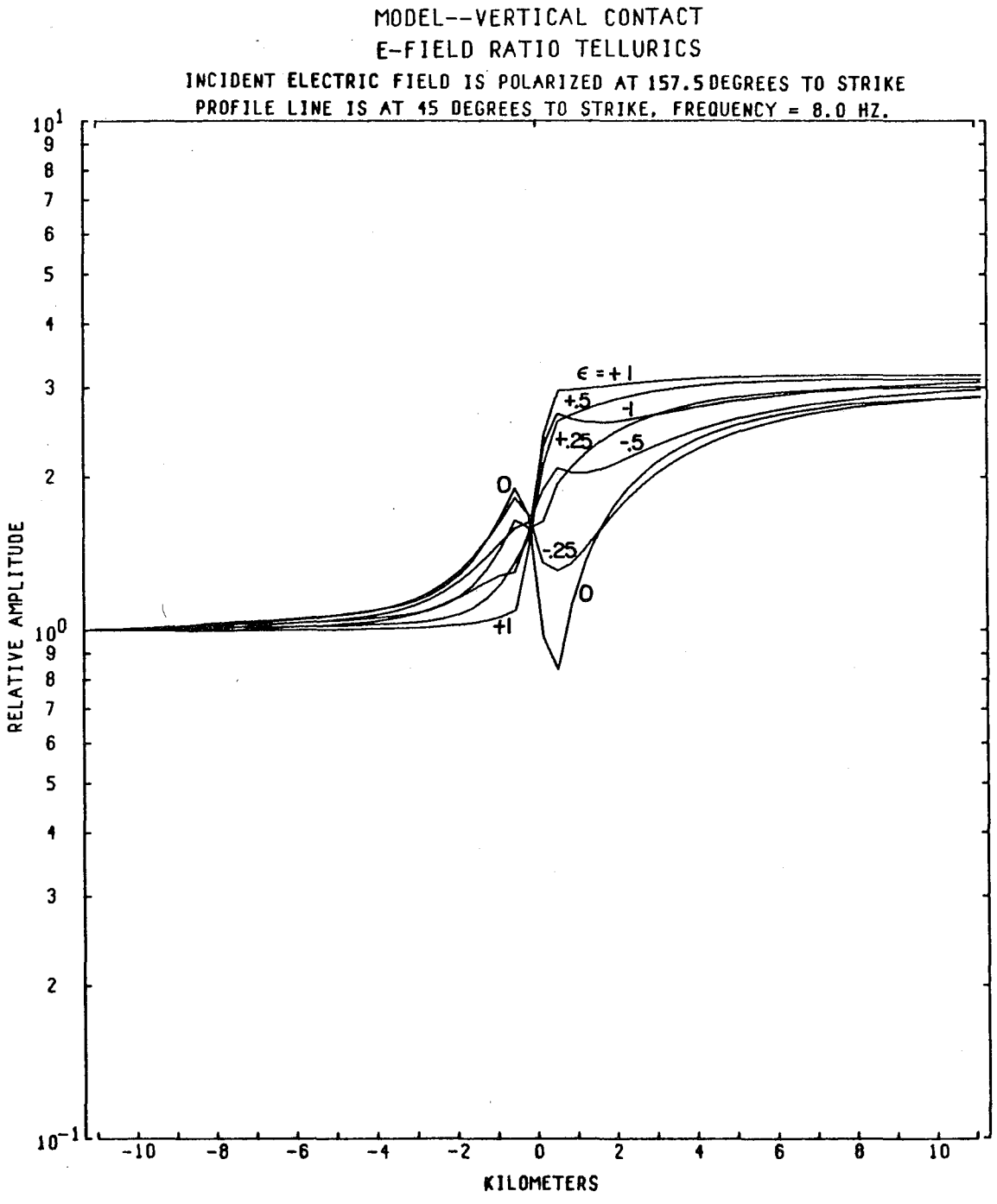

Figure I-C16

This report was done with support from the United States Energy Research and Development Administration. Any conclusions or opinions expressed in this report represent solely those of the author(s) and not necessarily those of The Regents of the University of California, the Lawrence Berkeley Laboratory or the United States Energy Research and Development Administration.